AD-A050 047 OHIO STATE UNIV COLUMBUS ELECTROSCIENCE LAB F/G 17/9
RADAR IDENTIFICATION OF NAVAL VESSELS.(U)
DEC 77 D L MOFFATT, C M RHOADS N00014-76-C-1079
UNCLASSIFIED ESL-784558-1 NL

1 OF 2
ADA
050047

UNCLASSIFIED

SECURITY CLASSIFICATION OF THIS PAGE (When Data Entered)

REPORT DOCUMENTATION PAGE

READ INSTRUCTIONS BEFORE COMPLETING FORM

1. REPORT NUMBER
2. GOVT ACCESSION NO.
3. RECIPIENT'S CATALOG NUMBER

4. TITLE (and Subtitle)

(6) RADAR IDENTIFICATION OF NAVAL VESSELS.

5. TYPE OF REPORT & PERIOD COVERED

(9) Annual Report,

6. PERFORMING ORG. REPORT NUMBER

(14) ESL-784558-1

7. AUTHOR(s)

(10) D. L. Moffat
C. M. Rhoads

8. CONTRACT OR GRANT NUMBER(s)

(15) Contract N00014-76-C-1079

9. PERFORMING ORGANIZATION NAME AND ADDRESS

The Ohio State University ElectroScience Laboratory, Department of Electrical Engineering, Columbus, Ohio 43212

10. PROGRAM ELEMENT, PROJECT, TASK AREA & WORK UNIT NUMBERS

11. CONTROLLING OFFICE NAME AND ADDRESS

Department of the Navy, Office of Naval Research
800 North Quincy Street
Arlington, Virginia 22217

12. REPORT DATE

December 1977

13. NUMBER OF PAGES

111 (12) 116 P.

14. MONITORING AGENCY NAME & ADDRESS (if different from Controlling Office)

15. SECURITY CLASS. (of this report)

Unclassified

15a. DECLASSIFICATION DOWNGRADING SCHEDULE

16. DISTRIBUTION STATEMENT (of this Report)

Approved for public release, distribution unlimited

17. DISTRIBUTION STATEMENT (of the abstract entered in Block 20, if different from Report)

18. SUPPLEMENTARY NOTES

19. KEY WORDS (Continue on reverse side if necessary and identify by block number)

Naval vessels
Identification
Scattering
Measurements
Natural resonances
Matched filter
Radar

20. ABSTRACT (Continue on reverse side if necessary and identify by block number)

This annual report summarizes research efforts on Contract N00014-76-C-1079 for the period 15 September, 1976 to 15 September 1977. An investigation of the feasibility of extending an existing radar target identification scheme to the case of naval vessels is reported. The existing scheme is based on the complex natural resonances of a target associated with transient responses synthesized from multiple frequency scattering data. To this end, multiple frequency scattering

DD FORM 1 JAN 73 1473 EDITION OF 1 NOV 65 IS OBSOLETE

UNCLASSIFIED

SECURITY CLASSIFICATION OF THIS PAGE (When Data Entered)

20.

data of good model targets of various vessel classes in a simulated ocean environment are reported. From these data special target response waveforms are generated and natural resonances extracted. Results are given showing the identification potential of both the response waveforms and the complex natural resonances. In a concluding section recommendations are made for a logical continuation of the research effort.

TABLE OF CONTENTS

I. INTRODUCTION

It is well understood that the primary, if undeclared, goal of any active radar system is the extraction of maximum target information. Detection of the target and estimation of parameters such as range, doppler and even attitude are routinely accomplished. What is not well understood, however, is the estimation of a target's physical properties such as size, shape and composition from radar signaling data. The extraction of these properties for naval vessels and their subsequent use in identification or discrimination of the target is the subject of this report. The identification of objects within a given class, i.e., discrimination and identification of an object without a priori class information, i.e., identification, are considered to be separate capabilities.

A basic understanding of the relationship between the physical properties of a target and its electromagnetic scattering behavior comes from the impulse response concept [1]. With the normalized scattered field in the far zone defined as

$$G(\theta,\phi,\hat{p},j\omega) = \frac{2r}{c} E^s(\theta,\phi,\hat{p},j\omega) \quad , \tag{1}$$

with r the range and c the velocity of light, the normalized scattered field and the normalized impulse response form a transform pair which is

$$G(\theta,\phi,\hat{p},j\omega) = \int_0^\infty F_I(\theta,\phi,\hat{p},t)e^{-j\omega t}dt \quad . \tag{2}$$

The triplet $\theta,\phi,\hat{p}$ denotes that a fixed target-observer orientation and fixed polarization of the incident field and transverse component of the scattered field have been selected. The impulse response waveform "sums up" the scattering properties of an object in one real time-dependent waveform. Thus specular contributions, creeping waves and other diffraction and reflection mechanisms are clearly identified. Using convolution, the response to any postulated interrogating waveform is obtained. The same approach yields the significant specular range of any particular scattering mechanism. The role of frequency becomes more evident from consideration of the ramp response waveform defined as

$$\frac{G(\theta,\phi,\hat{p},j\omega)}{(j\omega)^2} = \int_0^\infty F_R(\theta,\phi,\hat{p},t)e^{-j\omega t}dt. \tag{3}$$

Comparing Equations (2) and (3) it is seen that gross features of the target are defined at low frequencies, i.e., those frequencies which define the ramp response waveform, whereas successively more target detail is added by the step and impulse response waveforms. This conclusion is based on the fact that for most targets

$$\lim_{j\omega\to\infty} G(\theta,\phi,\hat{p},j\omega) = A(\theta,\phi,\hat{p}), \tag{4}$$

and for the worst case, finite flat surfaces viewed normal to the surface,

$$\lim_{j\omega\to\infty} G(\tfrac{\pi}{2},0,\hat{p},j\omega) = B(\hat{P})j\omega \quad . \tag{5}$$

Stated in the time domain, the highest possible singularity in the impulse response is an impulse (Equation (4)) for most targets while for a few targets (Equation (5)) a doublet can occur. This understanding of the role played by frequency illustrates why modulated short pulse-type radar systems can elicite the flare spots of a target but integrating such information into a composite picture of the target is, in general, a very difficult task.

With any radar target identification task there are two basic approaches to the problem, In the first approach the starting point is the radar scattering data available from presently operational systems. Based on such incomplete and nonidentification dictated information, an attempt is made to formulate methods and algorithms for identification. This approach has not been notably successful. A second approach starts with radar data known to be sufficient for the identification task. Note that this does <u>not</u> mean scattering data at all aspects and frequencies; admitting however that an exact inverse scattering solution probably exists with this much information. In the present context the required radar data are dictated by the impulse response concept. As will be seen, with this approach the remaining task is to simplify, as much as possible the required complexity of an identification radar system.

In this report the required radar data for conventional target identification is reviewed. Next, the special problems inherent to naval vessels are enumerated and suggested techniques for overcoming these difficulties are summarized. The suggested techniques are also shown to be applicable to more conventional identification problems. The next section of the report describes the reflectivity ranges and model targets used to obtain representative* radar scattering data

*Representative in the present context means data from which a possibly excitation invariant set of parameters can be obtained. No claim is made (see section on measurement range) that the data are valid cross sections in the usual sense of the term.

for naval vessels. These data are then presented together with special response waveforms synthesized from the data. It is also demonstrated that representative complex natural resonances can be extracted from the response waveforms. A final section of the report lists conclusions drawn from the research to date and recommends logical continuations and extensions of the research effort.

II. CONVENTIONAL TARGET IDENTIFICATION

A conventional method for target identification [2,3] is based on the fact that the ramp response waveform from a target can be synthesized as

$$F_R(\theta,\phi,\hat{p},t) \simeq \frac{-2}{\pi\omega_o} \sum_{n=1}^{2N-1} \frac{[1-(-1)^n]}{n^2} |G(\theta,\phi,\hat{p},jn\omega_o)| \cos[n\omega_o t + \xi(n\omega_o)], \tag{6}$$

using odd harmonics or as

$$F_R(\theta,\phi,\hat{p},t) \simeq \frac{-1}{\pi\omega_o} \sum_{n=1}^{2N} \frac{|G(\theta,\phi,\hat{p},jn\omega_o|}{n^2} \cos[n\omega_o t + \xi(n\omega_o)], \tag{7}$$

using even and odd harmonics.

In Equations (6) and (7)

$$\xi(n\omega_o) = \tan^{-1}\left\{\frac{Im[G(\theta,\phi,\hat{p},jn\omega_o)]}{Re[G(\theta,\phi,\hat{p},jn\omega_o)]}\right\} \quad . \tag{8}$$

Thus if L is a maximum linear target dimension then discrete spectral scattering data for an N of 5 and

$$\omega_o \simeq \frac{0.4\pi c}{L} \quad , \tag{9}$$

suffice to define the ramp waveform for most targets. The result in Equations (7) and (8) is coupled with the fact that the physical optics approximation to the ramp response waveform is

$$F_R(\theta,\phi,\hat{p},t) \propto \frac{-1}{\pi c^2} A(z)\Big|_{z = \frac{c(t-r/c)}{2}} \quad , \tag{10}$$

where A(z) is the projection of the illuminated portion of the target onto a plane perpendicular to the line of sight of the radar (z) with the illumination moving at 1/2 the free space velocity to account for the two way path. It is clear that the ramp response waveform contains basic information on the gross physical properties of the object. Moreover, the forced portion of the ramp response (Equation (10)) is directly related to the object's cross sectional area. This fact has been used to produce isometric three-dimensional images of the target [4,5].

Conventional target discrimination utilizes the fact that for the transient portion of the ramp response waveform a good approximation is

$$F_R(\theta,\phi,\hat{p},t) \simeq \sum_{m=1}^{M} Am(\theta,\phi,\hat{p})\, e^{\gamma_m(t-t_o)}\, \mu(t-t_o) \quad , \tag{11}$$

where t_o is the time the interrogating signal moves beyond the shadow boundary with zero at the point the response starts. Note in Equation (11) that the excitation coefficients contain the orientation and polarization dependence and the complex natural resonances

$$\gamma_m = \sigma_m \pm j\omega_m \quad , \tag{12}$$

are only a function of the size, shape and composition of the target, i.e., they are excitation invariant. Methods for finding the dominant complex natural resonances of a target from reaction integral equation formulations and from transient signals or their equivalent spectral samples (Equations (6) and (7)) have been discussed [2,3,6,7]. A relatively new method combining calculated spectral data and an integral equation formulation has also been given [8]. No single method has proven completely satisfactory and problems when noise and/or clutter contaminate the signal indicate additional research is needed. Also, while present methods do not preclude use of the complex natural resonances for target discrimination, they do dictate that the discrimination should <u>not</u> be based on extraction of complex natural resonances in real time from an unknown target signal.

If it is assumed that a library of natural resonances for a given class of objects is known, a priori, then discrimination is based on prediction-correlation as

$$\rho'' = 1 - \frac{\sum_n [F_{Rm}(n\Delta t) - F_{Rc}(n\Delta t)]^2}{\sum_n F_{Rm}^2(n\Delta t) + \sum_n F_{Rc}^2(n\Delta t)} \quad , \tag{13}$$

where F_{Rm} is the measured ramp response and F_{Rc} is a calculated ramp response. The calculated ramp response comes from the general predictor difference equation for transients [9]

$$f(t) = \sum_{n=1}^{N} B_{N,n}(-1)^{n+1} f(t-n\Delta t) \qquad t \geq N\Delta t, \qquad (14)$$

where N is the number of natural resonances and Δt the sample interval. The difference coefficients in Equation (14) are related to the natural resonances as

$$\prod_{n=1}^{N} (s-e^{\gamma_n \Delta t}) = \sum_{n=0}^{N} B_{N,n}\, s^{N-n} \qquad B_{N,0} \equiv 1, \qquad (15)$$

thus given the complex natural resonances, γ_n, for a given target the difference coefficients are known for arbitrary Δt. To reduce noise problems, Equation (14) is normalized by the magnitude of the largest difference coefficient. If this is done, with the N,k term say having the largest magnitude then

$$F_{Rc}(t-k\Delta t) = \sum_{\substack{n=1 \\ n\neq k}}^{N} \frac{B_{N,n}}{|B_{N,k}|} (-1)^{n+1} F_{Rm}(t-n\Delta t), \qquad (16)$$

and each calculated point comes from, in general, both prior and future samples of the measured waveform. Numerous examples of successful discrimination using Equations (13) and (16) have been given [2,3]. In the next section certain general limitations and the complications introduced by naval vessels are described. It should be noted however that there is nothing magic about the ramp response waveform beyond the discrimination against the influence of higher frequency scattering data. In principle, any transient response waveform from the target is sufficient. This assumes that a portion of the transient can be well approximated by a finite sum of exponentials.

There have been many applications of Prony's method and various modifications of the method reported. The references in a recent dissertation [10] are a good source for Prony's method. Two primary and different objectives characterize the numerous applications;

1) good, finite exponential fit of time-dependent signaling data,*

2) extraction of a finite set of complex natural resonances.

In the first application the "fit" to the data is all important - there is little interest in the exponential arguments. The second application stresses a physical significance for the exponential arguments, i.e., only left half-plane arguments with negative definite real parts are acceptable. For the identification problem, while the arguments or complex natural resonances are a parameter, it does not necessarily follow that a physical significance must be stressed completely. Our earliest applications of resonances to the identification problem used ramp response estimates [12]. In such data the inverse frequency squared weighting dictates only a few terms in the exponential approximation for all but very short times. For these problems the extracted resonances did have a physical meaning. However for complicated structures where the responses are obtained from signaling waveforms containing higher frequencies (synthetically or otherwise) it may not be possible to interpret physically the extracted resonances nor may it be possible to insist on precise excitation invariance. Thus it may be necessary to find that finite set of complex numbers which best satisfies several sets of data. This point will be discussed later.

Assume that a measured response signal is obtained as**

$$f_o(t) = f(t) + \underline{n}(t) \quad , \tag{17}$$

where $f(t)$ is the true response and $\underline{n}(t)$ an interfering signal which could be noise, clutter or roundoff error in a computer. The "measured" signal then can be experimentally or computationally obtained. Note that this discussion is concerned with the characterization of a target and not identification, i.e., Equation (17) are study signals used to obtain numbers for a library. The actual identification process does not extract such numbers. The approximation is

$$f_a(t) = \sum_{n=1}^{N} A_n e^{\gamma_n t} \approx f(t) + \underline{n}(t) \quad . \tag{18}$$

*A frequency approach has also been reported, see Reference [11].

**The position, polarization and delay dependence is assumed to be understood here and hence is suppressed.

The difference equations inherent in the solution of Equation (18) are

$$\sum_{m=1}^{M+1} \sum_{n=1}^{N+1} C_n \, f_o[t + (m+n-2)\Delta] = \sum_{m=1}^{M+1} \varepsilon_m \, , \qquad t_1 \leq t \leq t_2 \qquad (19)$$

where properly

$$\varepsilon_m = \varepsilon_m(N,M,\Delta,t_2-t_1) \, . \qquad (20)$$

That is, Equation (19) generates a system of M+1 equations in N+1 unknowns and the error in each equation is a function of the sample interval, t_2-t_1, the sample spacing, Δ, the order of the difference equation, N and the number of equations generated, M+1. The Prony method equates (19) to zero and sets C_1 to unity. In matrix form Equation (19) becomes

$$F \, C = \varepsilon \, , \qquad (21)$$

where

$$f_{ij} = f_o[t_1 + (i+j-2)\Delta] \, , \qquad \begin{matrix} i = 1,2, \cdots M+1 \\ j = 1,2, \cdots N+1 \end{matrix} \qquad (22)$$

$$C_{i,j} = C_{il} \, , \qquad i = 1,2, \cdots N+1 \qquad (23)$$

and

$$\varepsilon_{ij} = C_{il} \, , \qquad i = 1,2, \cdots M+1 \, . \qquad (24)$$

In general F is a rectangular matrix

$$M \geq 2N \, , \qquad (25)$$

with the equal sign in Equation (25) yielding a square matrix. The inequality in Equation (25) also follows from Equation (18) where there are 2N unknowns.

Before discussing solutions of Equation (18) or equivalently Equation (19) a difference in the approach adopted here should be noted. In Reference [13] and elsewhere the exponential sum is based on Singularity Expansion Method (SEM) ideas. That is, an impulse response is written as

$$h_I(t) = \sum_{n=1}^{\infty} A_n e^{S_n t} \mu(t-t_1) \quad , \tag{26}$$

where it is assumed that the singularities are simple poles (S_n), the transform of a possible entire function deleted and the A_n are products of the coupling coefficients and the natural modes. It is properly recognized that the transient must be delayed until the excitation is removed ($t_1>0$). If this line of reasoning is followed then for the ramp response

$$h_r(t) = \sum_{n=1}^{\infty} \frac{A_n}{(S_n)^2} \left[e^{S_n t} - e^{S_n t_1} (1+tS_n - t_1 S_n) \right] \mu(t-t_1) \quad . \tag{27}$$

Clearly the coefficients, A_n, can absorb the additional weighting in Equation (27) but the additional terms in Equation (27) must also be absorbed as exponentials and this in general cannot be done. We have for some time, however, used the form Equation (26) to fit ramp response waveforms and will continue the same type of approximation.

Returning to Equation (21) the solution of this equation is essentially a departure point for the two objectives mentioned earlier. If only a good fit to the waveform is desired then Prony's method is adequate except when signal/noise (S/N) power levels are low [10]*. If Equation (19) is solved in the least squares sense then the error in the fit to the waveform is minimized. This approach however does <u>not</u> optimize the exponential arguments. Simply stated, several different combinations of poles and residues can yield equally good fits to the response. The basic problem is that the waveform fit is relatively insensitive to the precise pole locations.

Consider again Equation (19), where there are two methods for solution which have been proposed. The first of these is Prony's method where C_1 is set to unity and the remaining coefficients are chosen such that

$$\sum_{m=1}^{M+1} \varepsilon_m^2 \quad , \tag{28}$$

*We do not feel that the S/N ratio of 30 dB (total) quoted in Reference [10] is realistic when the extraction process is in non-real time and not a one shot trial.

is minimized. This is the standard least squares or quasi-inversion procedure. A second method (eigenvalue) is to write Equation (19) in the quadratic form

$$\tilde{C}\,(S)\,C = \sum_{m=1}^{M+1} \varepsilon_m^{\,2} \quad , \tag{29}$$

where the quantity on the right of Equation (29) is a minimum,

$$\sum_{m=1}^{M+1} \varepsilon_m^{\,2} = 1, \tag{30}$$

and

$$s_{ij} = s_{ji} = \sum_{m=1}^{M+1} f_{oi}(t+(m+j-1)\Delta)\; f_{oj}(t+(m+i-1)\Delta), \tag{31}$$

are the components of the symmetric matrix S. The coefficients (C) are then the eigenvectors of the minimum eigenvalue. It has been shown [14] via a specific example that the two methods lead to different squared errors, with the minimum obtained using the eigenvalue approach.

The error parameters in Equation (20) present difficulties. Unfortunately these parameters are not independent, i.e., setting one parameter imposes restrictions on certain other parameters. For example the order of the difference equation, N, must clearly be related to the investigation interval t_2-t_1. If the interval t_2-t_1 is progressively expanded to include earlier times it follows that additional exponential terms may be needed. Conversely if the difference equation order is fixed and not over specified then the interval t_2-t_1 should be bounded. It has been suggested [15] that the eigenvalue approach can be used to establish N. This however is based on t_2-t_1 being fixed and the use of noise-free data. With noise, clutter and roundoff error present, as is always the case, this approach rapidly deteriorates. There is also the problem that if N becomes large discrimination procedures become unwieldy [16]. Thus it is advantageous to keep N as small as possible. We postulate that N is best determined from trials on various data sets corresponding to the same target which precludes real time resonance extraction but is compatible with a predictor-correlator approach.

The sample interval Δ must be carefully considered. It is not sufficient to use the Nyquist rate

$$\Delta < \frac{1}{2F_{max}} \quad , \tag{32}$$

where F_{max} is the highest frequency in $f_o(t)$. This will yield an upper bound but not a lower bound. Numerous examples with prediction-correlation, where the same difference equation as in Equation (19) is used, have shown that Δ also has a lower bound

$$\Delta_{min} < \Delta < \frac{1}{2F_{max}} \quad . \tag{33}$$

If Fourier synthesis is used to obtain the transient then prior results [16] indicate

$$0.02 \leq \frac{\Delta}{T_o} \leq 0.035 \quad , \tag{34}$$

but this is based on a particular interval

$$t_2 - t_1 = T_o - 0.33T_o \quad . \tag{35}$$

However, even within the acceptable limits, Equation (34), the results are not constant, i.e., the coefficients in Equation (19) are a function of Δ. Simply stated, the rectangular matrix generated by Equation (19) is poorly conditioned numerically. One attempt at a partitioning scheme to improve the conditioning [11] (a frequency domain approach) was unsuccessful.

Our best results to date have been obtained using programs which systematically vary each of the error parameters [16]. When applied to numerous data sets for a given target, the results are acceptable. The formulation in [14] uses a Z-domain approach and eigenvalue solution, but the Z-domain at least appears to be incidental. On the present program research has not yet reached the stage where the nuances of Prony's method are of vital importance. It is sufficient that characteristic complex numbers can be extracted from the data and that these numbers are, via prediction-correlation, an adequate representation of the data. It should be noted that for the matched filter responses of naval vessels the extracted (Prony) resonances have oscillatory parts in excess of the highest input frequency. This is not surprising because the purpose of the matched filter response is to obtain a rapidly damped response.

III. SPECIAL PROBLEMS OF NAVAL VESSELS

It is evident from Equation (9) and the discussion on conventional target discrimination that relatively low frequencies are required for the ramp excitation. The reason for this is that dominant complex natural resonances have been emphasized. For example, aircraft target natural resonances are used where the wing and fuselage lengths are approximately one-half wavelength at the oscillatory part of the natural complex frequency. Therefore the required excitation frequencies for the transient response are quite low. Also, using

Equation (6) or Equation (7), complex radar scattering data, i.e., amplitude and phase, are required. For naval vessels, if the hull length is considered the dominant linear dimension, the required frequencies are very low. For example destroyers, with a nominal hull length of 130 meters would require a fundamental excitation frequency of 0.462 MHz. Thus one special problem of naval vessels is very evident.

Assuming that singularities of the target scattering function can continue to be modeled as simple poles at higher frequencies, there is no basic reason why higher frequencies cannot be used. Clearly as frequency increases smaller target dimensions approach an oscillatory resonant length. Thus target identification based on what can be termed "substructure resonances" is a possibility. A number of complications can be anticipated. As already noted, the substructure resonances must be well modeled by simple poles. It must also follow that in a particular spectral range such substructure resonances must be dominant. That is poles associated, for example, with certain superstructure features must have real parts at least comparable to those of larger structural features. Using an aircraft example, vertical and horizontal stabilizers must have resonances similar to those of the wings and fuselage but at higher oscillatory frequencies. To be useful the damping part of such resonances should not be much greater than those dominant for the wings and fuselage. It also follows that for a complex structure the density of complex natural resonance locations must increase as the oscillatory frequency is increased. That is, multiple resonances of longer structures may be in close proximity to the first or dominant resonance of a smaller structure. For this reason it may be necessary to use a larger number of poles to describe the transient response than that necessary for the ramp response. Alternatively, special interrogating signals based on knowledge of the higher order resonances may be needed.

It is well known that radar signals from naval vessels exist in a clutter background produced by the sea. A rare exception can occur when radar beamwidths are such that only portions of the vessel are effectively illuminated. An explanation of the possible complicated electromagnetic interactions between the vessel and the sea is beyond the scope of this study. In fact, a valid mathematical model for the complex radar return from the sea alone at arbitrary frequencies is not yet available. Admittedly some success in predicting sea return at particular frequencies has been reported, but a general model has not emerged. The sea then is an added complication for naval vessels. Note also that the sea presence essentially precludes obtaining good radar return data from models of naval vessels for higher full scale frequencies because a physical model of the sea surface becomes prohibitively difficult. For our purpose we assume that if the full scale frequencies are such that*

*The highest permissible frequency is somewhat arbitrary, but it is felt that Equation (36) is reasonable if possibly optimistic.

$$F_{FS} \leq 25 \text{ MHz}, \tag{36}$$

then the sea can be modeled electromagnetically as a perfectly conducting ground plane. With a highest model frequency of (see next section)

$$F_M = 10.8 \text{ GHz} \quad , \tag{37}$$

a scale factor for the model of 432 or greater is required. Actually, the choice of scale factors was dictated by that available from suppliers of plastic models.* It was decided that silver-painted plastic models, despite the size restrictions, were more realistic than very crude homemade versions of the vessels. It is apparent however that in order to investigate full scale frequencies higher than 25 MHz, modeling would be a most difficult problem. The dilemma is serious because both mathematical and experimental models of the clutter at full scale frequencies greater than 25 MHz can be seriously questioned. We have circumvented the problem for the moment by restricting initial attention to the lower frequencies. The rationale being that vessel identification should first be established in spectral ranges where reasonably good scattering data can be obtained on a model basis.

IV. MULTIPLE FREQUENCY REFLECTIVITY FACILITY AND MODEL TARGETS

The nine model targets used to obtain the reflectivity measurements reported in this study are tabulated in Table I. Only the nominal lengths of the models are given, other pertinent dimensions can be found in Jane's Ships of the World, 1973. Admittedly, minor differences can and do exist between the vessels reported in the reference and the actual models used in this study. However, over the span of frequencies covered minor structural differences should not produce appreciable changes in the scattered field. A possibly more serious problem is the maze of antennas known to exist on modern naval vessels. Long, wire-like communications antennas could seriously alter the scattered field. No attempt has been made to include antenna structures on the model targets. In this initial phase of the study it was felt that principles could be explored without the necessity of detailed antenna modeling. This amounts to assuming that antenna structures do not dominate the scattered field over the span of frequencies covered. There are obviously complex natural resonances associated with the antennas but these resonances in general would be a poor identification tool because the antenna structures would be approximately the same size on most vessels. Associated vessel structures would alter the

*We are indebted to Dr. Arthur Jordon of the Naval Research Laboratory for supplying, on a loan basis, three good 500:1 scale factor metal and wood models of naval vessels.

TABLE I. MODELS

Name	Classification	Scale	Scaled f_o	Model Length	L/λ_o	Construction
Midway	Aircraft carrier	1:500	2.17 MHz	58.7 cm (23.1 in)	2.12	Silver painted, wooden hull, metal superstructure
Missouri	Battleship	1:500	2.17 MHz	54.0 cm (21.3 in)	1.95	Silver painted, wooden hull, metal superstructure
Sverdlov	Cruiser	1:500	2.17 MHz	47.0 cm (16.5 in)	1.52	Metal
Missouri	Battleship	1:700	1.55 MHz	38.4 cm (15.1 in)	1.39	Plastic, silver painted
Iowa	Battleship	1:700	1.55 MHz	38.4 cm (15.1 in)	1.39	Plastic, silver painted
Bismark	Battleship	1:700	1.55 MHz	35.5 cm (14.0 in)	1.28	Plastic, silver painted
Mogami	Heavy Cruiser	1:700	1.55 MHz	28.1 cm (11.1 in)	1.02	Plastic, silver painted
Hayanami	Destroyer	1:700	1.55 MHz	18.5 cm (7.3 in)	0.67	Plastic, silver painted
Shimokaze	Destroyer	1:700	1.55 MHz	16.9 cm (6.7 in)	0.61	Plastic, silver painted

f_o = 1.085 GHz, λ_o = 27.63 cm (10.88 in)

resonance locations slightly between vessel classes but probably not sufficiently to affect identification. Photographs of the model vessels on the ground plane are shown in Figures 1 and 2. In every case, non-metallic portions of the models were silver painted to ensure realistic scattering data. As noted, the targets used in this study were for the most part commercially available scale-model plastic ships. The models were waterline, i.e., simulating a floating structure. The models were spray painted with silver-loaded paint to simulate conducting metal targets. A list of the models used and their major characteristics is given in Table I. While some of these targets are not United States Navy ships or even fairly recent foreign ships, their major features are similar to those of ships in use today and it was felt that they would be adequate for our purpose.

The measurement facility used to obtain data on the ship models is a unique bistatic radar system using the first ten harmonics of a harmonically rich crystal controlled 1.085 GHz source, $f_o(f_o)10f_o$. All data collection is performed under computer control using an IBM Minimal Informer. A simplified block diagram of the system is shown in Figure 3. Once the data taking sequence is initiated, requests are made to the operator for the parameters of the range geometry. The computer uses these data to control a stepping motor which moves the target one-half wavelength along the range vector from the target to either antenna. Thus the two way path differential is one wavelength at the fundamental. At the fundamental, this results in one cycle of a slow-doppler interference pattern, two cycles at the second harmonic, etc. Since several frequencies are used on any one run the return contains a superposition of the interference patterns. The individual components are separated by multiplying the sample values by sin(nx) and summing for n=1,2,...10. This is also done for cos(nx). In essence this yields the Fourier Coefficients of a ten frequency periodic pattern. These complex coefficients therefore contain the magnitude and phase information on the target.

For the scattering coefficients of an unknown target, three sets of data are taken. These are:

(1) No target run (NT_M)

(2) Unknown target run (U_M)

(3) Reference (conducting hemisphere) target run (R_M),

where the M subscript denotes measured values. Also, a calculated set of scattering coefficients for the reference target at the ten frequencies is required (designated R_C). By the linearity property of the Fourier Series the NT_M term can be subtracted from both U_M and R_M since it represents the stationary clutter return. By forming the ratio R_C over R_M a set of complex calibration coefficients is formed. The calibrated unknown target scattering coefficients (designated U_C) are then found by multiplying by the calibration coefficients. This is simply shown by:

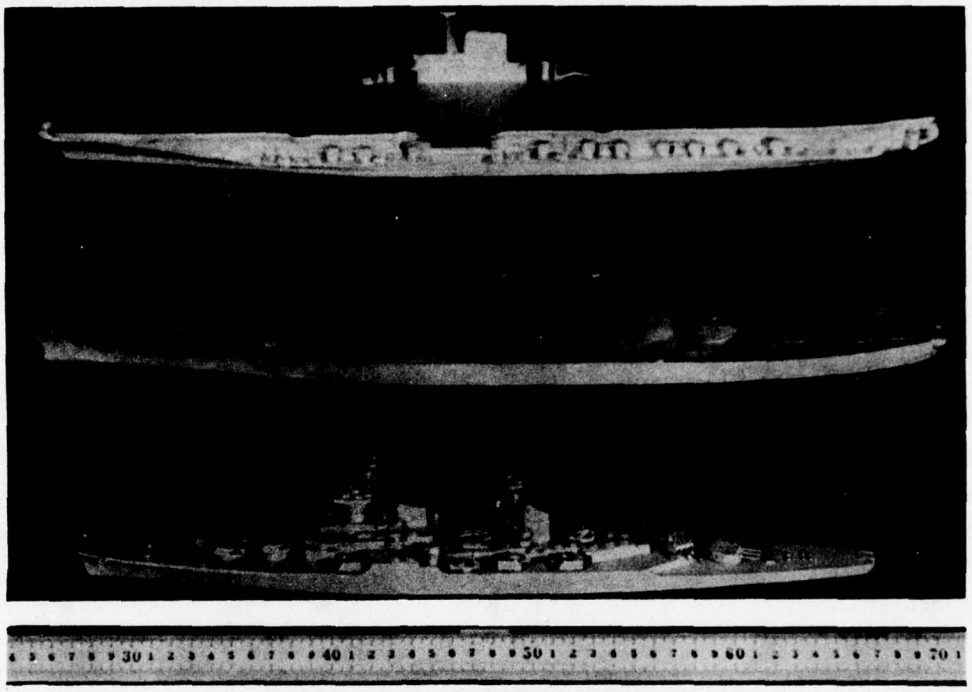

Figure 1. -1/500 scale models.

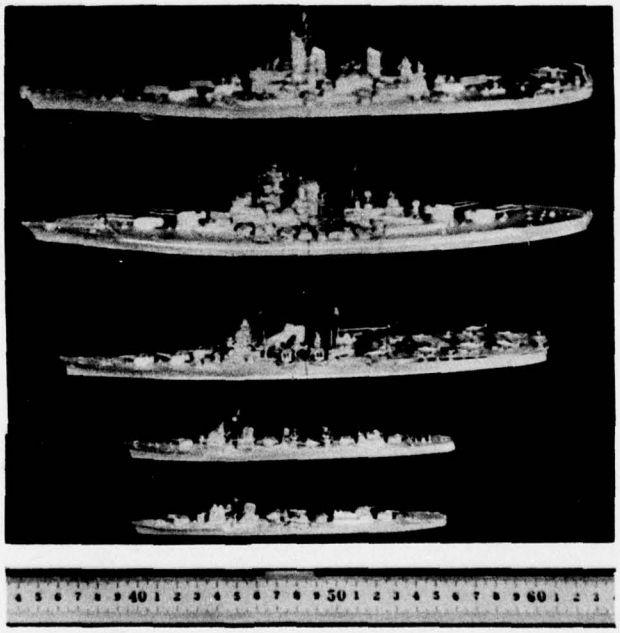

Figure 2. -1/700 scale models.

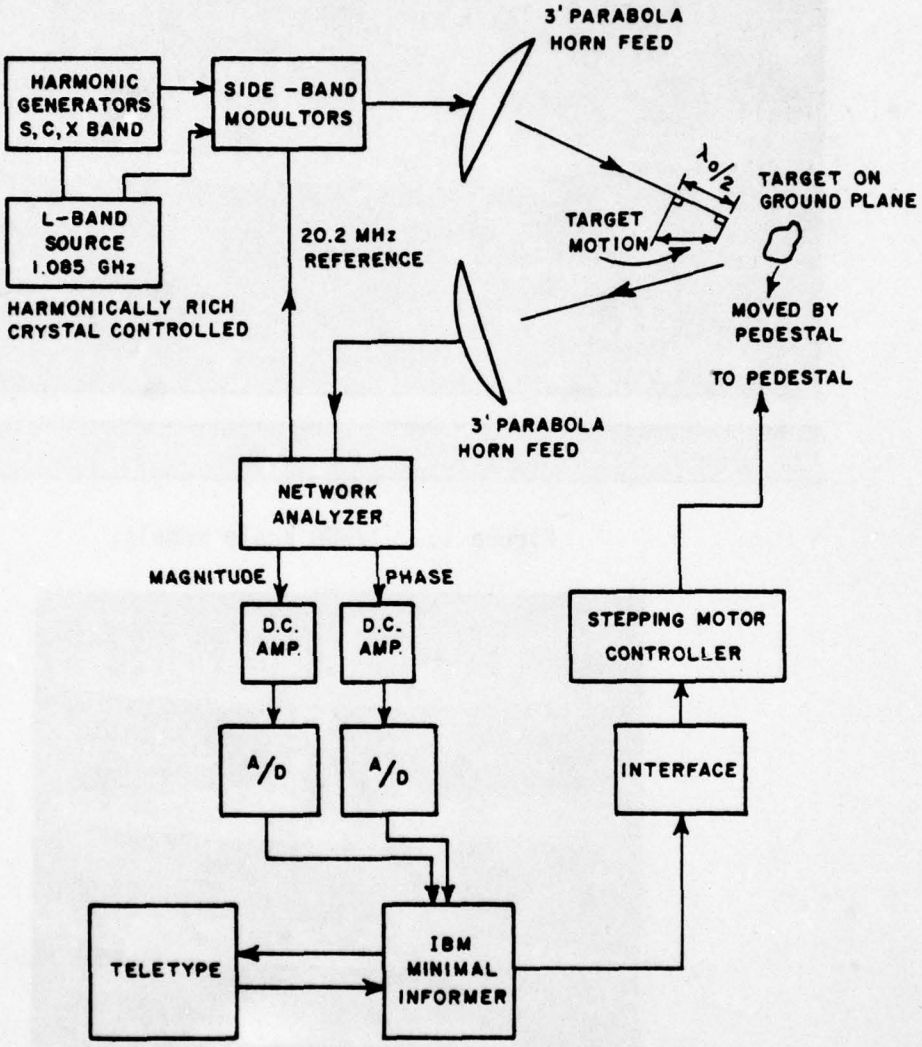

Figure 3--Multifrequency system configuration.

$$U_C = (U_M - NT_M) \times \frac{R_C}{(R_M - NT_M)} \quad . \tag{38}$$

Using this method, ten frequency scattering data (both magnitude and phase) for a given target and aspect can be quickly obtained.

System accuracy is determined by running another target (designated the check target) for which scattering data are known. Acceptable data are usually based on allowable errors of ≈5% in amplitude and ≈10% in phase for the check target. For matched filter responses which alleviate the foldover errors, the 10% phase error limit was relaxed since phase data are not used. For the ground plane range, hemispheres were used for both the reference and check targets. These were modeled as perfectly conducting hemispheres on an infinite perfectly conducting ground plane. A far field source and a far field receiver both having theta (vertical) polarization were assumed. The reference coordinate origin is at the hemisphere center (on the ground plane) with the z-axis perpendicular to the ground plane and the x-axis in the plane bisecting the radar bistatic angle. The hemisphere was then modeled, using image theory, as a sphere with an image transmitting antenna, see Figure 4. A computer program was written to generate the required magnitude and phase data. The magnitude data were output as the square-root of the radar cross section which is proportional to scattered field strength. The phase data are referenced to the center of the hemisphere at its base. It is for this reason that all included ramp response waveforms for the hemispheres appear to start at a maximum which corresponds to the incident plane wave passing through the phase center and also intersecting the greatest cross-sectional area.

One major problem with the present system is violation of the far-field approximation at all but the lowest harmonics. Using a crude $2\,D^2/\lambda$ approximation for the n-th harmonic, the far-field range is approximately

$$r_{ff} = n\left(\frac{2\,D^2}{\lambda_o}\right) \quad . \tag{39}$$

The antennas used are 3 foot parabolas with horn feeds (see Figures 5, 6 and 7). With the fundamental of 1.085 GHz ($\lambda_o \cong 10.88$ inches) this yields:

$$r_{ff} \cong n(19.6 \text{ ft}) \quad . \tag{40}$$

With the present range of about 10 feet it is clear that the targets are not in the far-field. Note that the tenth harmonic would require a range greater than 196 feet - a very difficult requirement. Our purpose, however, is <u>not</u> to produce cross section data. The ship parameters we seek are independent of the excitation and therefore any excitation which produces an extractable transient is sufficient. To

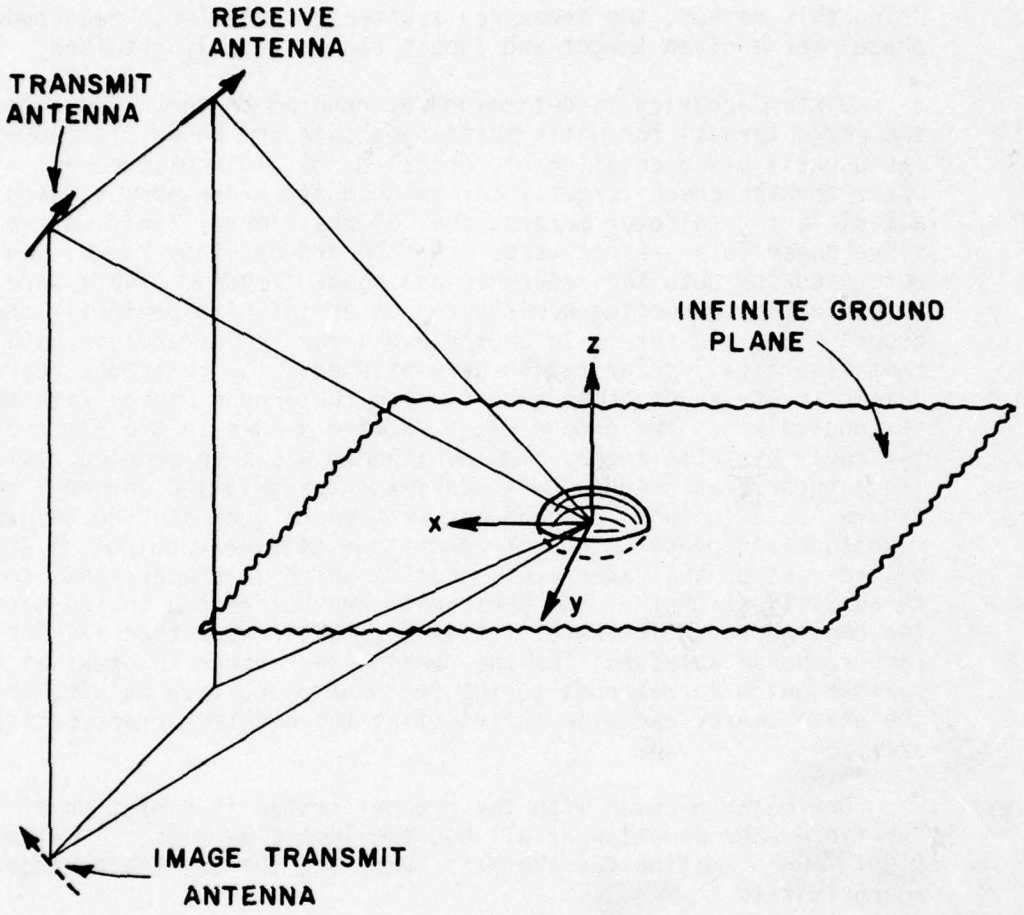

Figure 4. Calibration hemisphere geometry from image theory.

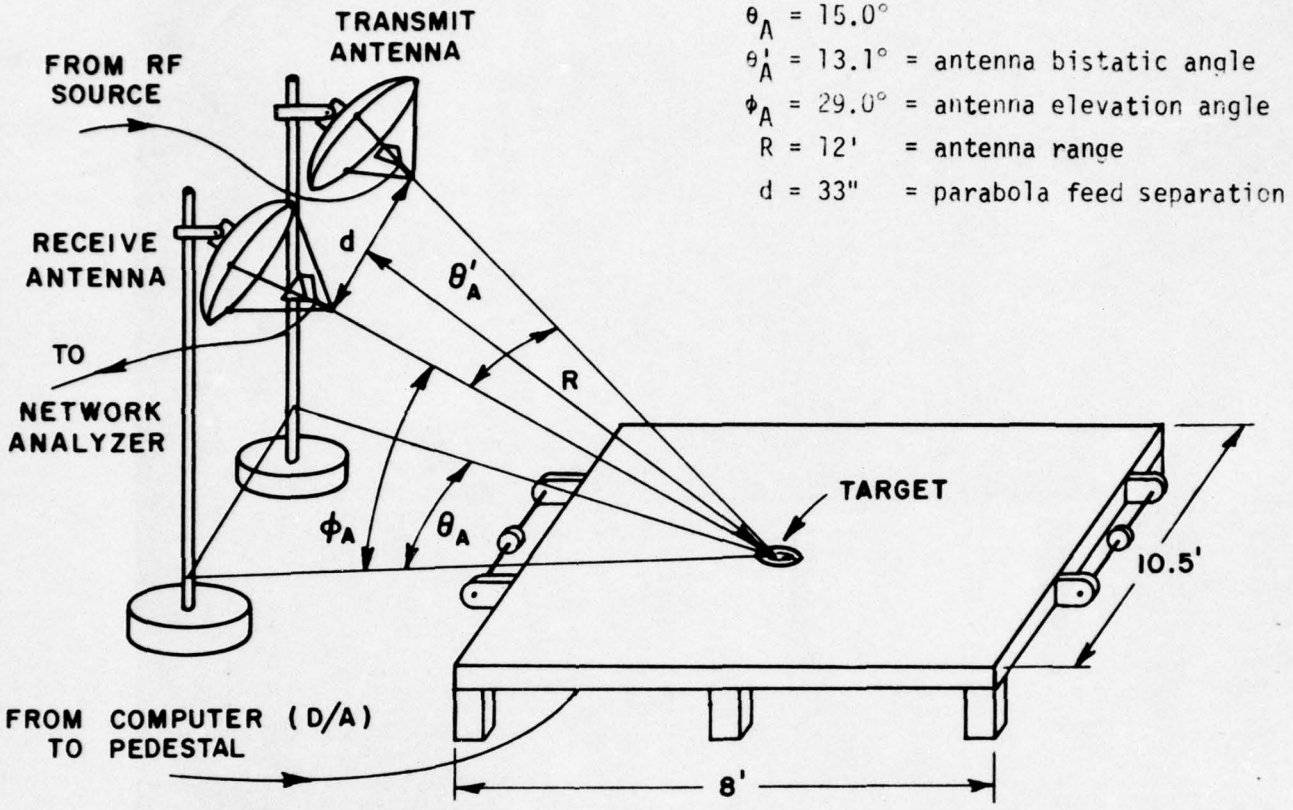

Figure 5. Multifrequency ground plane range geometry.

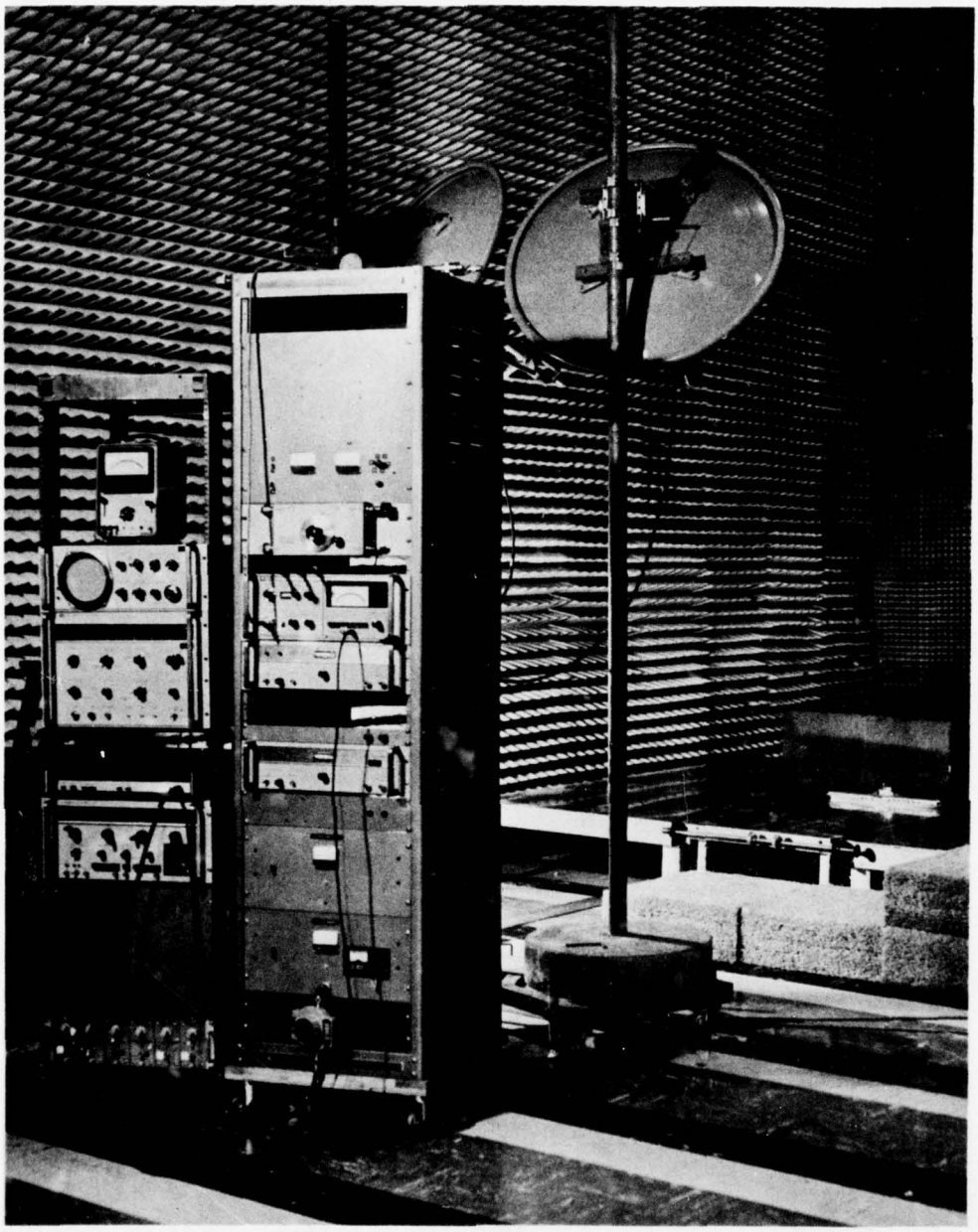

Figure 6. Multi-frequency system with ground plane.

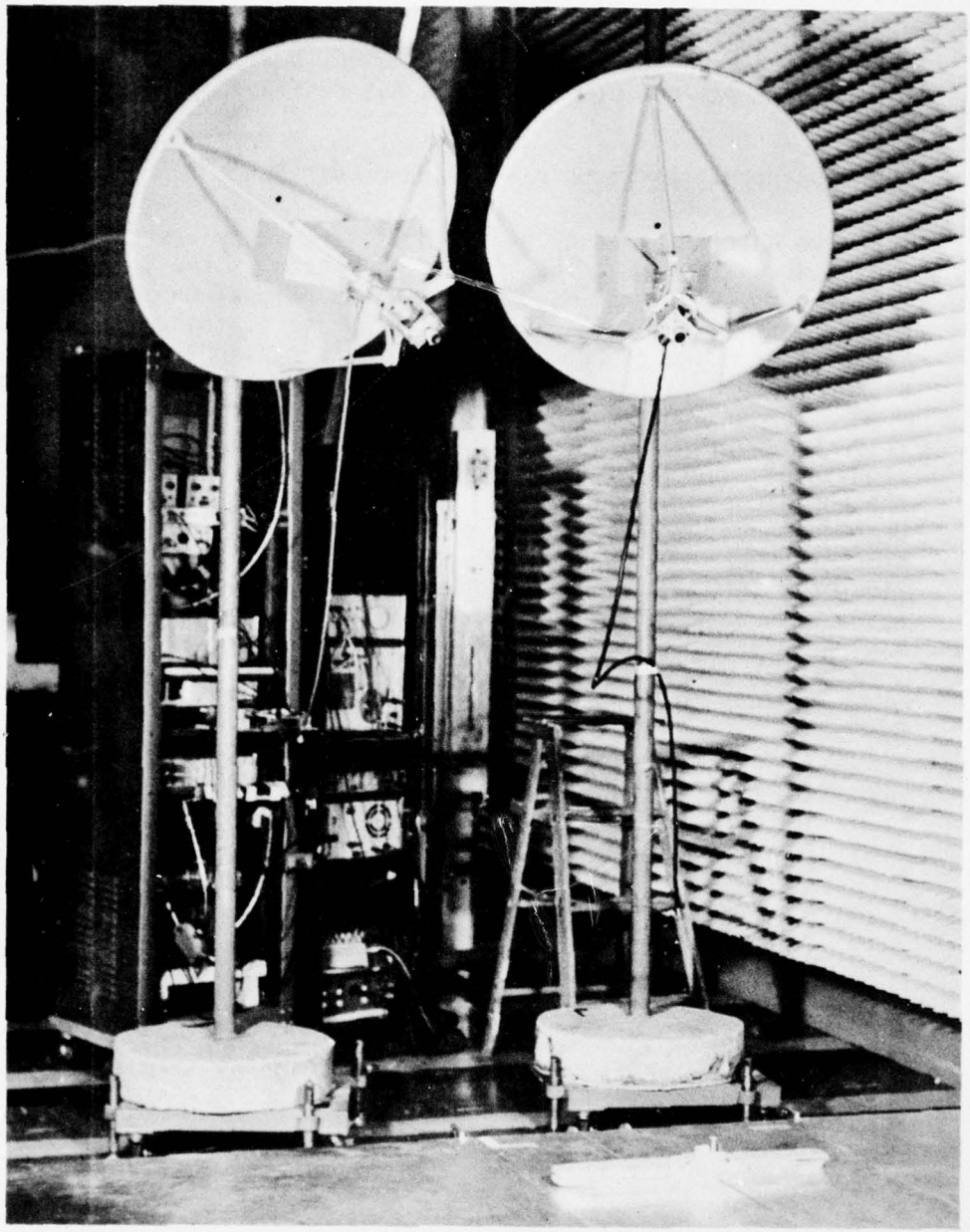

Figure 7. Multi-frequency system with ground plane.

instrument a model range satisfying the above requirements would require major changes including TWT or equivalent amplifiers. This type of expenditure was not planned and is not considered necessary for the program.

V. MEASURED SCATTERING DATA OF NAVAL VESSELS

The data obtained using the Multi-frequency System are given in magnitude-phase form. The unit of magnitude is the square-root of cm^2 yielding cm. Thus the magnitude is proportional to the received electric field strength. The unit of phase is the degree. Phase is measured from the center of the reference hemisphere at its base. As stated elsewhere, the phase data obtained have not been used extensively due to the use of the matched filter step weighted responses. These response waveforms are constructed using a finite cosine series of the magnitudes squared with a $1/n^2$ weighting factor on the n-th term and with the phases set equal to zero. For this reason the phase data have not been included in this report, although they are implicit in the synthetic ramp responses. The amplitude data are presented in graphical form in Figures 8 through 37. For comparison an interpolated spectrum is given with each set of data. It has been assumed that the spectra have zero value at dc and the eleventh harmonic. This grossly simulates the lowpass nature of our finite cosine series and Rayleigh scattering as the frequency approaches zero. The interpolation process is given by

$$|G(j\omega)|^2 = \frac{\sum_{n=0}^{N} |C'_N\, G(jn\omega_o)|^2 \left[\frac{\sin(\frac{\omega}{\omega_o} - n)\pi}{(\frac{\omega}{\omega_o} - n)\pi} + \frac{\sin(\frac{\omega}{\omega_o} + n)\pi}{(\frac{\omega}{\omega_o} + n)\pi} \right]}{\sum_{n=0}^{N} C'_N \left[\frac{\sin(\frac{\omega}{\omega_o} - n)\pi}{(\frac{\omega}{\omega_o} - n)\pi} + \frac{\sin(\frac{\omega}{\omega_o} + n)\pi}{(\frac{\omega}{\omega_o} + n)\pi} \right]}$$

$$N = 11 \qquad \text{for ten harmonics} \tag{41}$$

where $G(jn\omega_o)$ is the complex scattering coefficient at the n-th harmonic and the C'_n are modified impulse coefficients

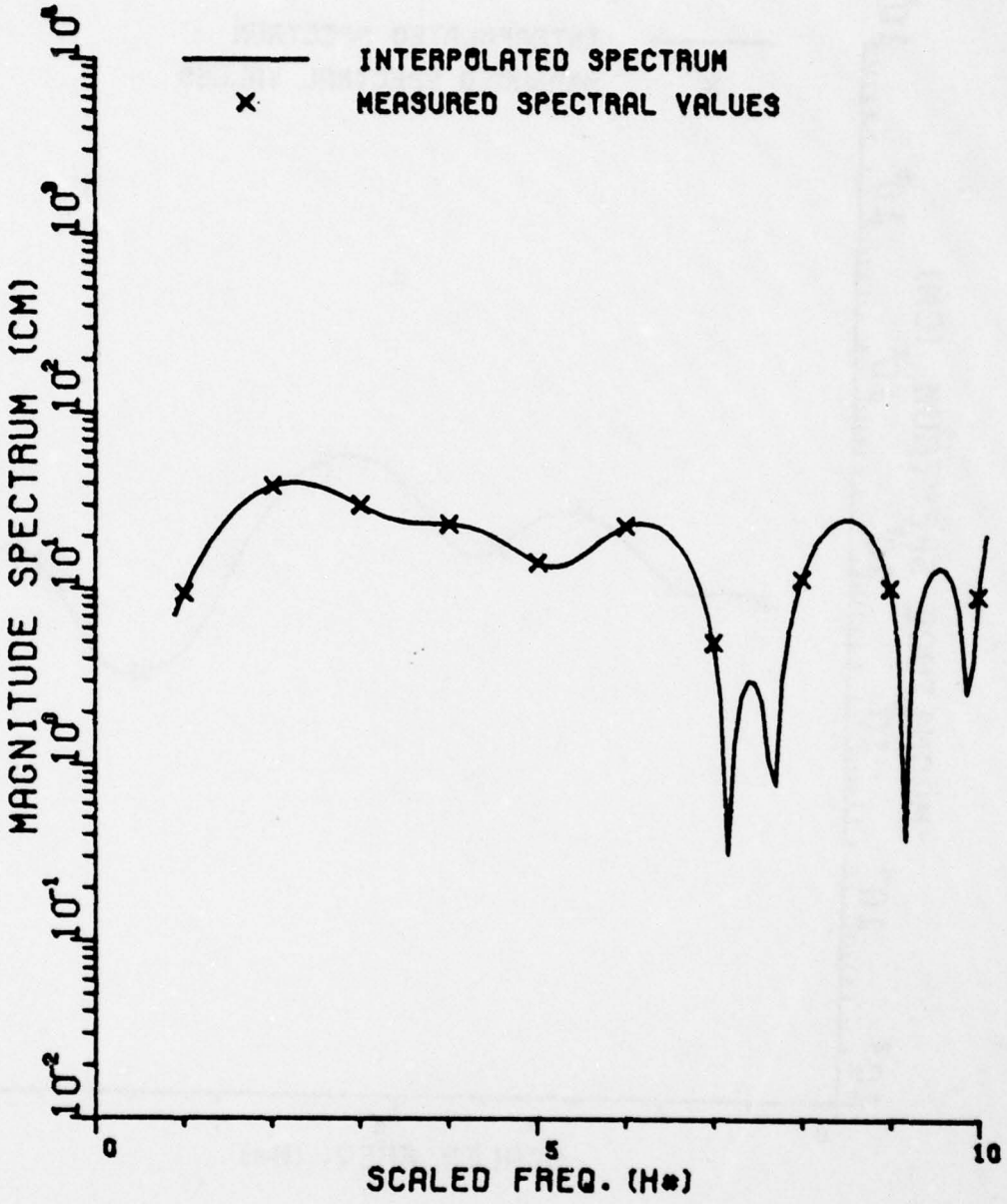

MIDWAY (1/500) -BOW ON

Figure 8

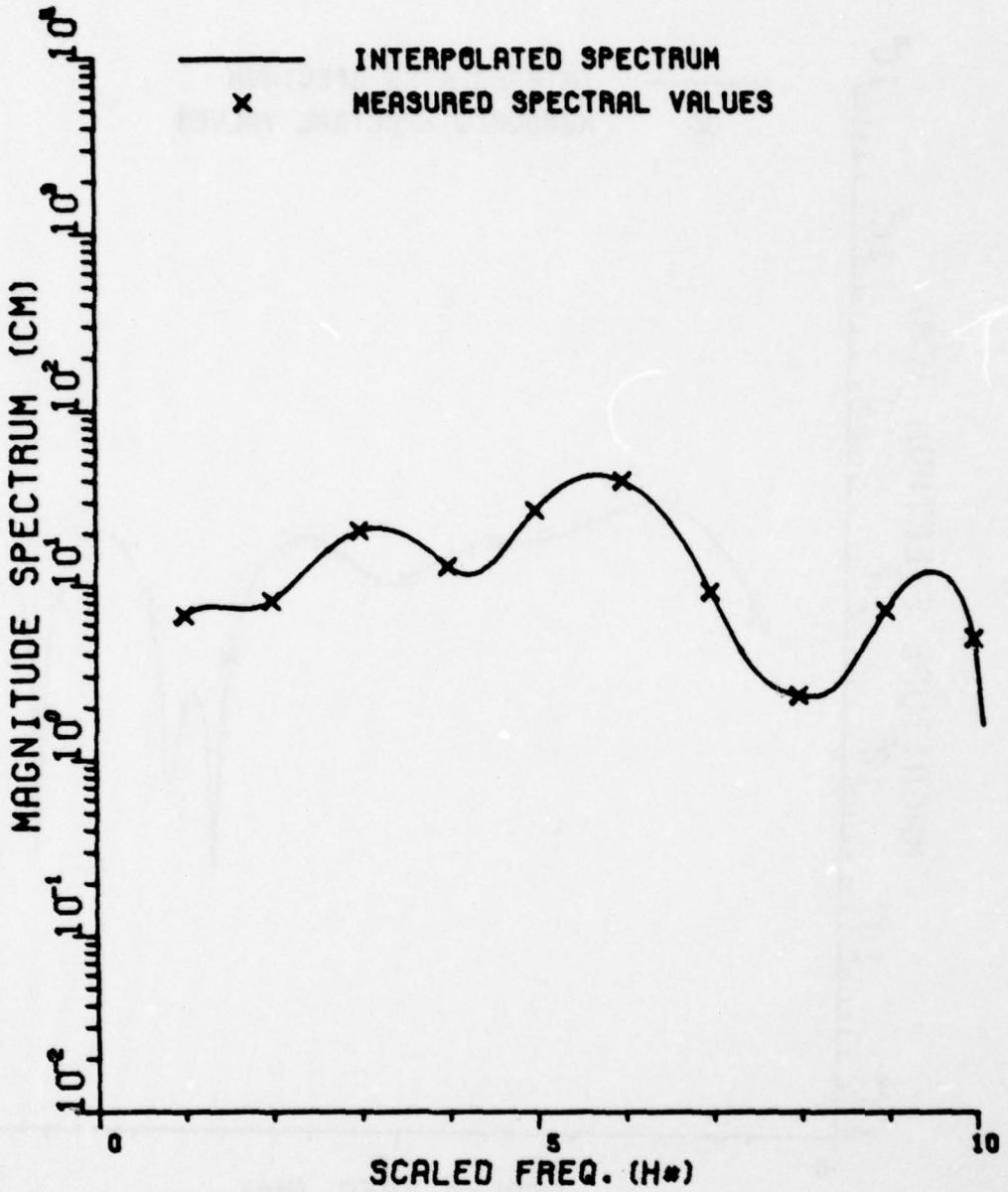

MIDWAY (1/500) -STERN

Figure 9

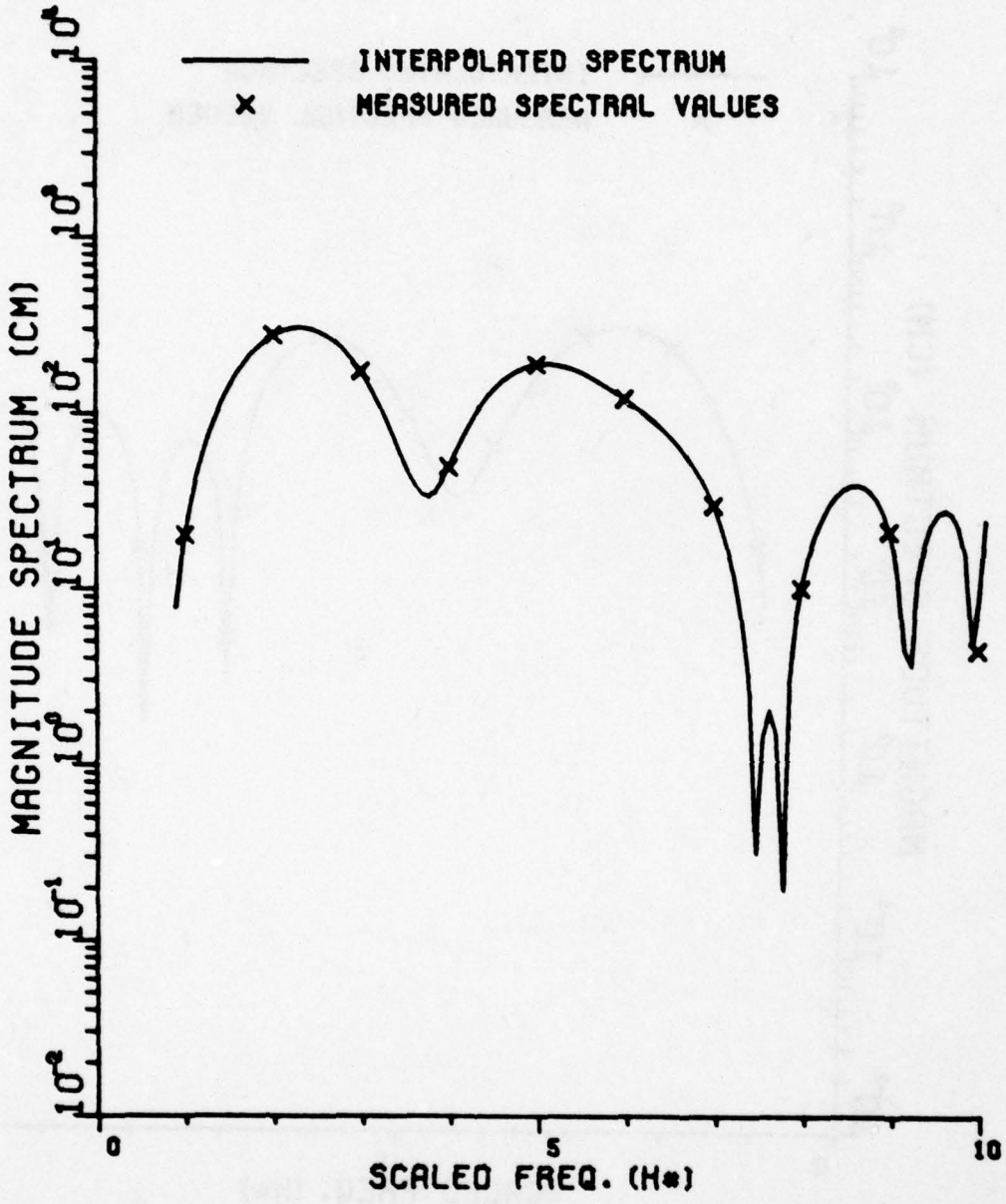
INTERPOLATED SPECTRUM
MEASURED SPECTRAL VALUES
MAGNITUDE SPECTRUM (CM)
10^{-2}
10^{-1}
10^{0}
10^{1}
10^{2}
10^{3}
10^{4}
0
5
10
SCALED FREQ. (H*)
MIDWAY (1/500) -STARBOARD

Figure 10

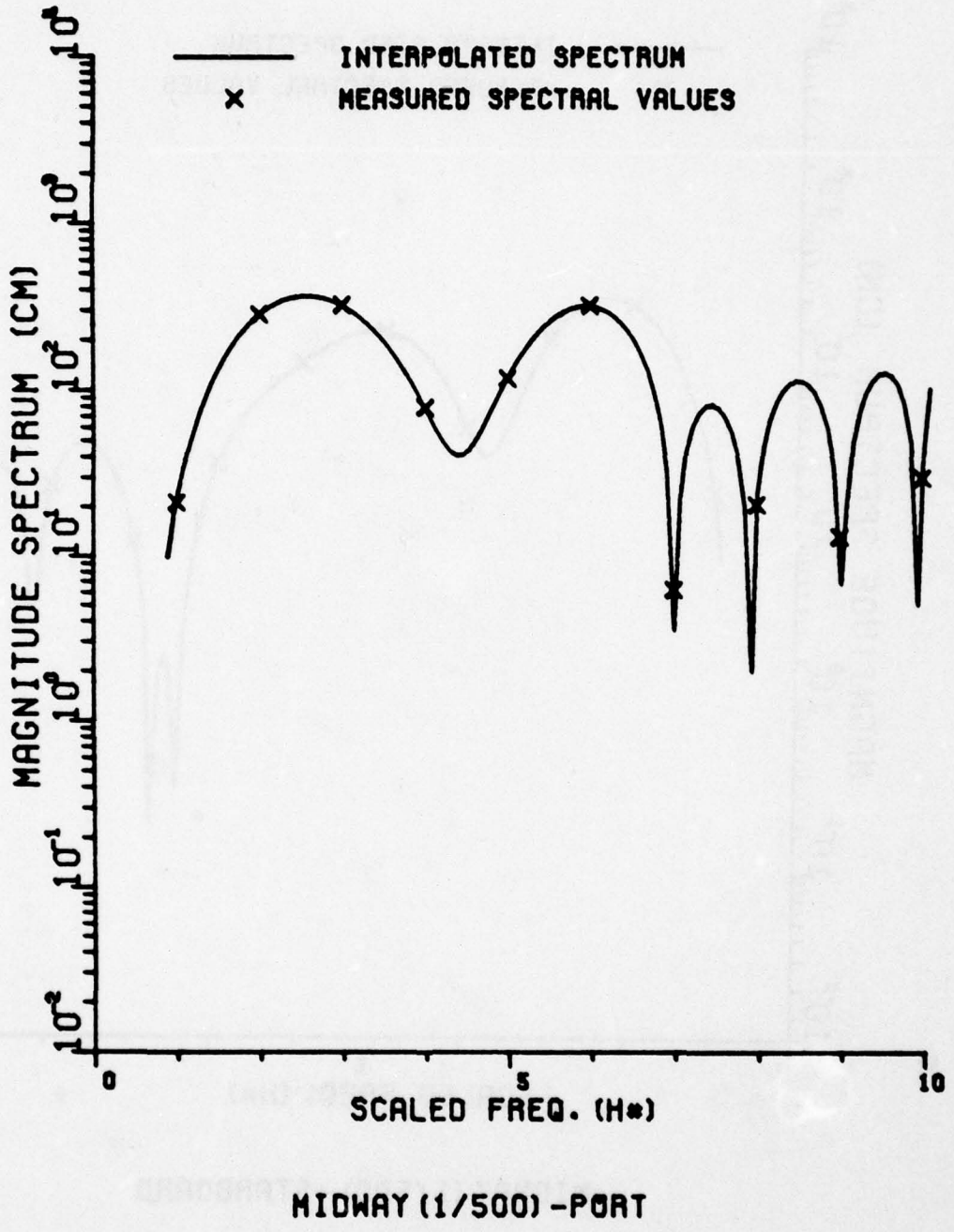
INTERPOLATED SPECTRUM
MEASURED SPECTRAL VALUES
MAGNITUDE SPECTRUM (CM)
10^{2}
10^{1}
10^{0}
10^{1}
10^{2}
10^{3}
10^{4}
0
5
10
SCALED FREQ. (H*)
MIDWAY (1/500) -PORT

Figure 11

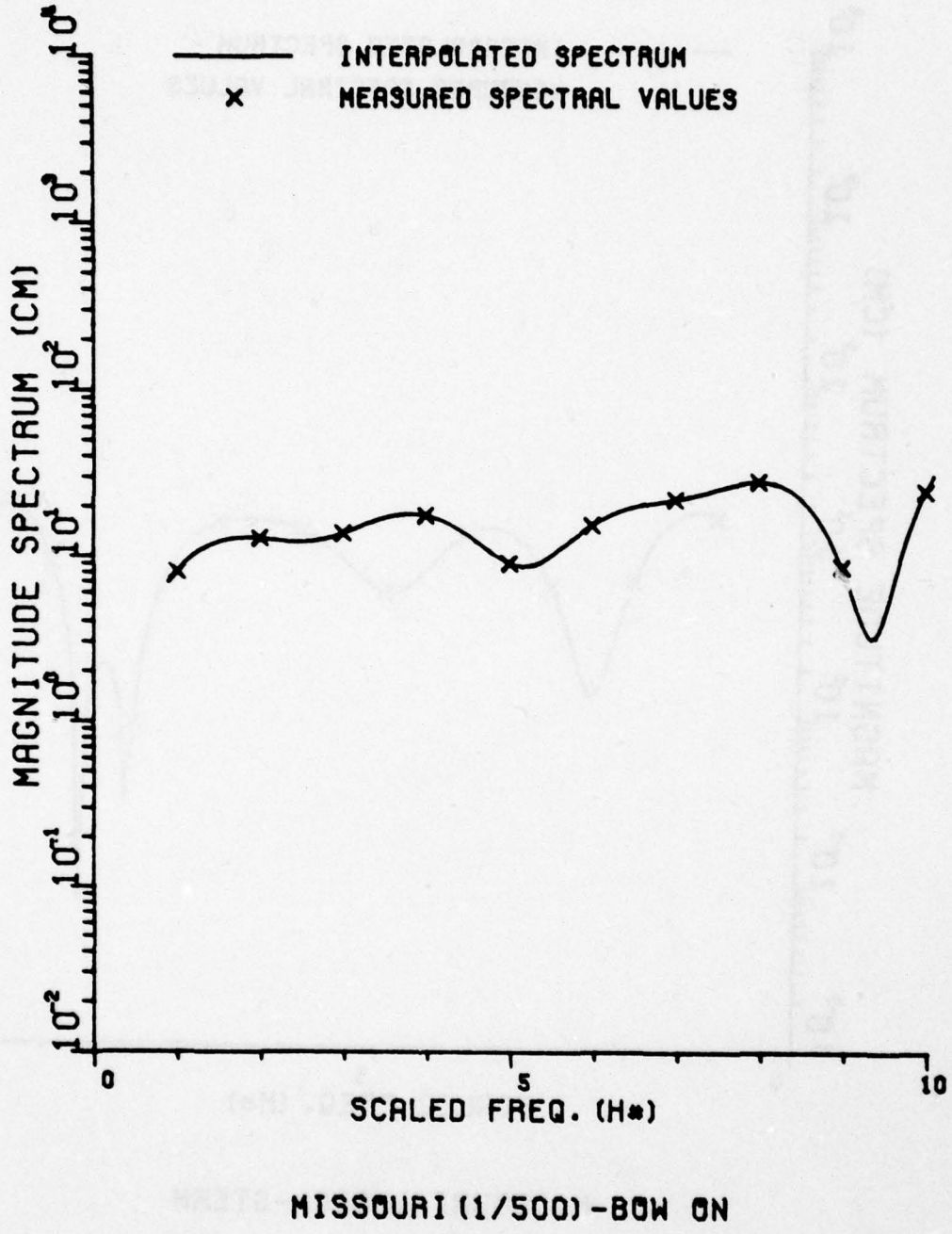

MISSOURI (1/500) -BOW ON

Figure 12

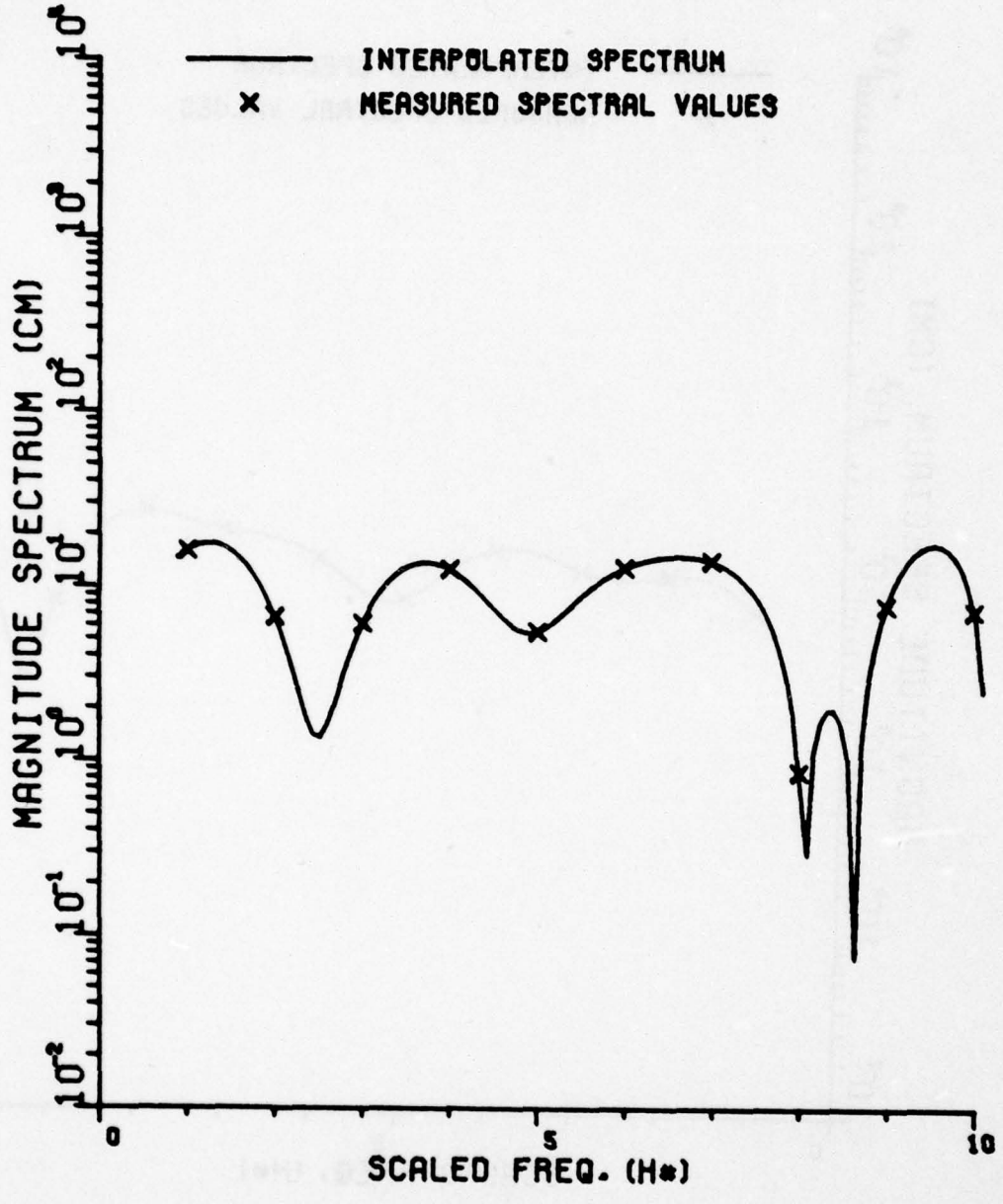
INTERPOLATED SPECTRUM
MEASURED SPECTRAL VALUES
MAGNITUDE SPECTRUM (CM)
10^{-2}
10^{-1}
10^{0}
10^{1}
10^{2}
10^{3}
10^{4}
0
5
10
SCALED FREQ. (H*)
MISSOURI (1/500) -STERN

Figure 13

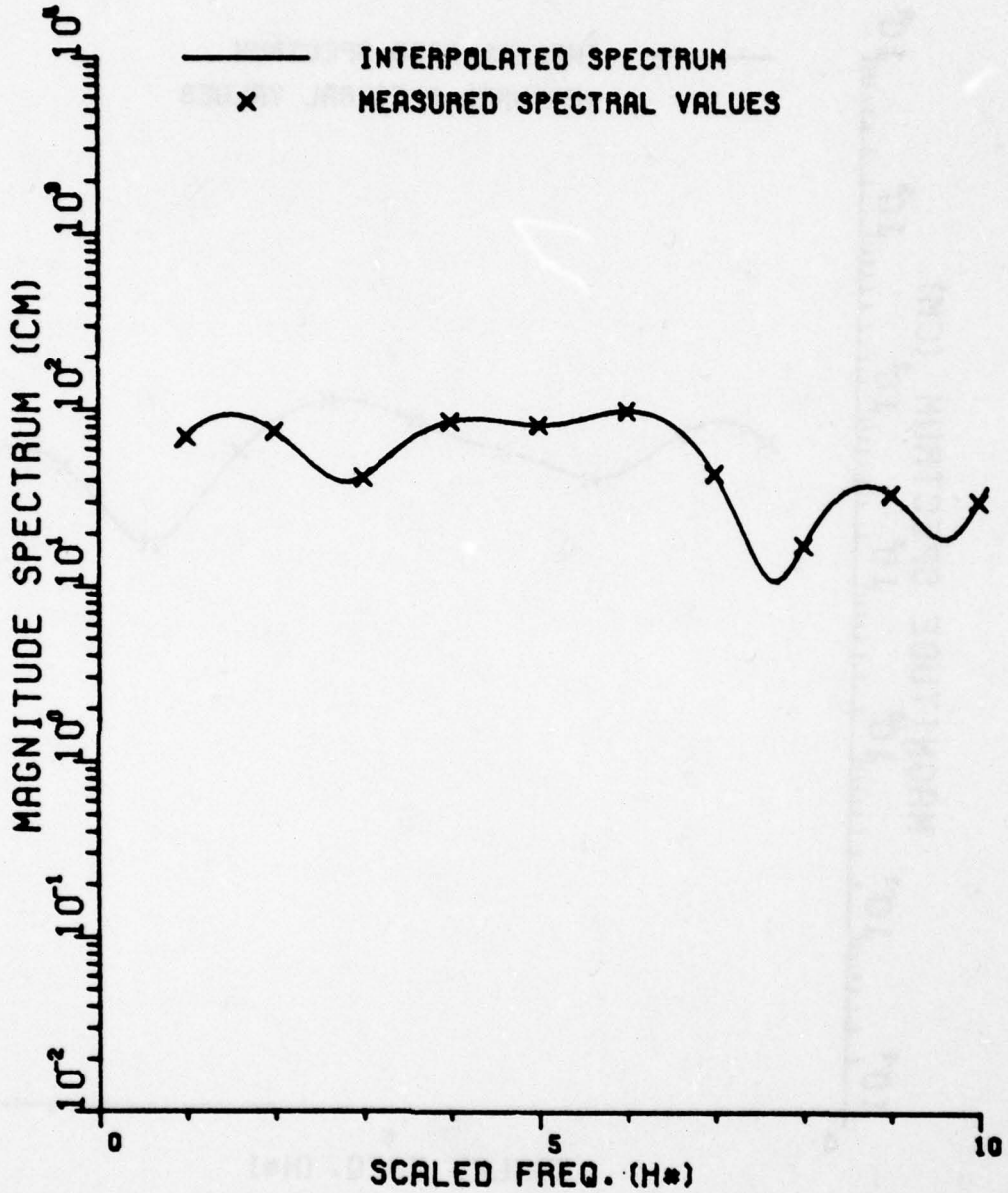

MISSOURI (1/500) -STARBOARD

Figure 14

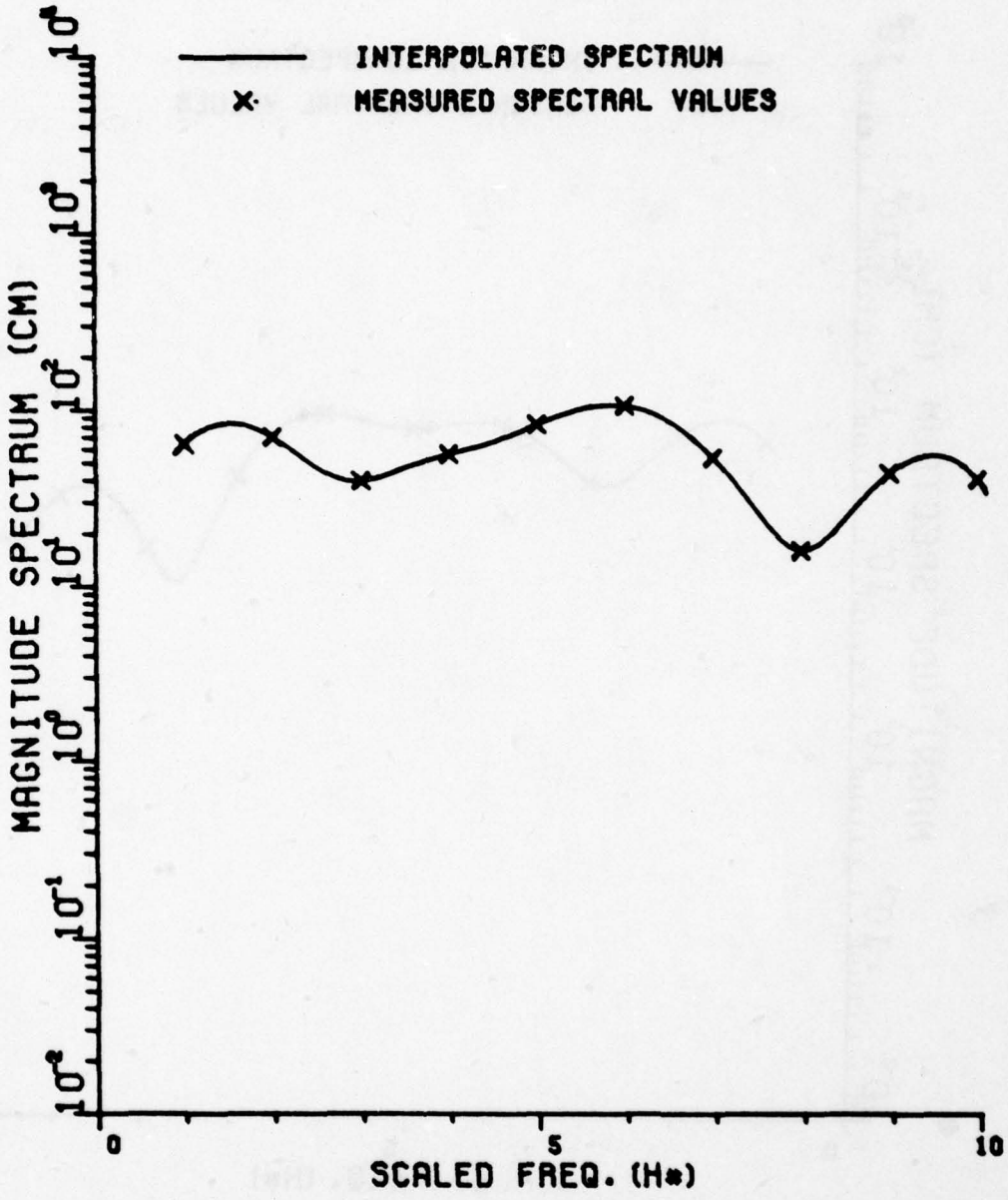

MISSOURI (1/500) -PORT

Figure 15

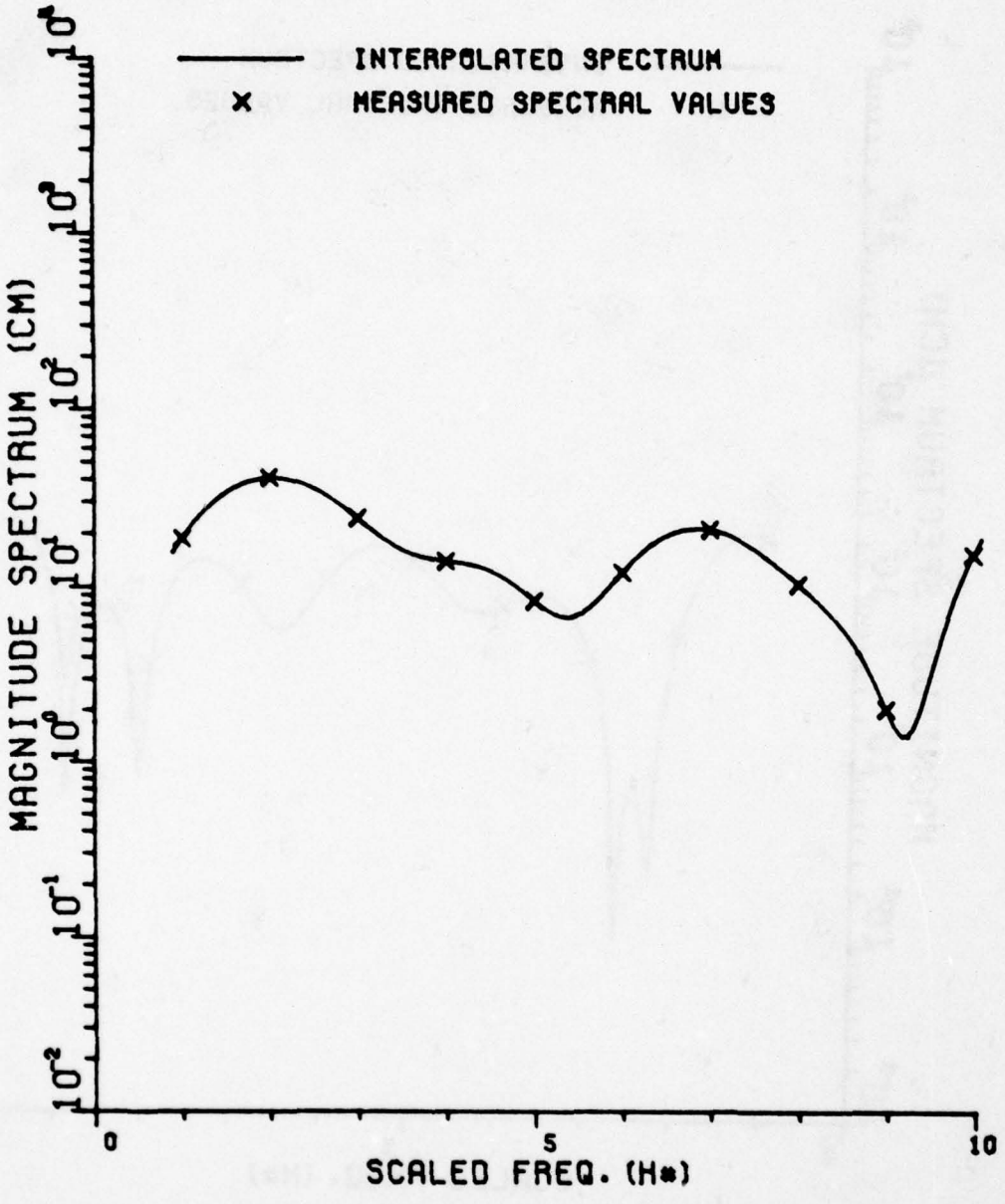
INTERPOLATED SPECTRUM
MEASURED SPECTRAL VALUES
MAGNITUDE SPECTRUM (CM)
10^{-2}
10^{-1}
10^{0}
10^{1}
10^{2}
10^{3}
10^{4}
0
5
10
SCALED FREQ. (H*)
SVERDLOV (1/500) -BOW ON

Figure 16

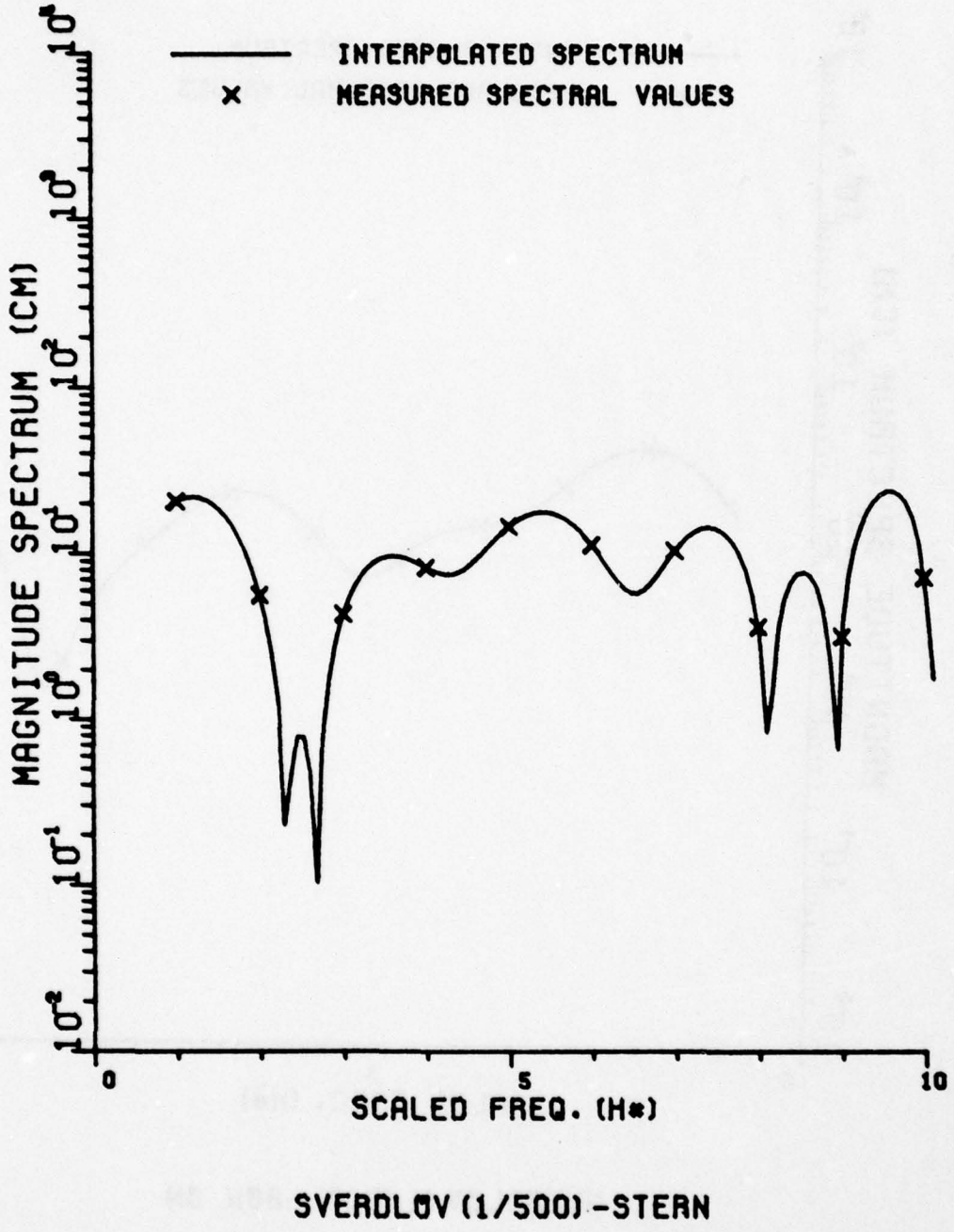
INTERPOLATED SPECTRUM
MEASURED SPECTRAL VALUES
MAGNITUDE SPECTRUM (CM)
10^{-2}
10^{-1}
10^{0}
10^{1}
10^{2}
10^{3}
10^{4}
0
5
10
SCALED FREQ. (H*)
SVERDLOV (1/500) -STERN

Figure 17

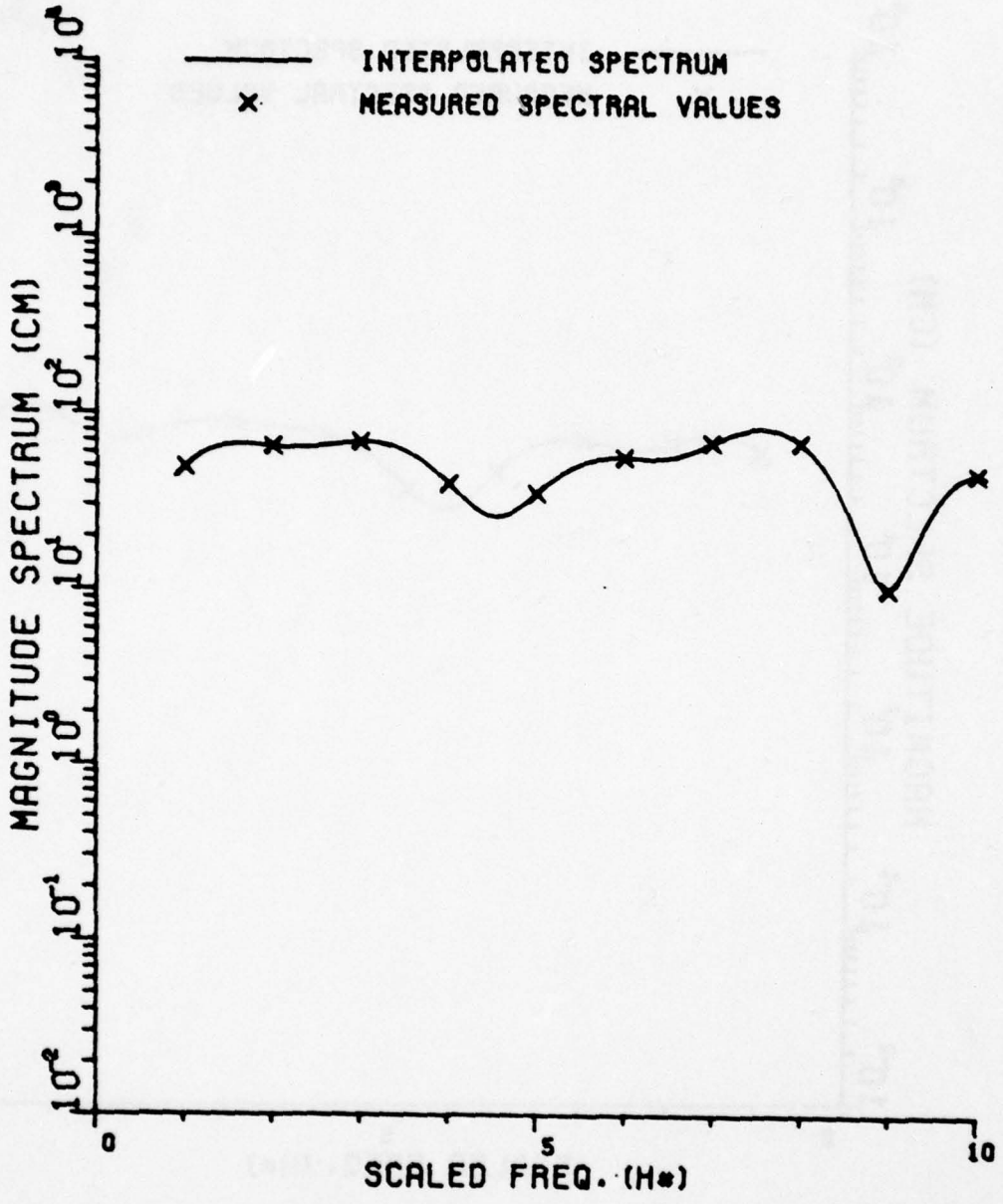

SVERDLOV (1/500) -STARBOARD

Figure 18

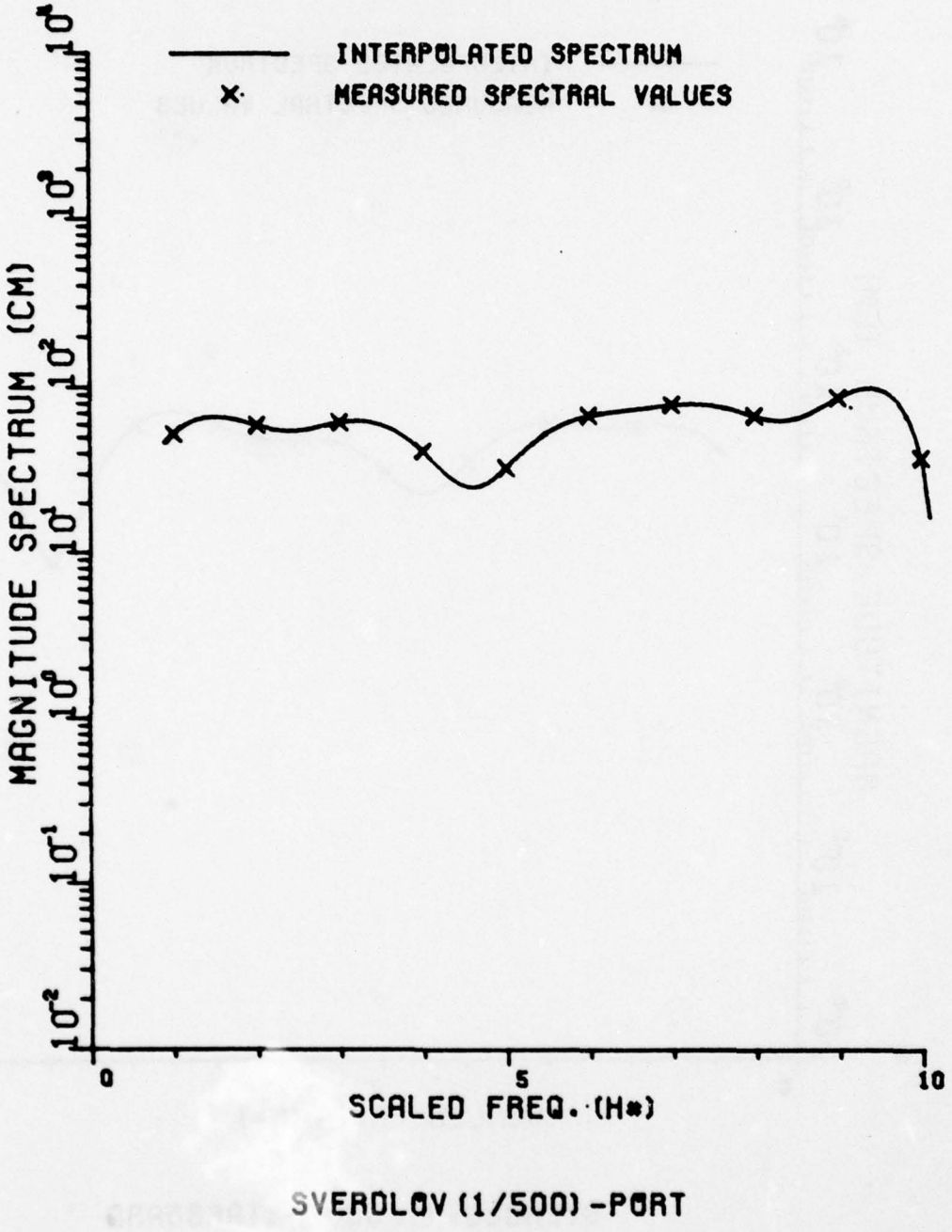
INTERPOLATED SPECTRUM
MEASURED SPECTRAL VALUES
MAGNITUDE SPECTRUM (CM)
10^{-2}
10^{-1}
10^{0}
10^{1}
10^{2}
10^{3}
10^{4}
0
5
10
SCALED FREQ. (H*)
SVERDLOV (1/500) -PORT

Figure 19

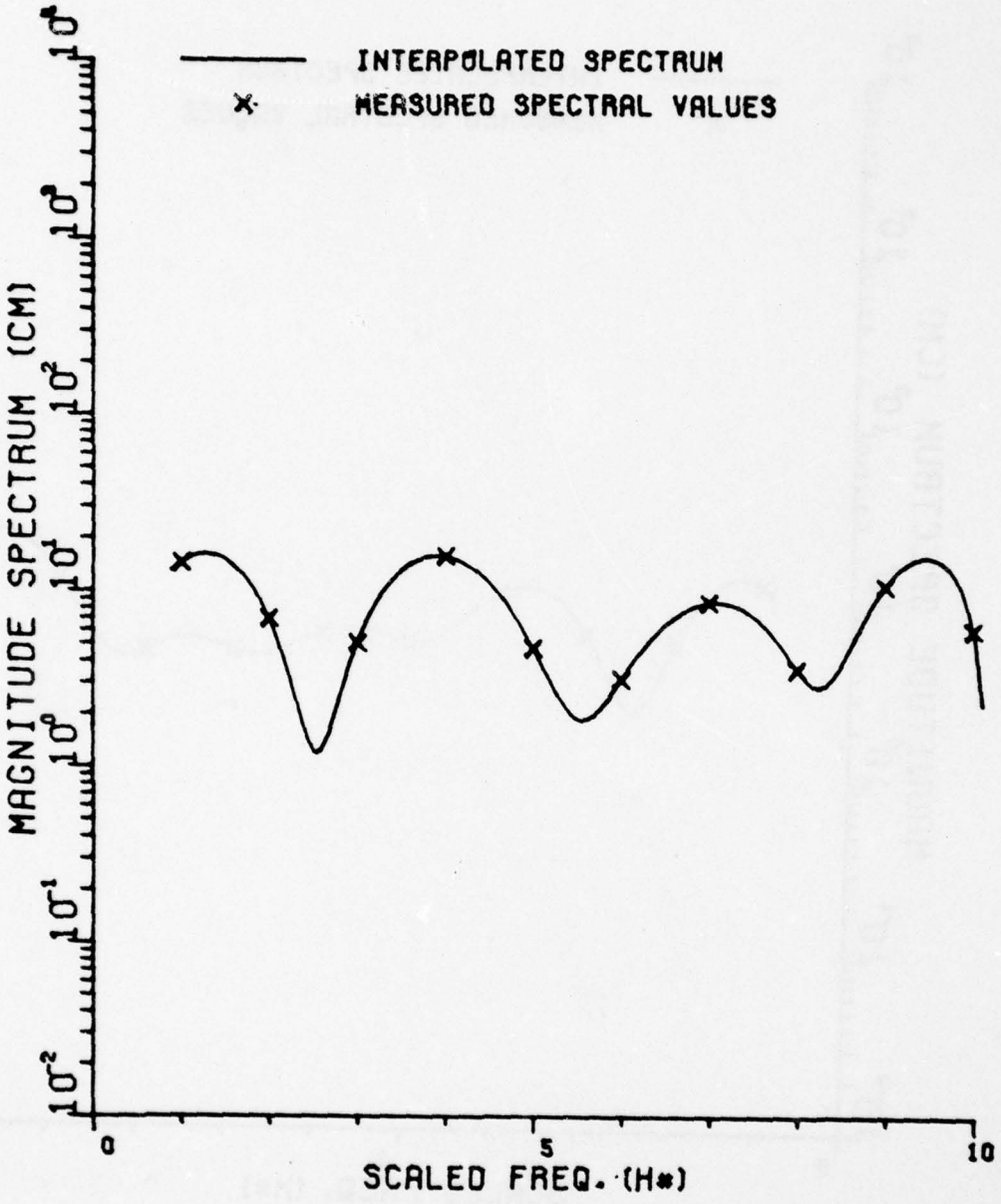

MISSOURI (1/700) -BOW ON

Figure 20

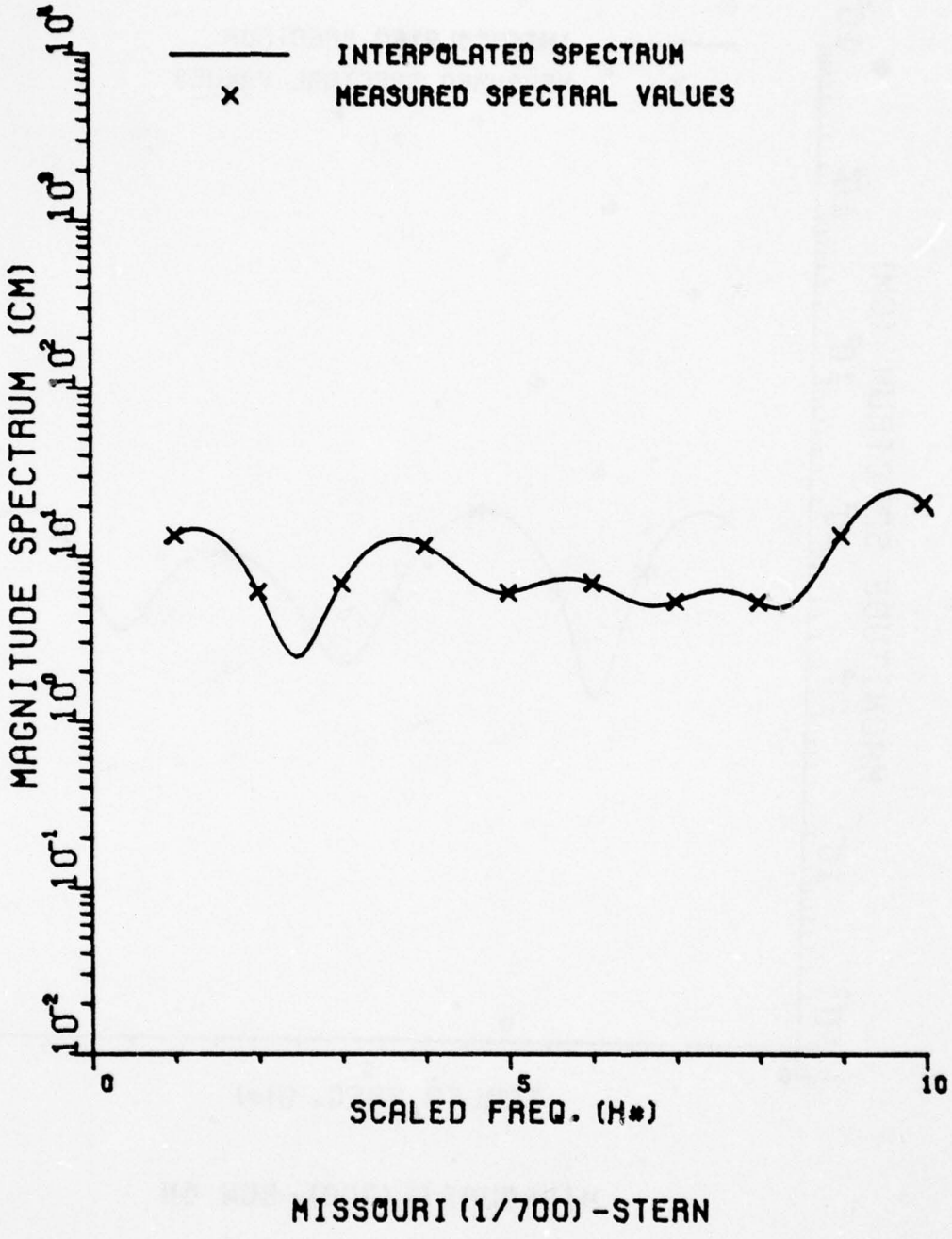

MISSOURI (1/700) -STERN

Figure 21

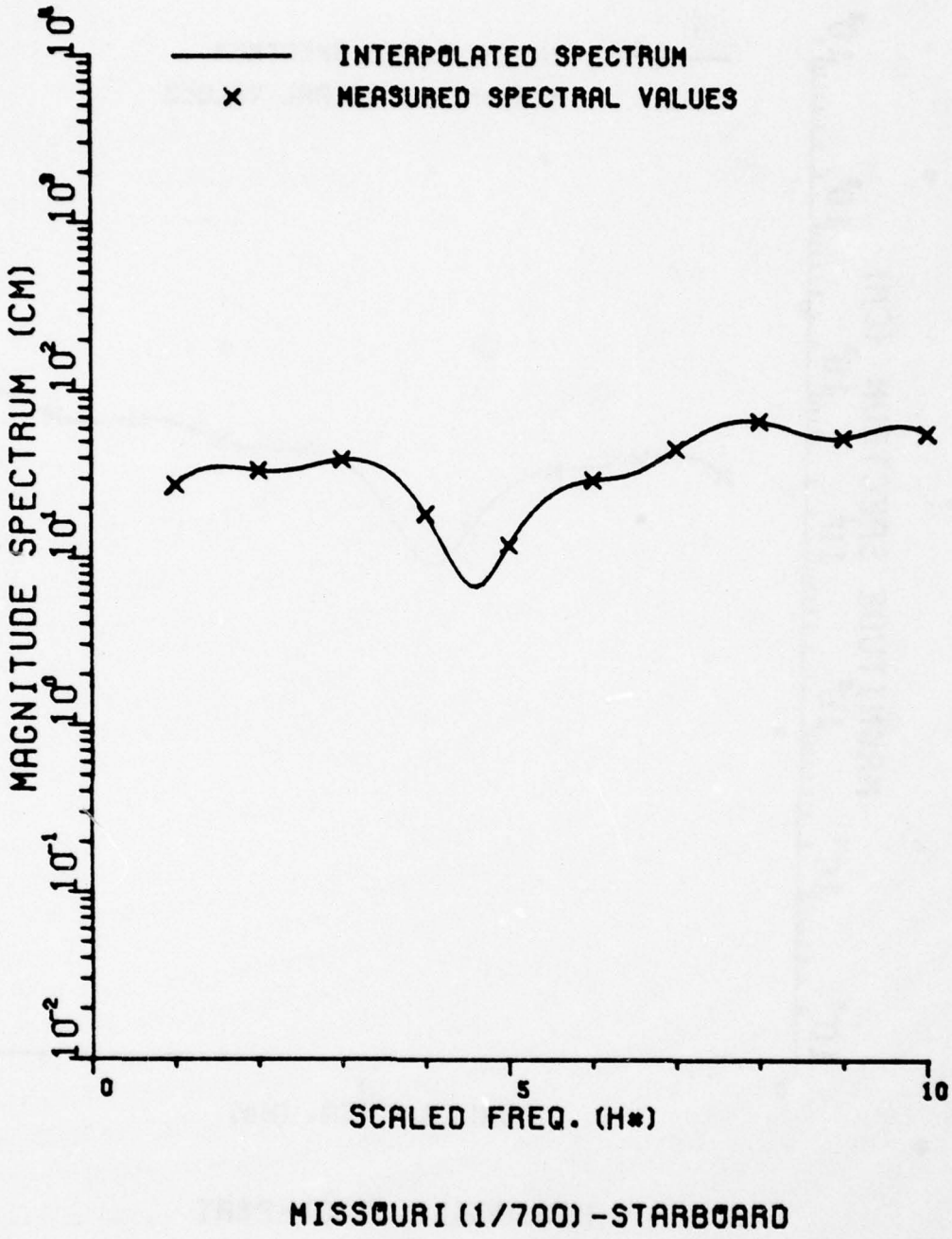
INTERPOLATED SPECTRUM
MEASURED SPECTRAL VALUES
MAGNITUDE SPECTRUM (CM)
10^{-2}
10^{-1}
10^{0}
10^{1}
10^{2}
10^{3}
10^{4}
0
5
10
SCALED FREQ. (H*)
MISSOURI (1/700) -STARBOARD

Figure 22

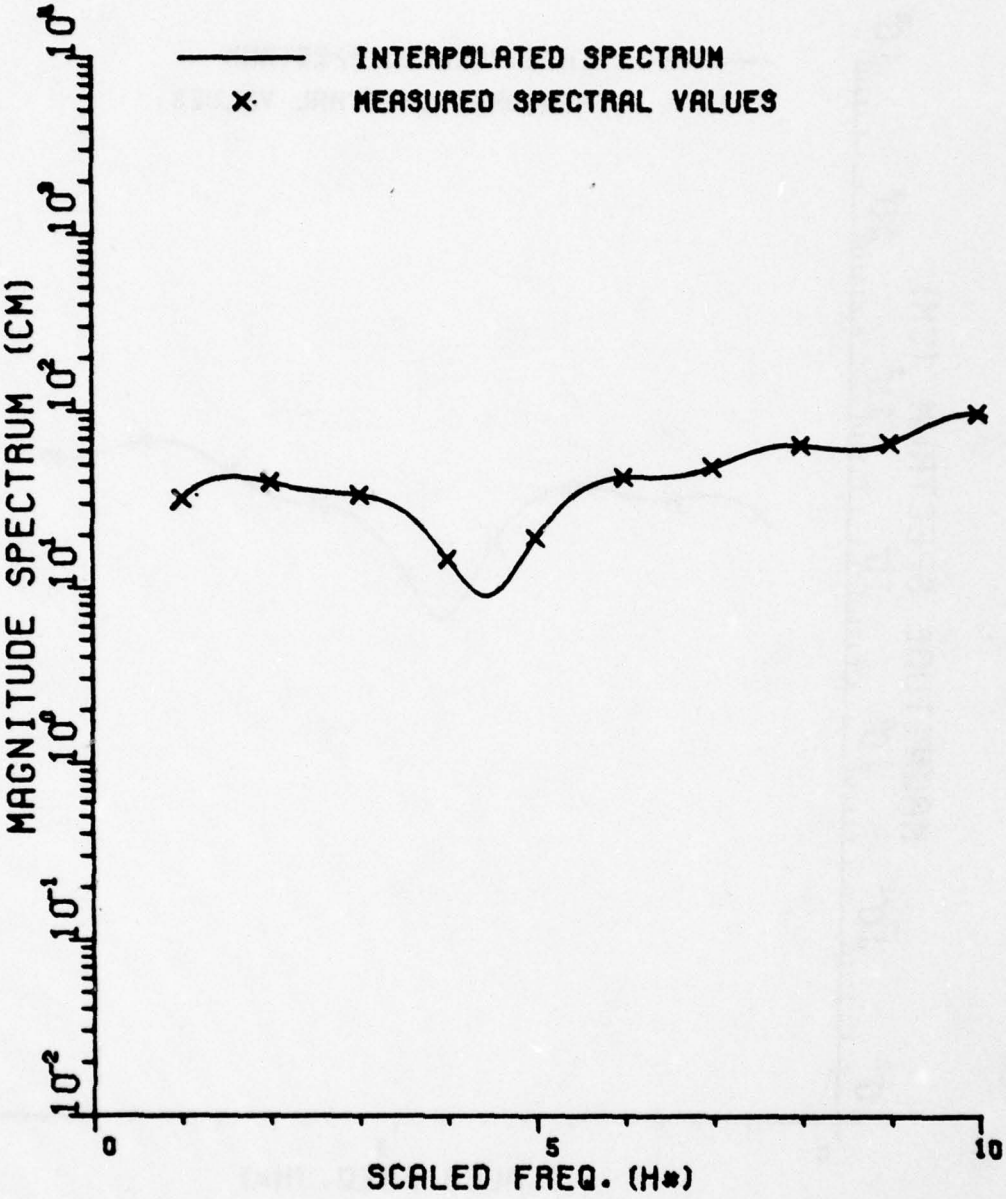

MISSOURI (1/700) -PORT

Figure 23

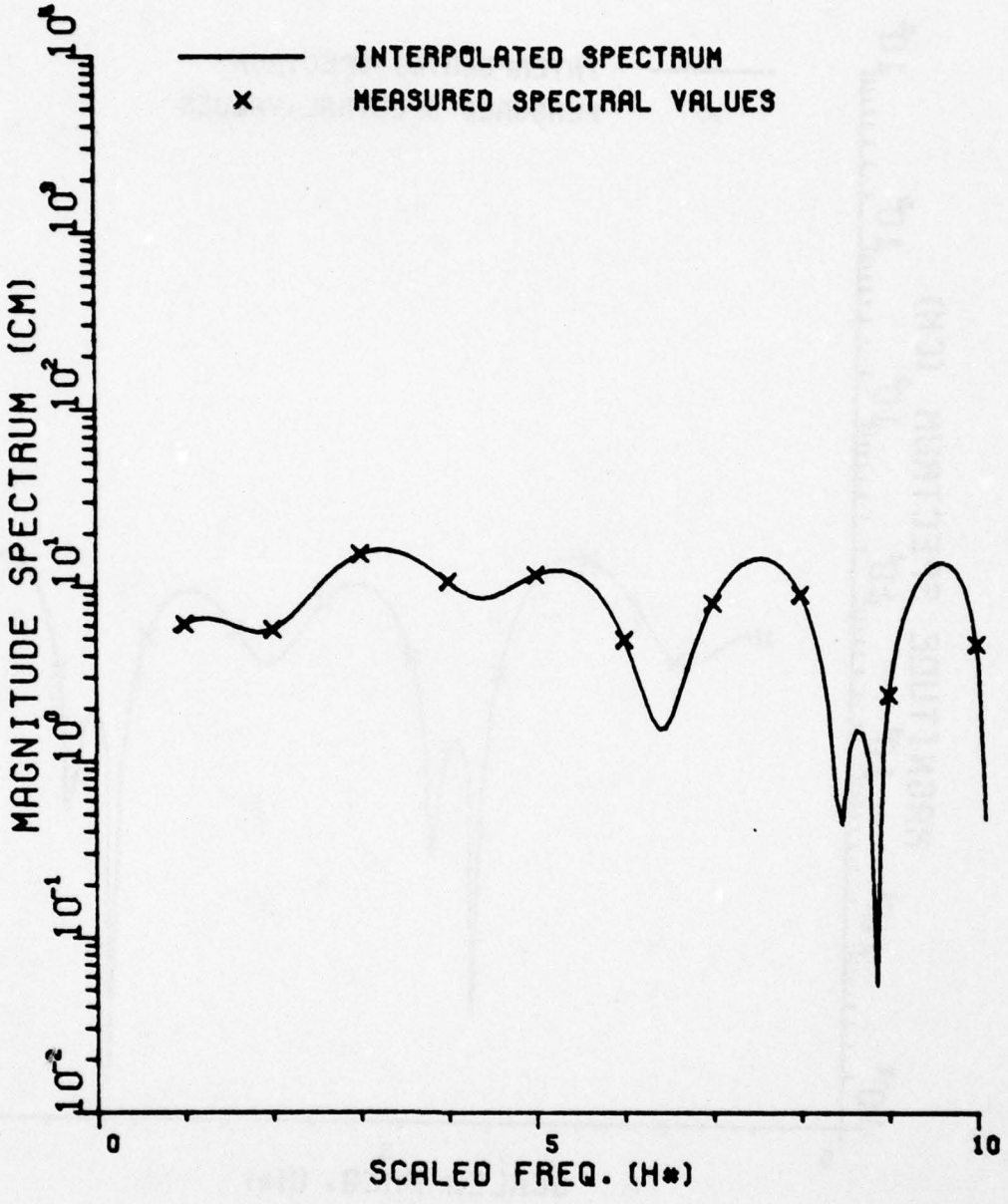

BISMARK (1/700) -BOW ON

Figure 24

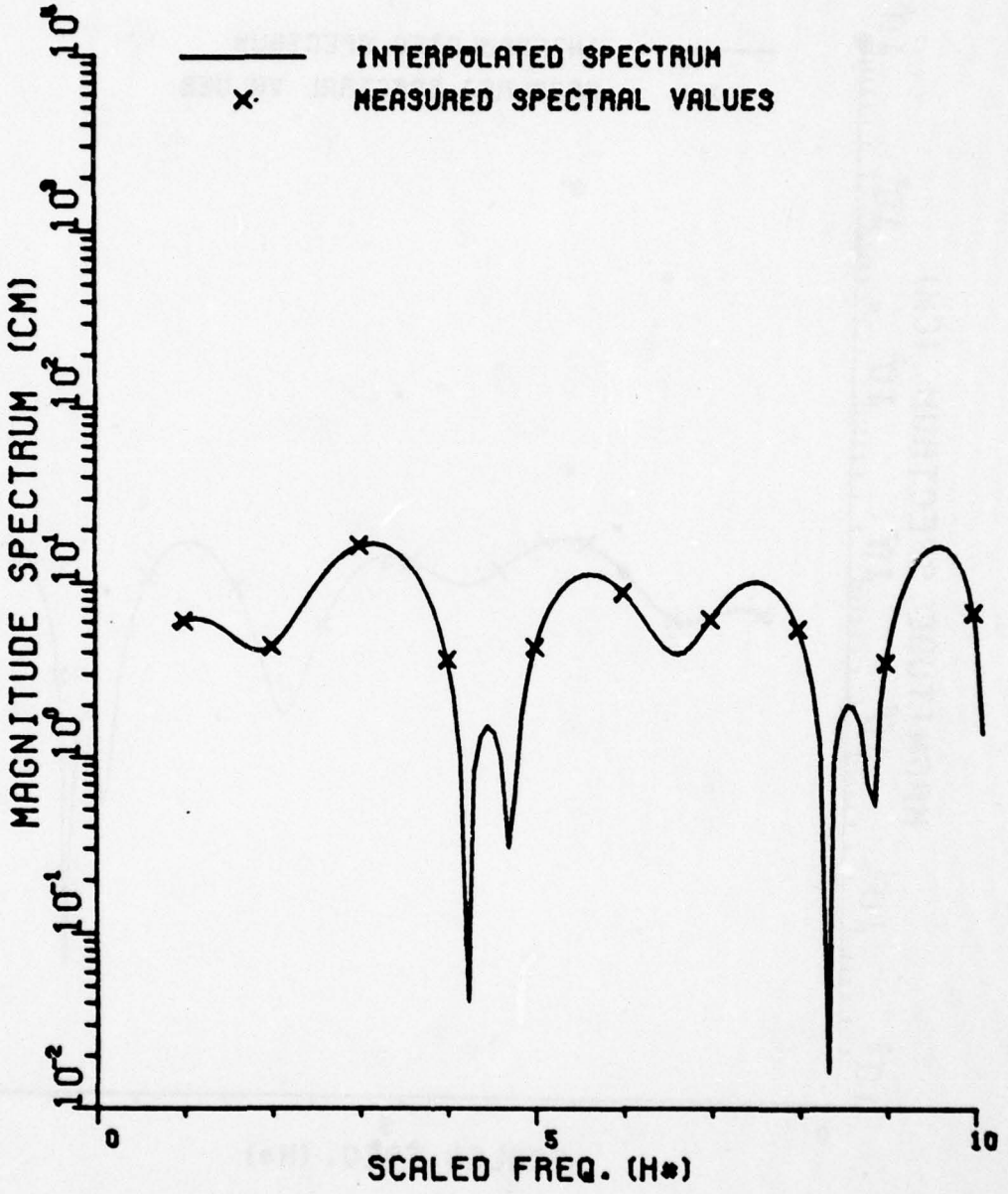

BISMARK (1/700) -STERN

Figure 25

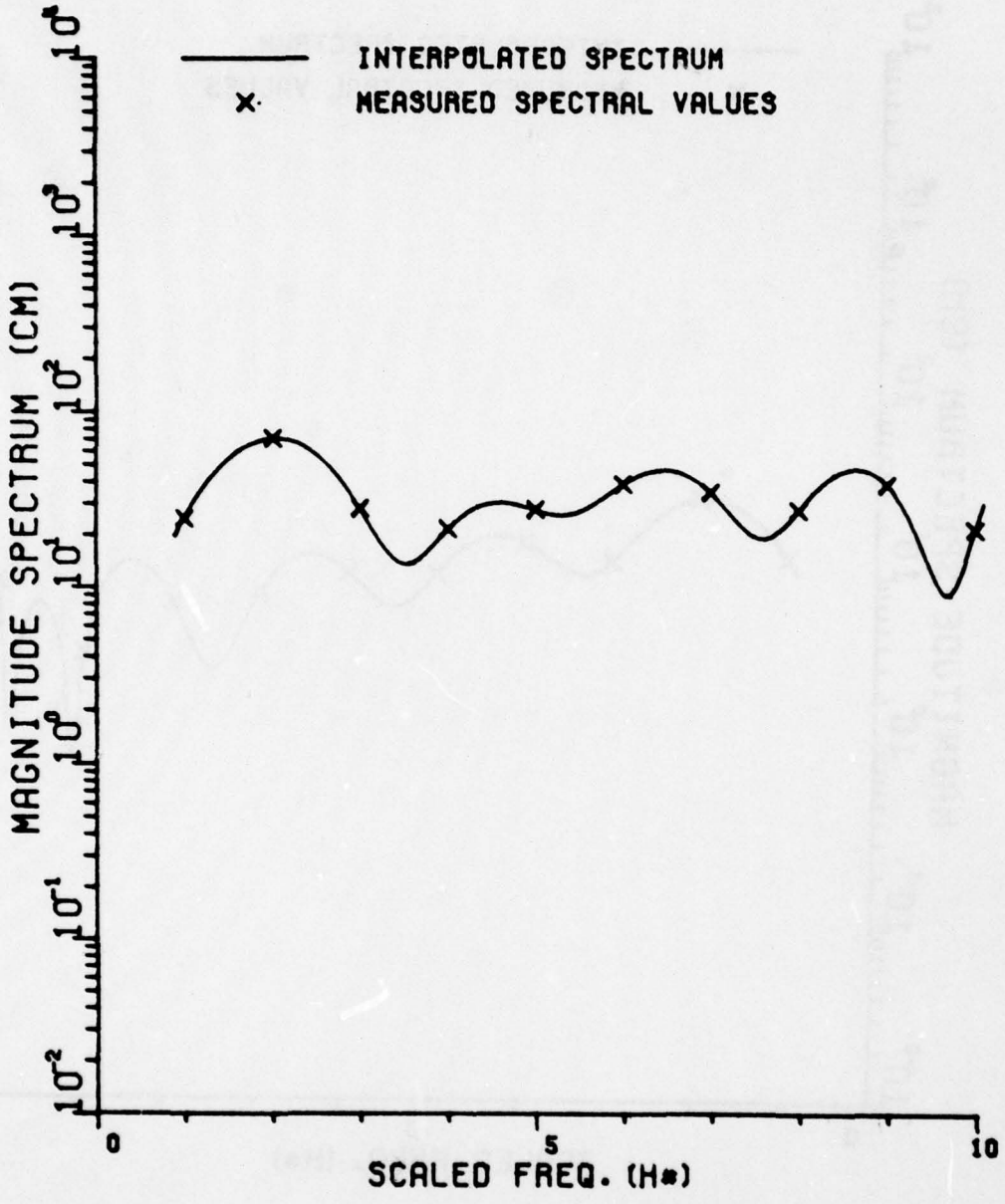
INTERPOLATED SPECTRUM
MEASURED SPECTRAL VALUES
MAGNITUDE SPECTRUM (CM)
10^{2}
10^{1}
10^{0}
10^{1}
10^{2}
10^{3}
10^{4}
0
5
10
SCALED FREQ. (H*)
BISMARK (1/700) -STARBOARD

Figure 26

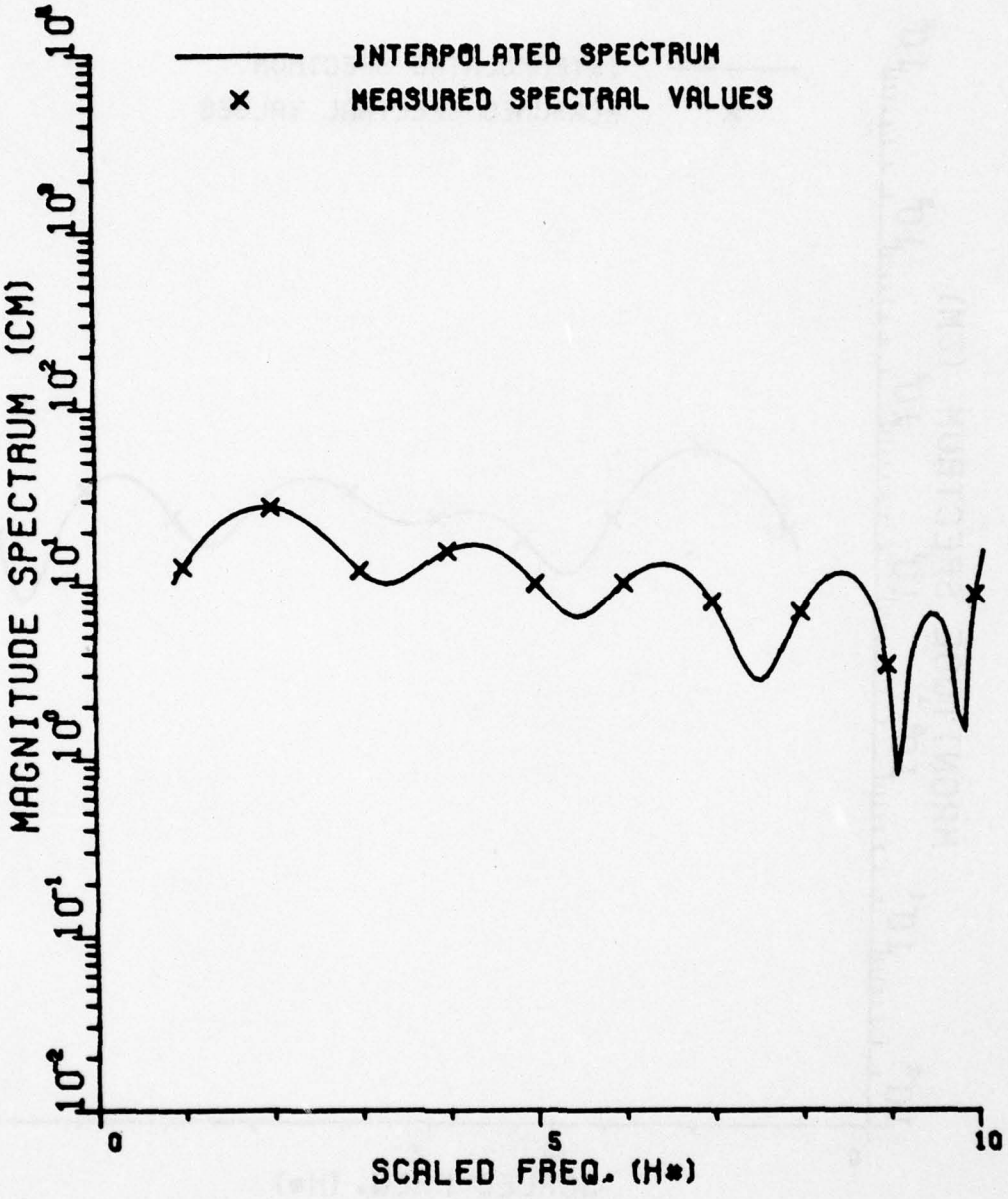

MOGAMI (1/700) -BOW ON

Figure 27

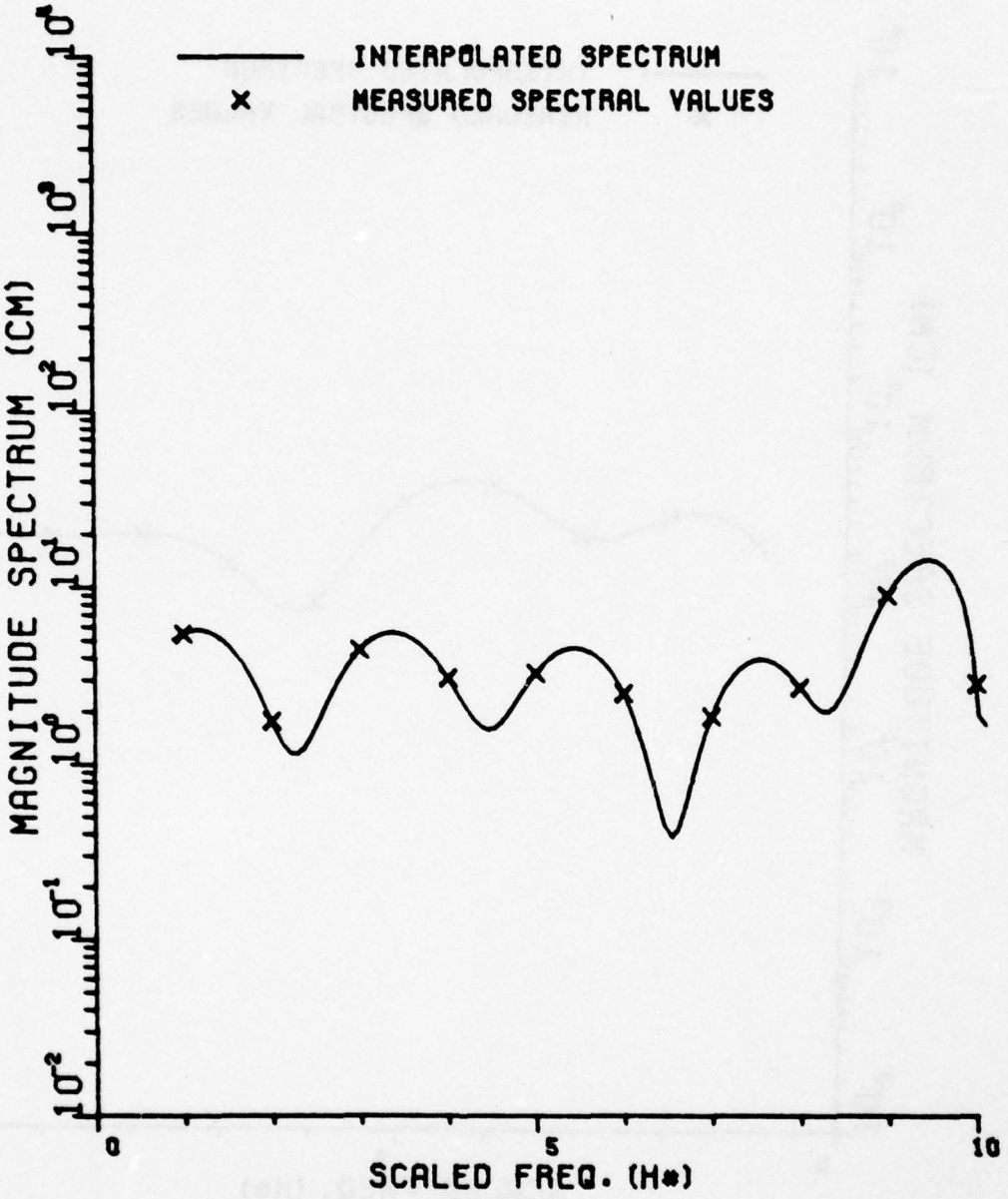

MOGAMI (1/700) -STERN

Figure 28

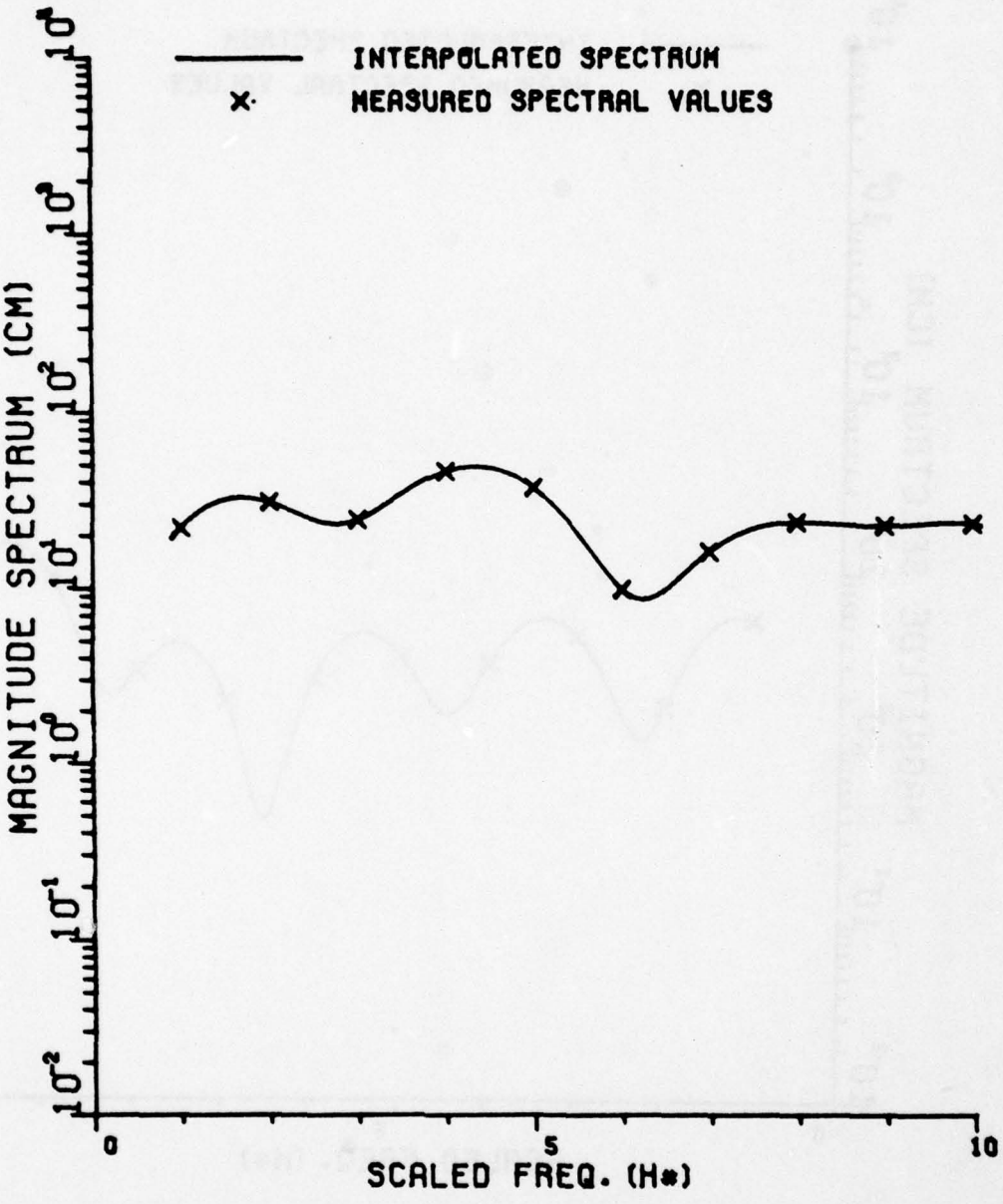

MOGAMI (1/700) -STARBOARD

Figure 29

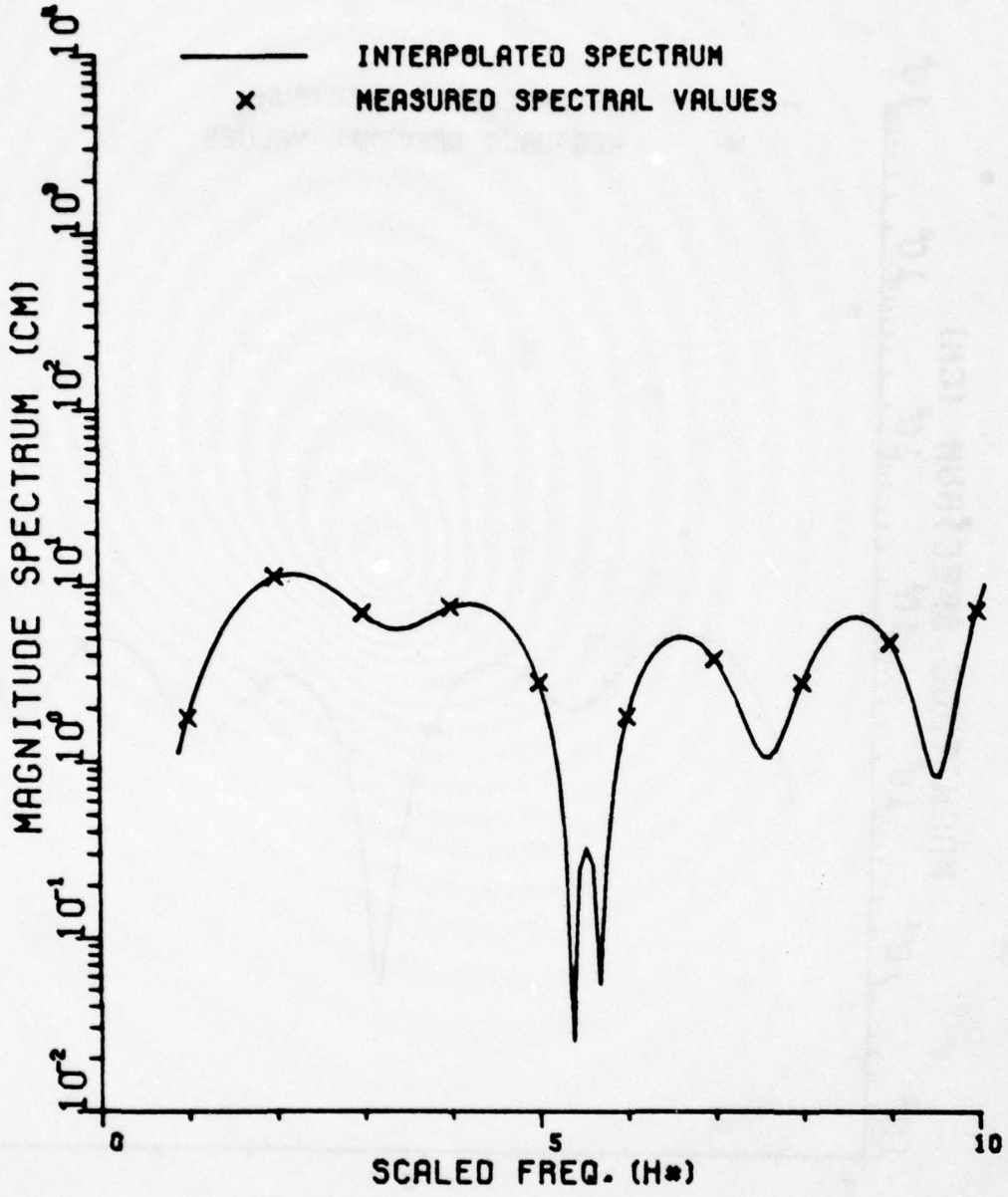

HAYANAMI (1/700) -BOW ON

Figure 30

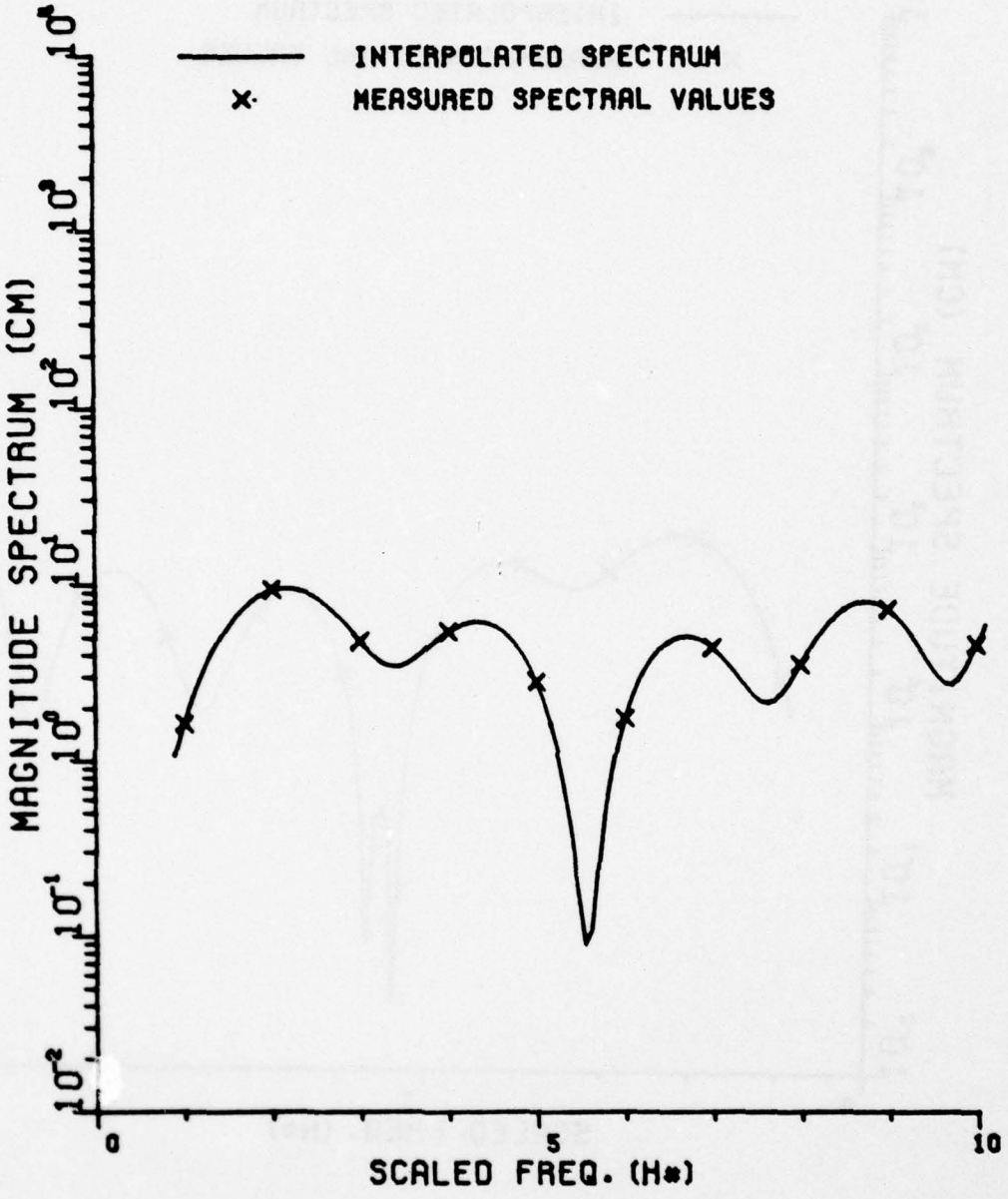
INTERPOLATED SPECTRUM
MEASURED SPECTRAL VALUES
MAGNITUDE SPECTRUM (CM)
10^{-2}
10^{-1}
10^{0}
10^{1}
10^{2}
10^{3}
10^{4}
0
5
10
SCALED FREQ. (H*)
HAYANAMI (1/700) -STERN

Figure 31

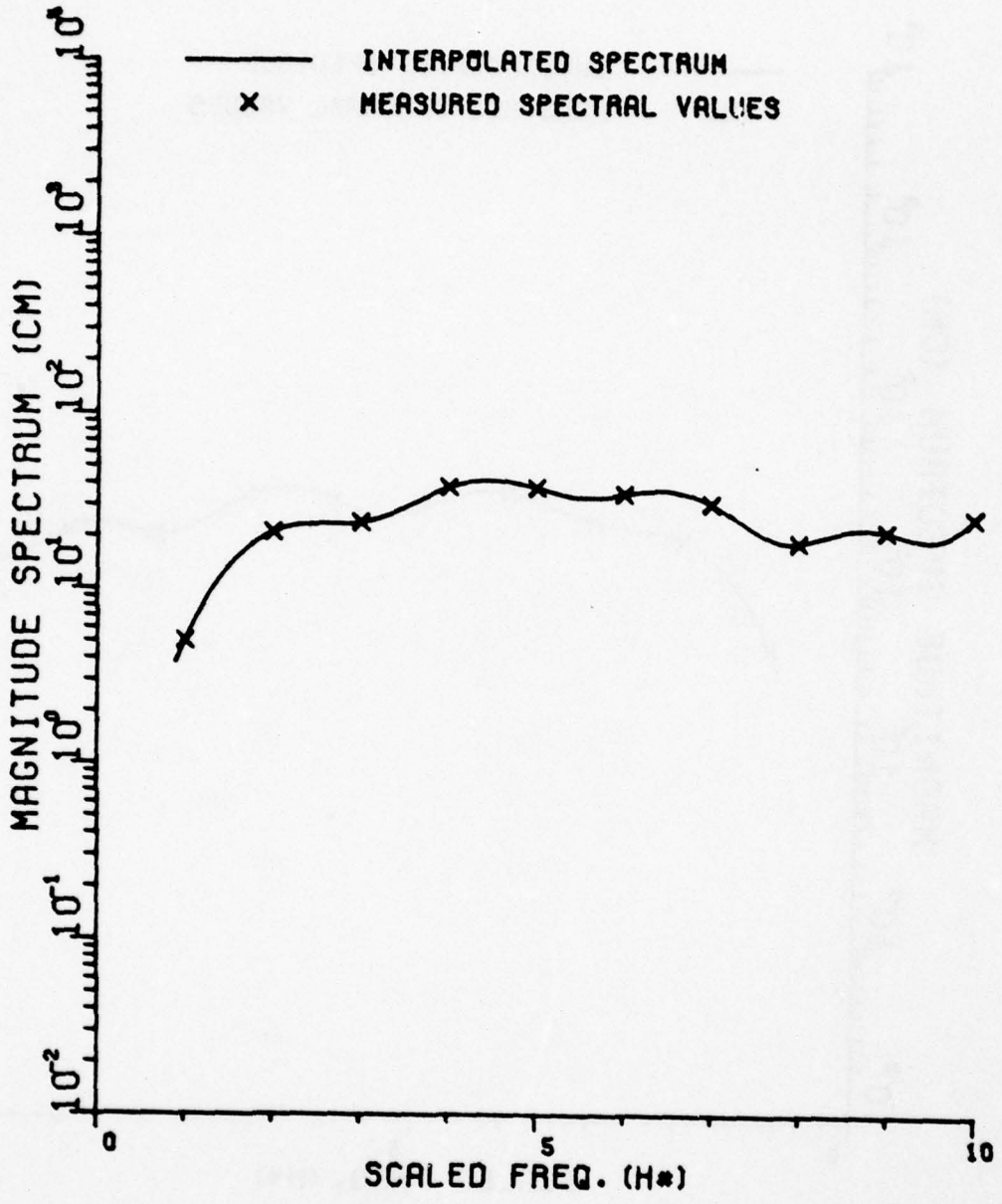

HAYANAMI (1/700) -STARBOARD

Figure 32

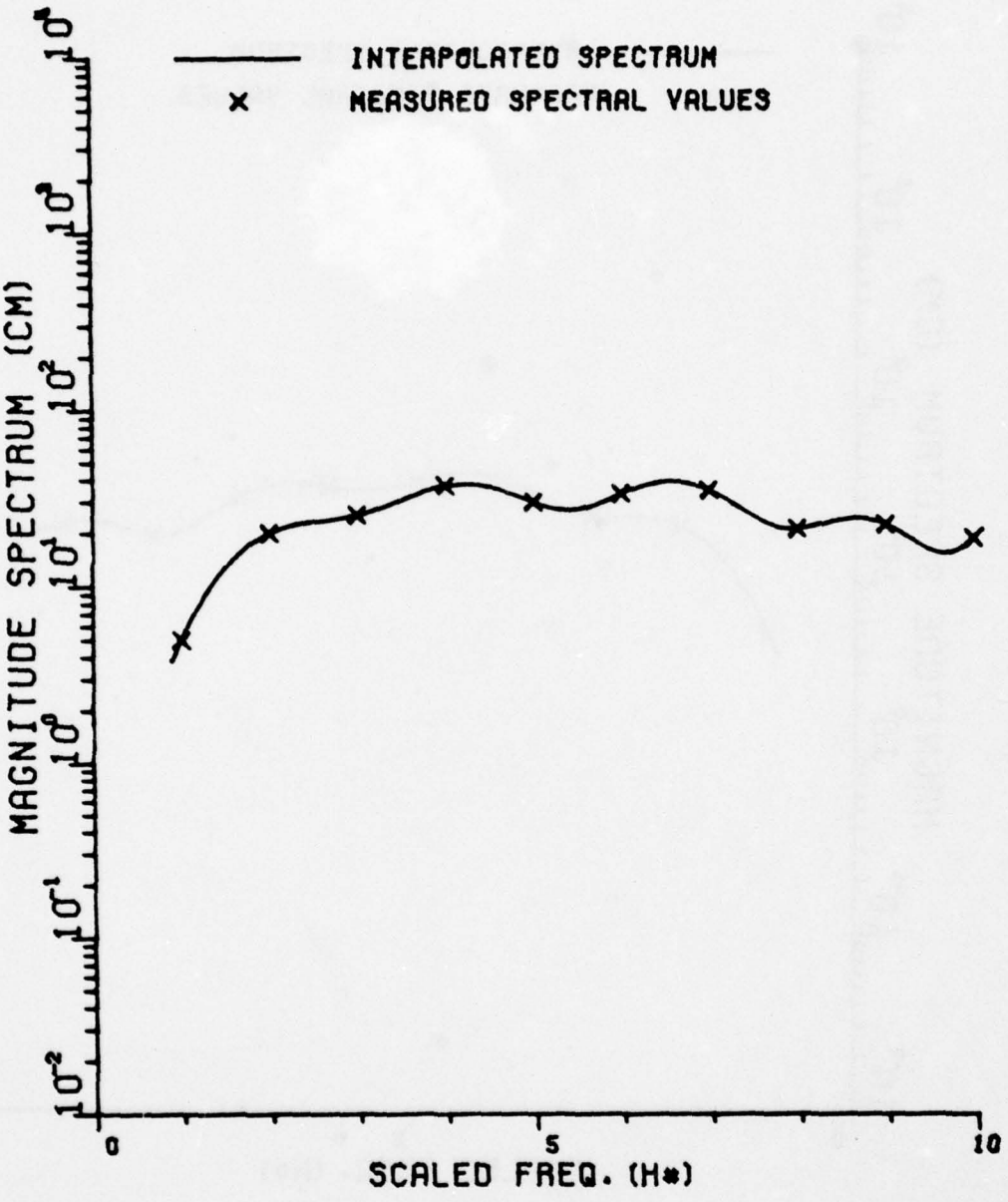

HAYANAMI (1/700) -PORT

Figure 33

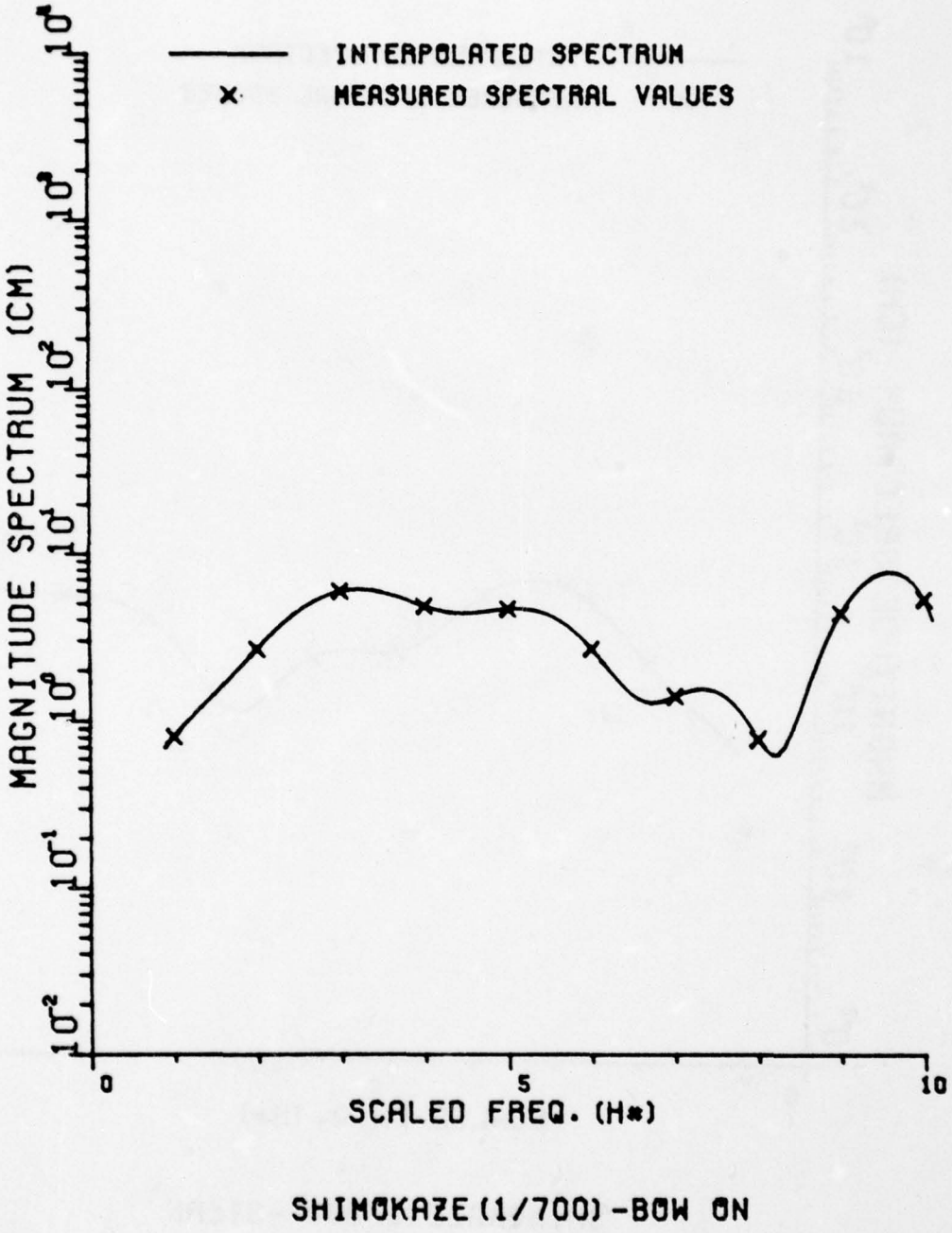

SHIMOKAZE (1/700) -BOW ON

Figure 34

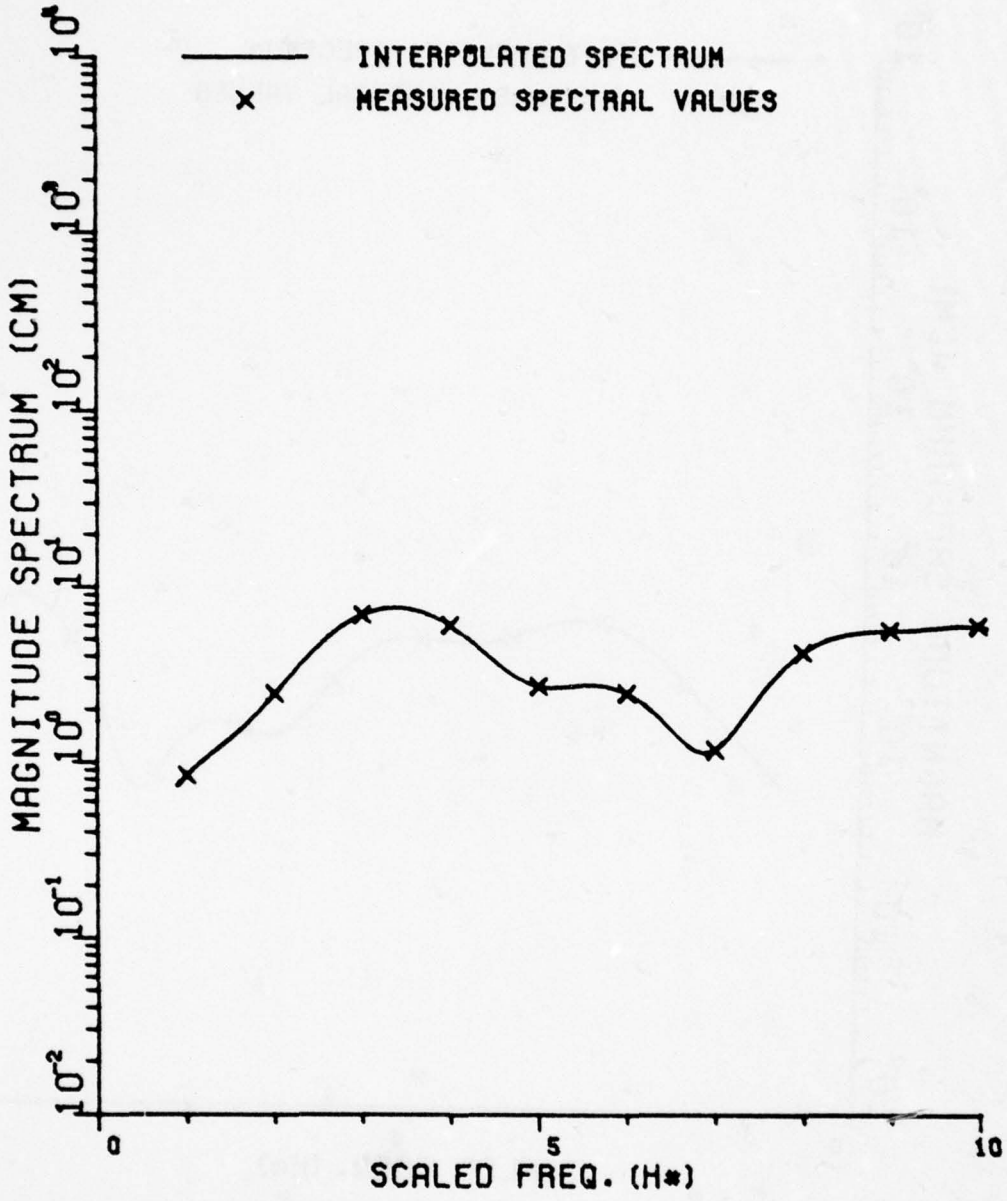

SHIMOKAZE (1/700) -STERN

Figure 35

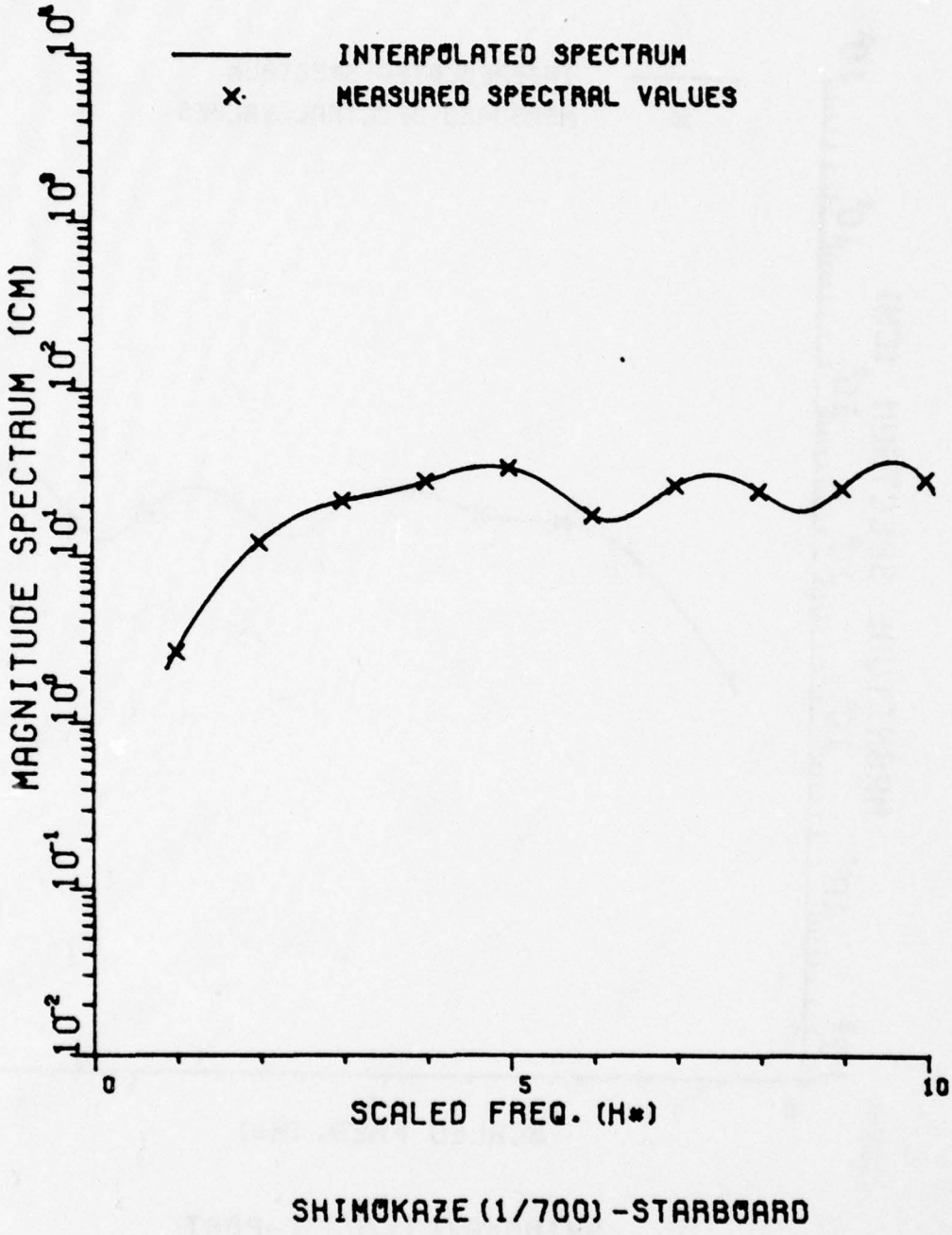
INTERPOLATED SPECTRUM
MEASURED SPECTRAL VALUES
MAGNITUDE SPECTRUM (CM)
10^{-2}
10^{-1}
10^{0}
10^{1}
10^{2}
10^{3}
10^{4}
0
5
10
SCALED FREQ. (H*)
SHIMOKAZE (1/700) -STARBOARD

Figure 36

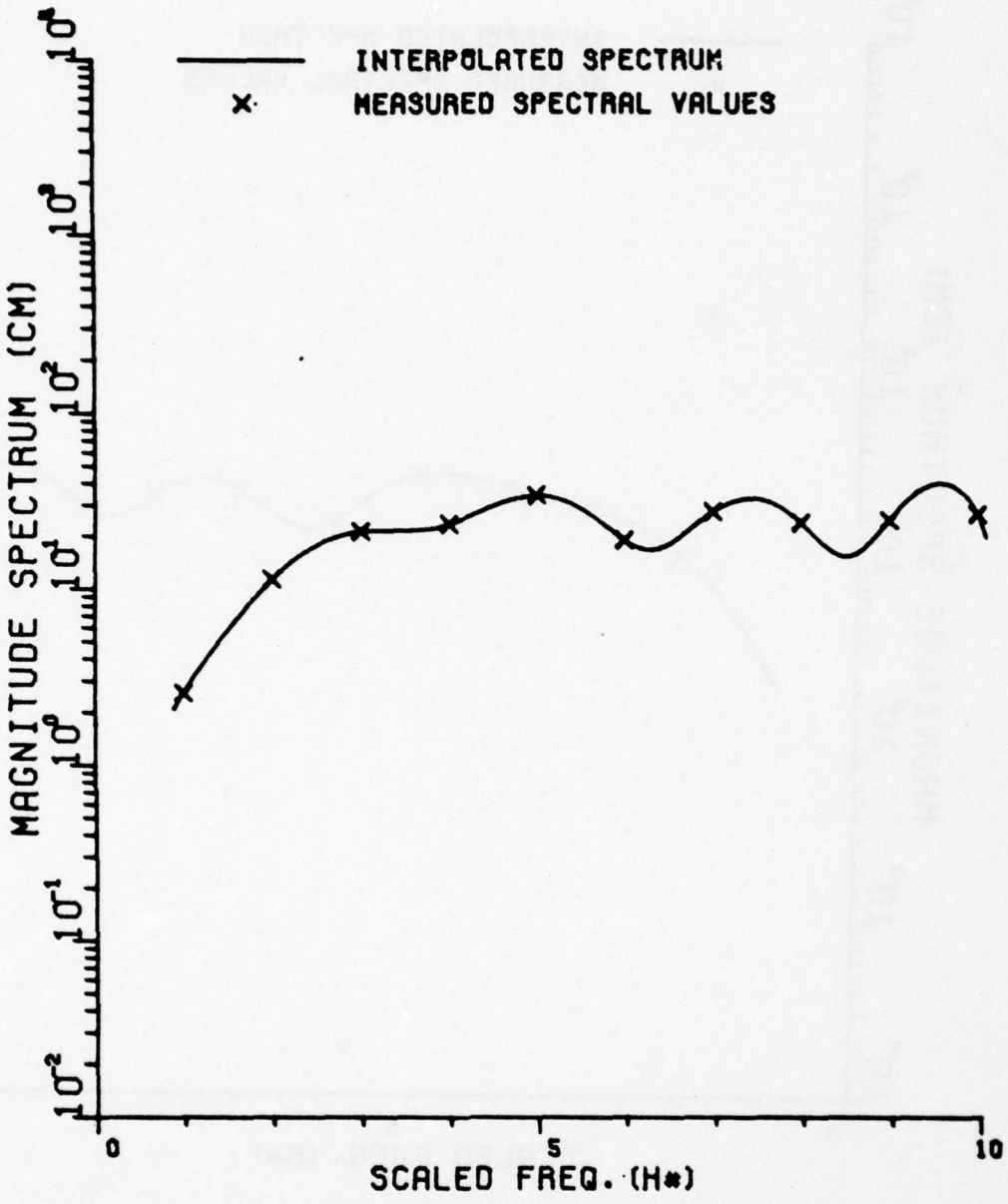

SHIMOKAZE (1/700) -PORT

Figure 37

$$C_n = \frac{1}{1-\left(\frac{2n}{N}\right)^2} \times \frac{\sin\left(2\pi\frac{n}{N}\right)}{\left(2\pi\frac{n}{N}\right)} \tag{42a}$$

$$C_0' = \frac{1}{2} + \frac{C_1}{4} \tag{42b}$$

$$C_N' = \frac{C_{N-1}}{4} + \frac{C_N}{2} \tag{42c}$$

$$C_n' = \frac{C_{n-1}}{4} + \frac{C_n}{2} + \frac{C_{n+1}}{4} \qquad 0 \neq n \neq N \quad . \tag{42d}$$

It is not intended to imply that the interpolated curves can necessarily be taken as valid estimates of the scattered field amplitude between test frequencies. The data curves shown are simply intended as a more meaningful display than tables of amplitude data versus frequency. The curves obtained via Equation (41) were also found to yield smoother results than rational function fits of the same amplitude data (crosses in the figures). A more complicated version of Equation (41) can also be used to estimate continuous amplitude and phase spectra with the added capability of simulating "chirp-type" responses. This type of processing is currently under study.

VI. PROCESSED RESPONSE WAVEFORMS OF NAVAL VESSELS

The tabulated electrical sizes of the model ships given in Table I make it clear that true ramp response waveforms cannot be synthesized from the measured scattering data. Simply stated, the fundamental period is such that the transient signal does not decay to negligible values within this period (Fourier synthesis automatically involves periodic waveforms). Therefore foldover errors occur in the synthesized waveform. The profile or area function interpretation (Equation (10)) cannot be made and it does not necessarily follow that complex natural resonances extracted from the waveform (Equation (11)) can be related to the physical target structure in a simple manner. It is noted however, as will be shown, that the ramp response waveforms obtained from Equation (6) or Equation (7) are characteristic of the target. It is instructive to examine the near foldover error for a calibration target; in this case a conducting hemisphere on a conducting ground plane. For convenience, all of the processed response waveforms given in this report are normalized such that the peak magnitude of the waveform is unity. A vertical scale factor given on each figure is used to determine the actual peak value of the waveform. The abscissa scale can be given equivalently in either length or time. For our

purpose the scale is in samples of the fundamental period ($\frac{1}{1.085 \times 10^9}$) and 400 samples span the fundamental period. For ramp waveform synthesis, the ordinate scale is in units of centimeters normalized by π. The synthesized ramp response waveform of a 1.5 inch diameter conducting hemisphere on a ground plane is shown in Figure 38. The waveform was synthesized from calculated 10 frequency harmonic scattering data corresponding to the reflectivity facility (fundamental frequency of 1.085 GHz). Note that the waveform assumes a constant value over a portion of the fundamental period showing that foldover problems are not present. Because the phase reference is at the center of the sphere, the peak response happens to occur at the start and end of the period. The same waveform, shifted such that the ramp response actually starts at the beginning of the period and with the constant term removed is shown in Figure 39. The negative sign in Equation (7) has also been included. It would be a simple matter to calibrate the response in Figure 39 in terms of the profile function (Equation (10)). However, if the diameter of the hemisphere exceeds the imposed limit (Equation (9)) this interpretation is no longer possible. The near maximum hemisphere diameter case is illustrated in Figure 40, where the synthesized ramp response waveform of a 2.5 inch diameter hemisphere is shown. Figure 40 should be compared with Figure 38 and Figure 41 with Figure 39. The waveform in Figure 40 is still a true ramp response for a hemispherical target on a ground plane but note that without the aid of Figure 39 the start of the waveform is questionable because a constant return over some portion of the period is not readily obtained. Increasing the diameter of the hemisphere beyond 2.5 inches will yield other characteristic waveforms, all different in general from those in Figures 39 and 40. Decreasing the electrical size of the hemisphere below that shown in Figure 40 will yield waveforms of the same shape as shown in Figure 40. An exception to this occurs when all frequency samples are in the Rayleigh region. In this case the synthesized waveform will depart from the anticipated shape. In fact a sum of equally weighted cosine harmonics is obtained. Finally it is clear by comparing Figures 38 and 40 that the maximum hemisphere diameter which will yield a true ramp response waveform is roughly

$$d_{max} \leq 2.5 \text{ inches.} \tag{43}$$

The above remarks are perhaps obvious to one well-versed in Fourier synthesis but may need clarification for other engineers.

For further discussion of these concepts the reader is referred to any general text on Fourier synthesis (Reference [17]). Selected ramp response waveforms of the model naval vessels tested are given in this section to illustrate that characteristic waveform signatures are obtained. The phase reference for the scattering data used to synthesize these waveforms is normally at the center and base of each hull length. With this information one can estimate the point at which each response waveform should start using the hemisphere results. For

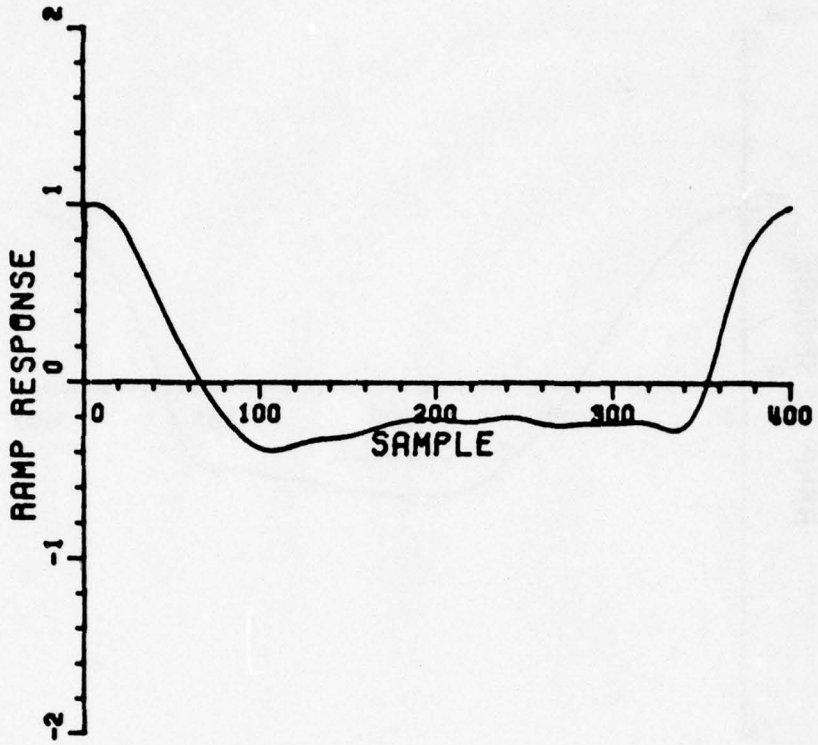

Figure 38. 1.5" Hemisphere; Scale: 0.346

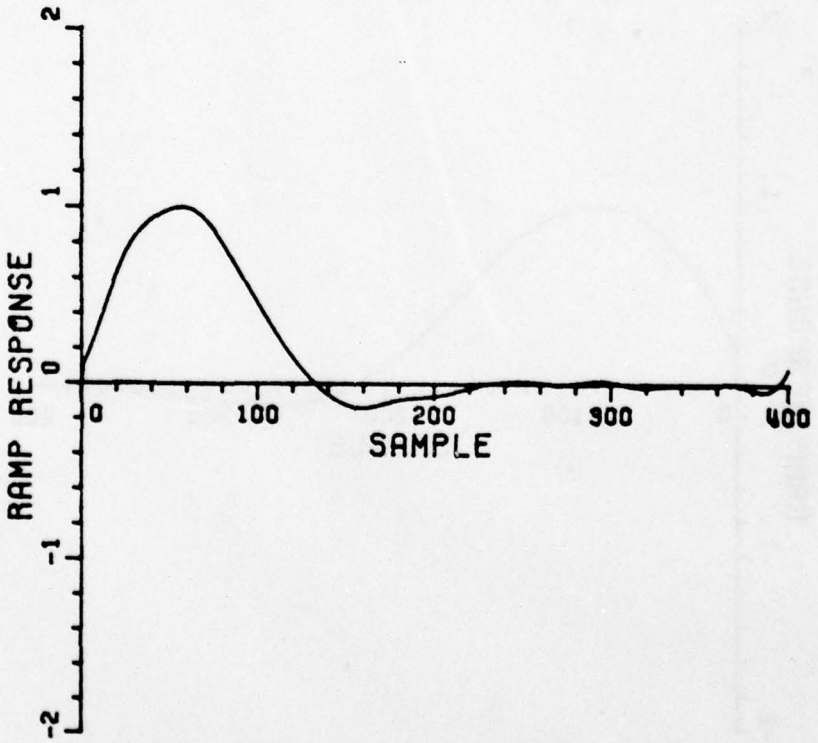

Figure 39. 1.5" Hemisphere; time shifted, constant removed; scale: 0.423.

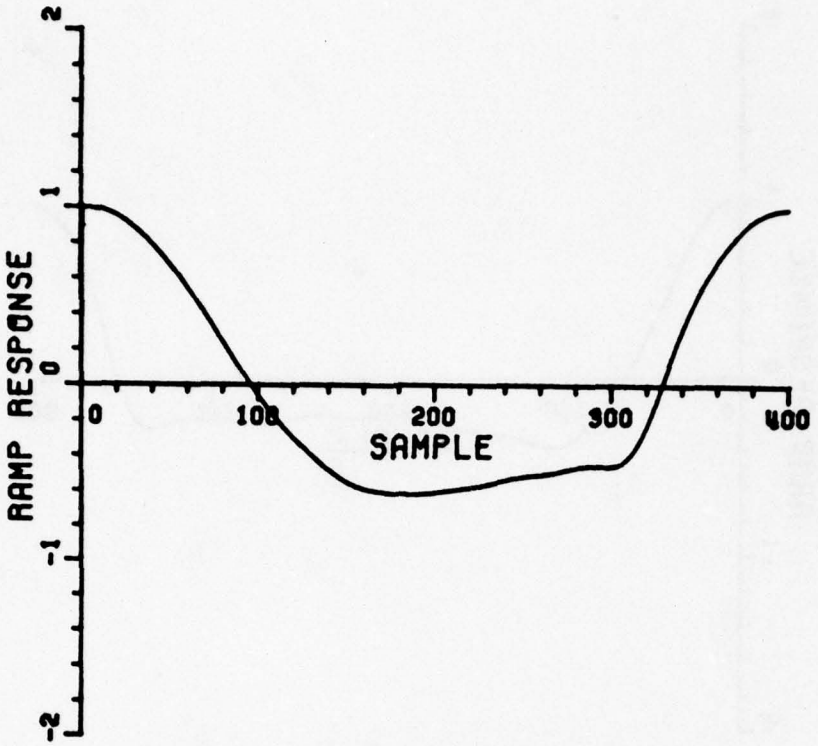

Figure 40. 2.5" Hemisphere; Scale: 0.825.

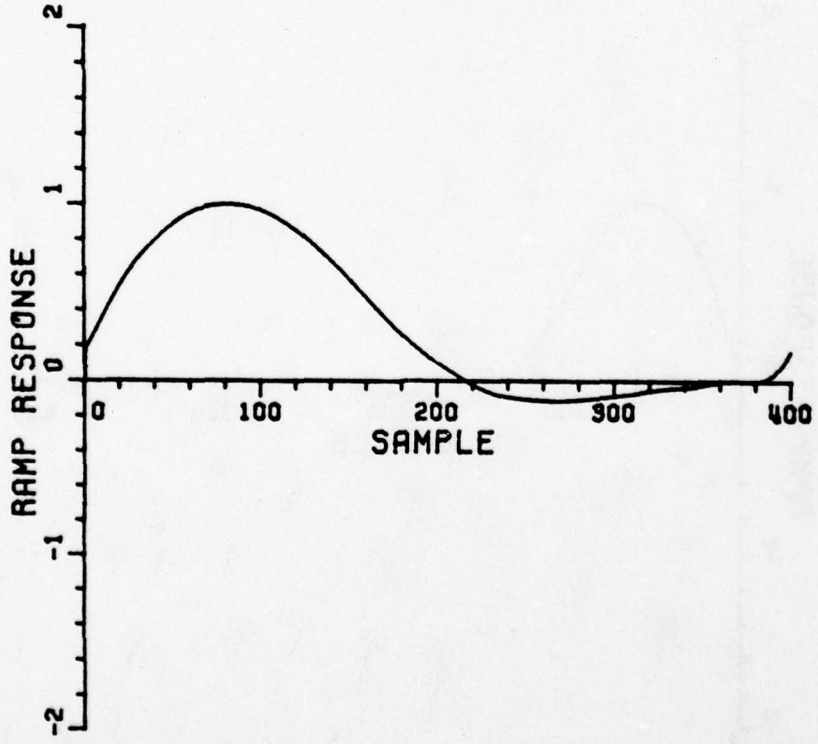

Figure 41. 2.5" Hemisphere; time shifted, constant removed; Scale: 1.201.

example, the response of the 1.5 inch hemisphere starts at roughly 340 samples. The response of the 2.5 inch diameter hemisphere starts at 310 samples. Thus a length increase ratio of 2.5/1.5 yields a reduction of 30 samples in the starting point. Estimated starting points are indicated on the various ship responses, based on the appropriate hull length or beam width of the models. If the ship responses were true ramp responses then a constant level could be removed from the waveforms. In the present case this cannot be done and each waveform must be examined with an understanding that an unknown vertical shift is needed. The starting points indicated for the ship waveforms are obviously gross estimates because of the foldover errors.

In Figures 42 through 49 synthesized ramp response waveforms of the vessels given in Table I are presented in the order listed in Table I.* Each figure has three waveforms (a, b and c) corresponding respectively to bow, stern and starboard beam incidence. These waveforms are included primarily to illustrate that in most cases characteristic waveforms are obtained. There is no way that a detailed analysis of the waveforms can be made. Note, however, that in some of the bow and stern responses one can discern an approach to a reasonably constant level from the origin and then larger magnitude returns. This would be anticipated as the incident signal washes over the relatively clean hull and then encounters the superstructure. The beam waveforms differ in that the superstructure is encountered immediately.

From a complex natural resonance viewpoint the ramp response waveforms are not convenient. Admittedly for most waveforms there is a portion of the return which could be approximated by a finite, decaying exponential sum. But there is little or no consistency among the various waveforms and consequently less likelihood of obtaining excitation invariant parameters. For this reason a different type of response waveform was desirable. It was also known that the accuracy of the recorded phase data was not good. A synthetic matched filter-type response can be written as

$$f_M(\theta,\phi,\hat{p},t) = \sum_{n=1}^{2N} |G(\theta,\phi,\hat{p},jn\omega_o)||T(\theta,\phi,\hat{p},jn\omega_o)|\cos[n\omega_o t+\xi(n\omega_o)+\beta(n\omega_o)] \tag{44}$$

where $G/\underline{\xi}$ and $T/\underline{\beta}$ are respectively the scattered field and filter in phasor notation. Discarding the phase data and using a step weighting

*The Iowa (1:700) is not included since it is identical in construction to the Missouri.

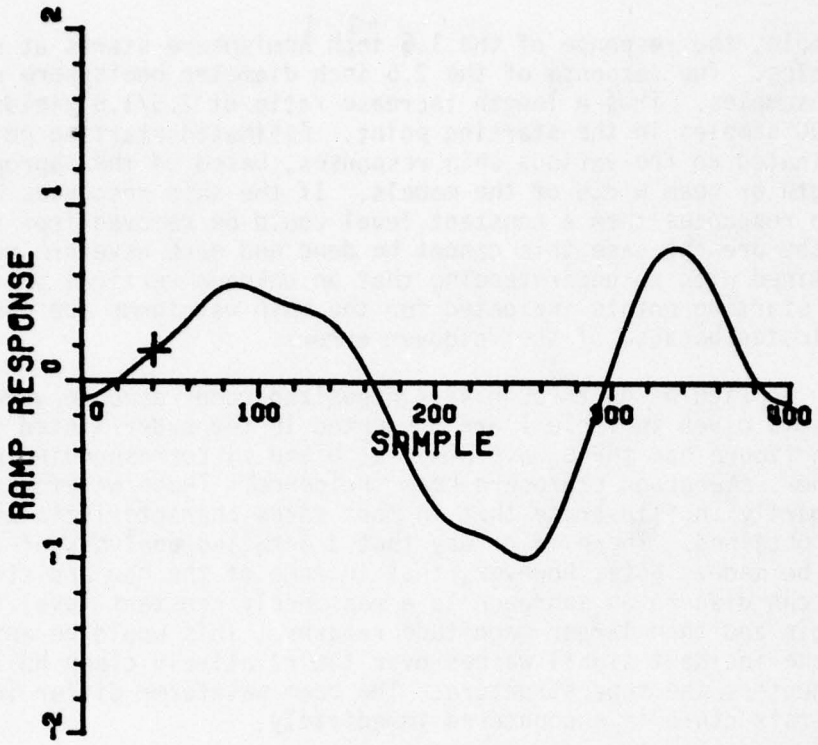

Figure 42(a). Midway (1/500) - Bow on; Scale: 0.437.

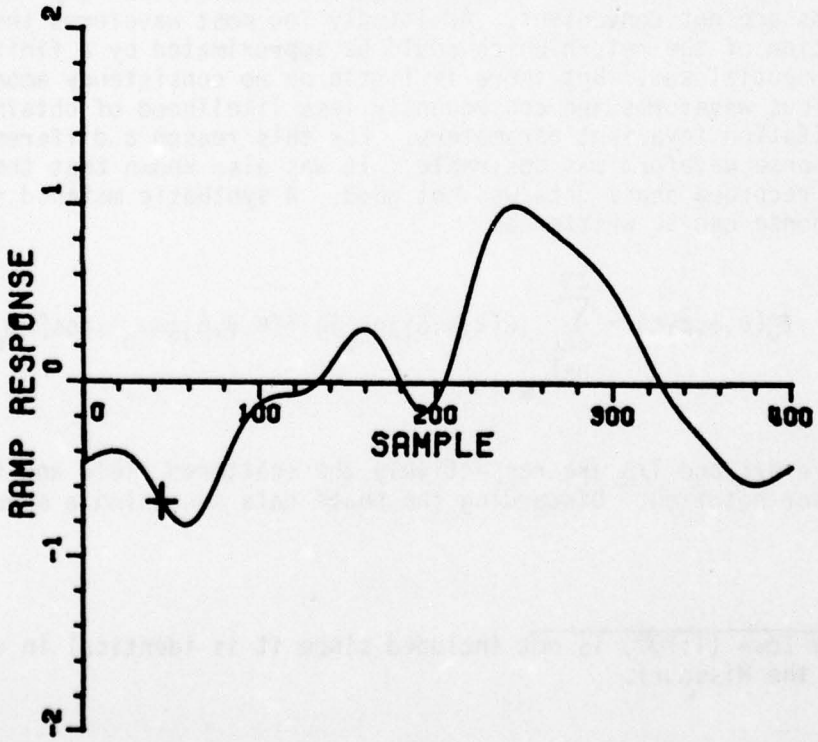

Figure 42(b). Midway (1/500) - Stern; Scale: 0.246.

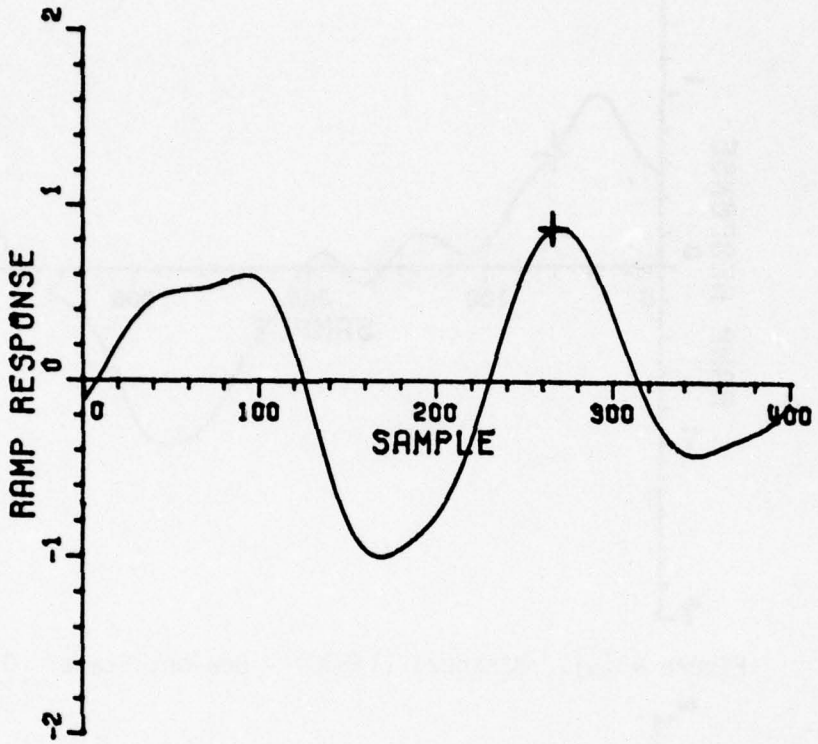

Figure 42(c). Midway (1/500) - Starboard; Scale: 2.265.

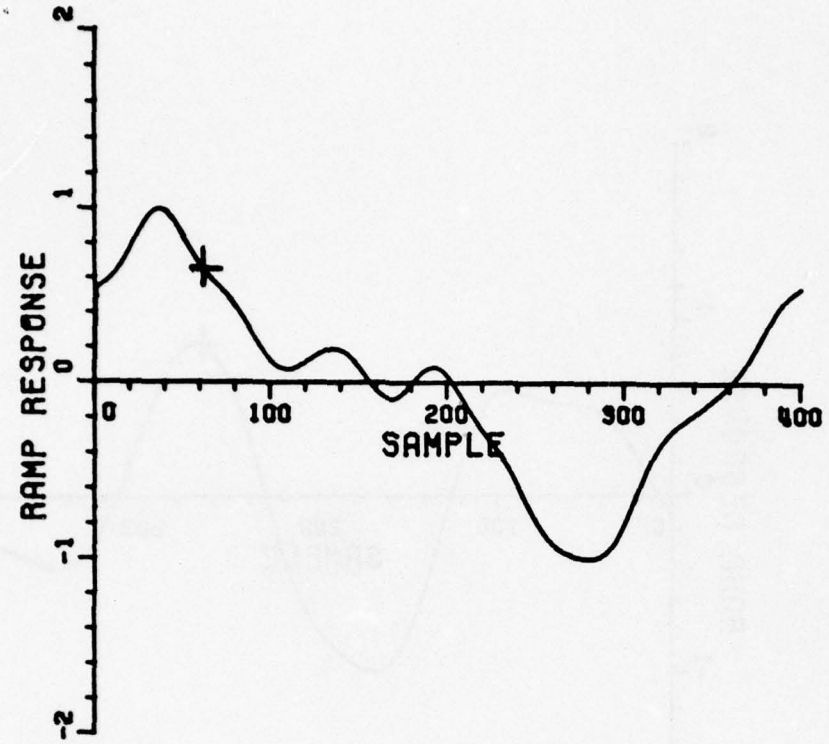

Figure 43(a). Missouri (1/500) - Bow on; Scale: 0.276.

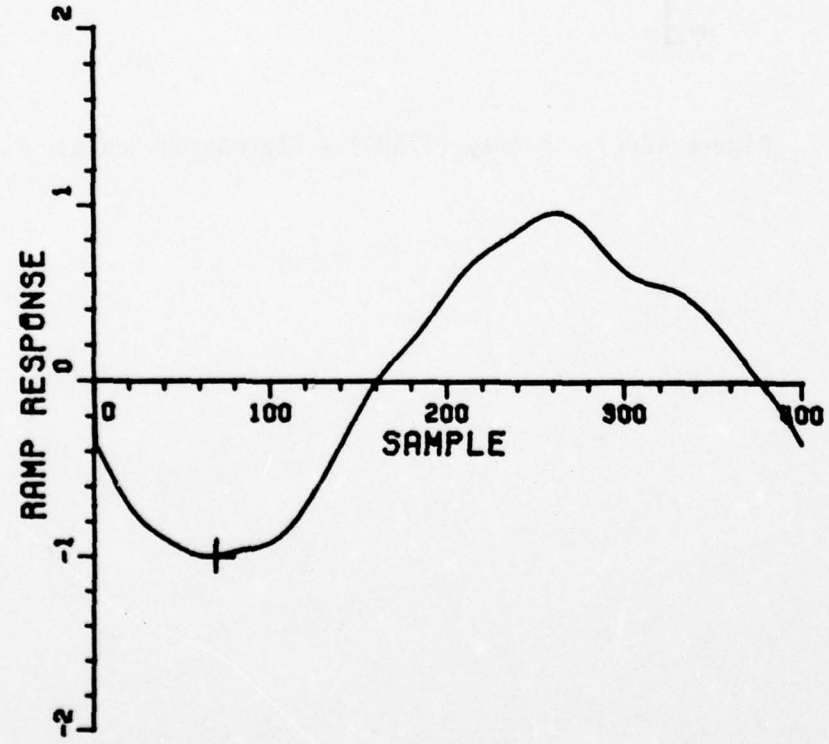

Figure 43(b). Missouri (1/500) - Stern; Scale: 0.402.

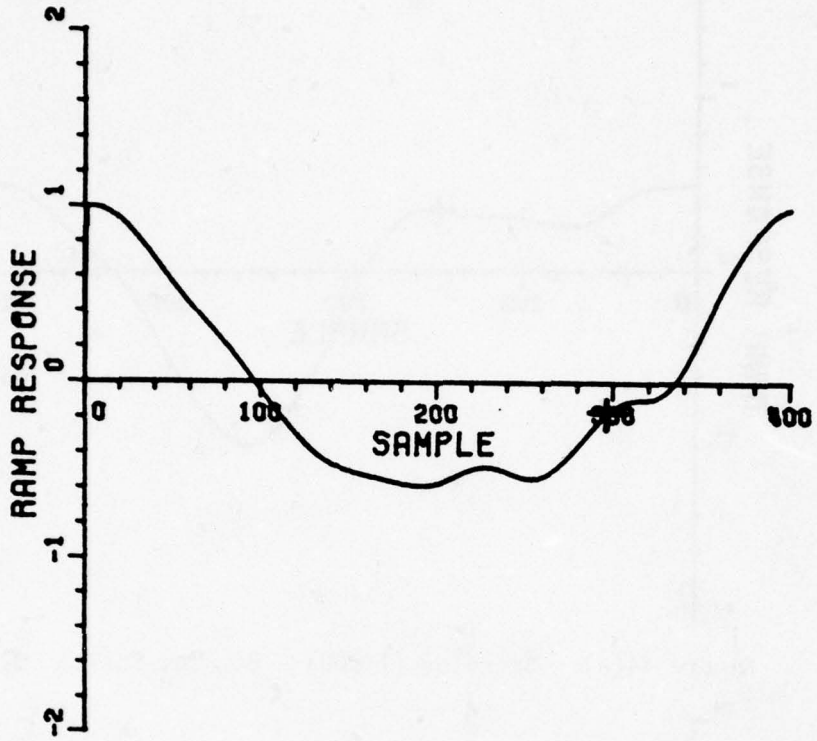

Figure 43(c). Missouri (1/500) - Starboard; Scale: 2.281.

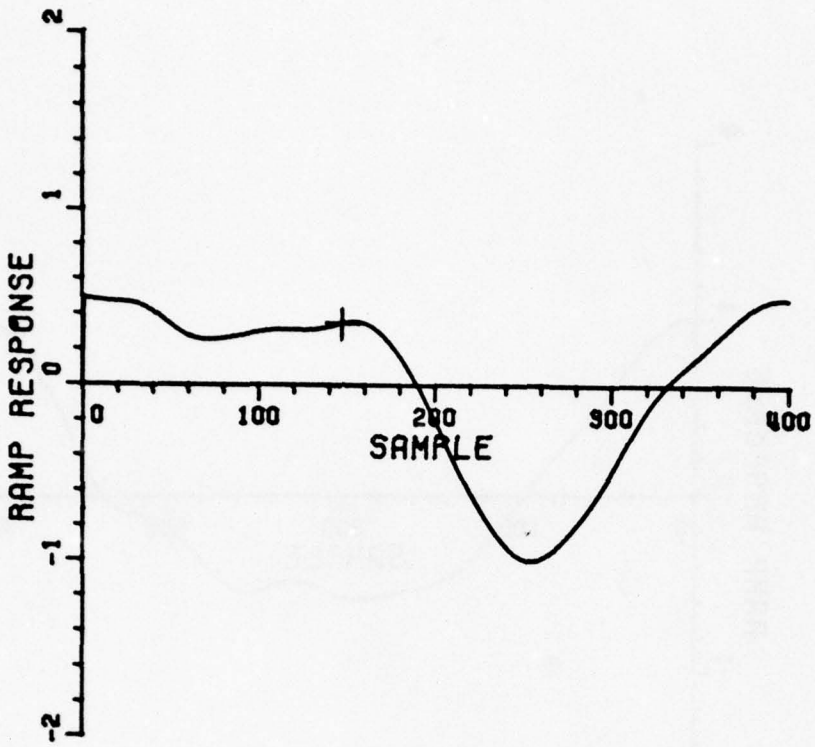

Figure 44(a). Sverdlov (1/500) - Bow on; Scale: 0.743.

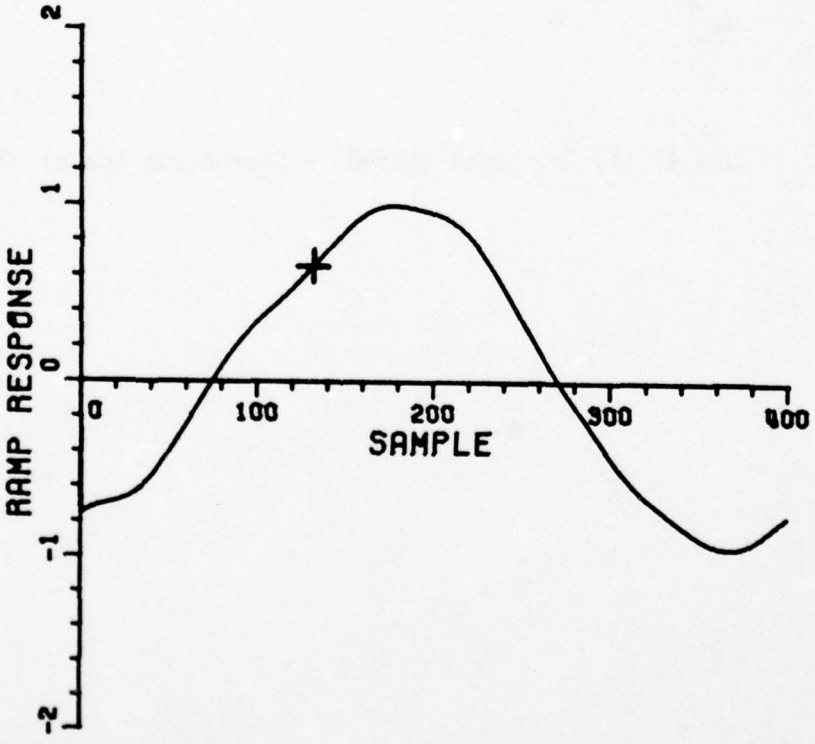

Figure 44(b). Sverdlov (1/500) - Stern; Scale: 0.506.

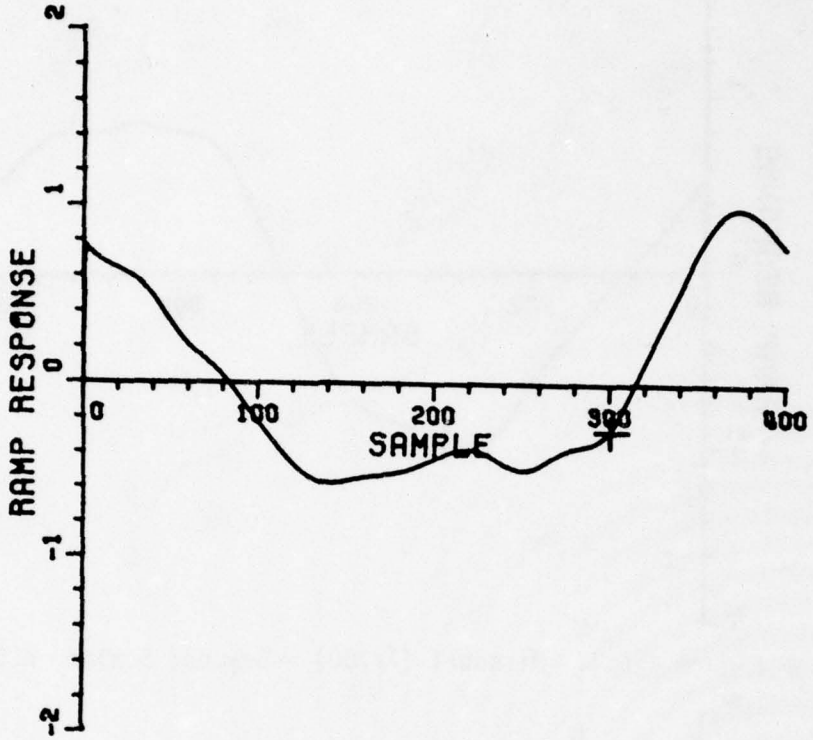

Figure 44(c). Sverdlov (1/500) - Starboard; Scale: 1.665.

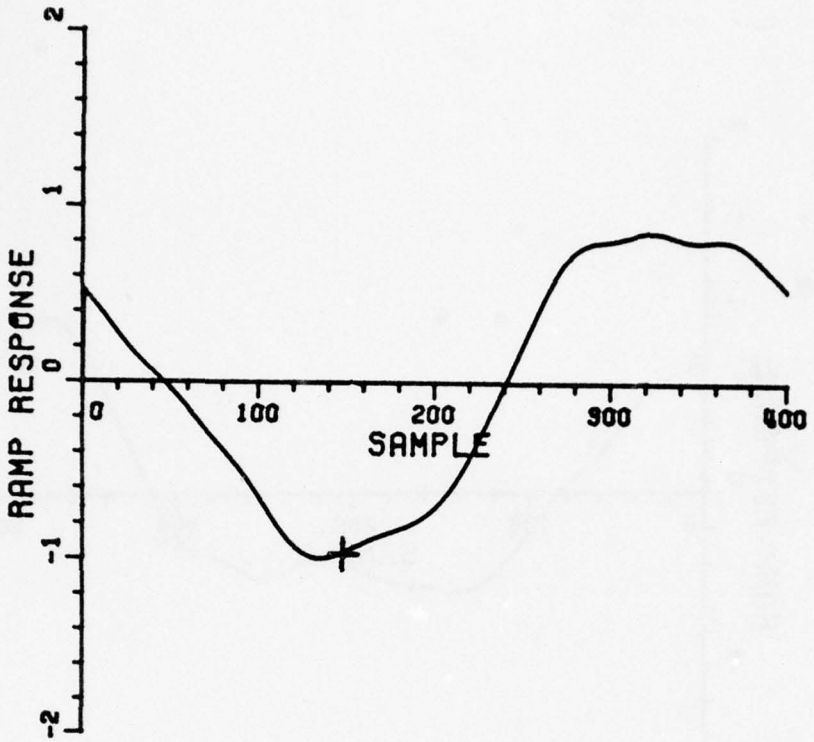

Figure 45(a). Missouri (1/700) - Bow on; Scale: 0.503.

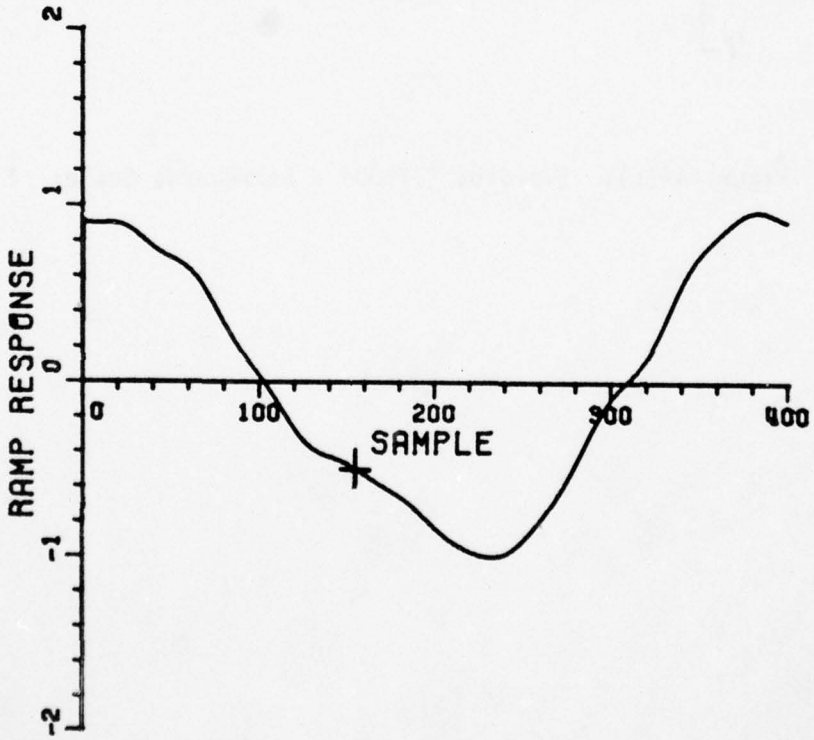

Figure 45(b). Missouri (1/700) - Stern; Scale: 0.463.

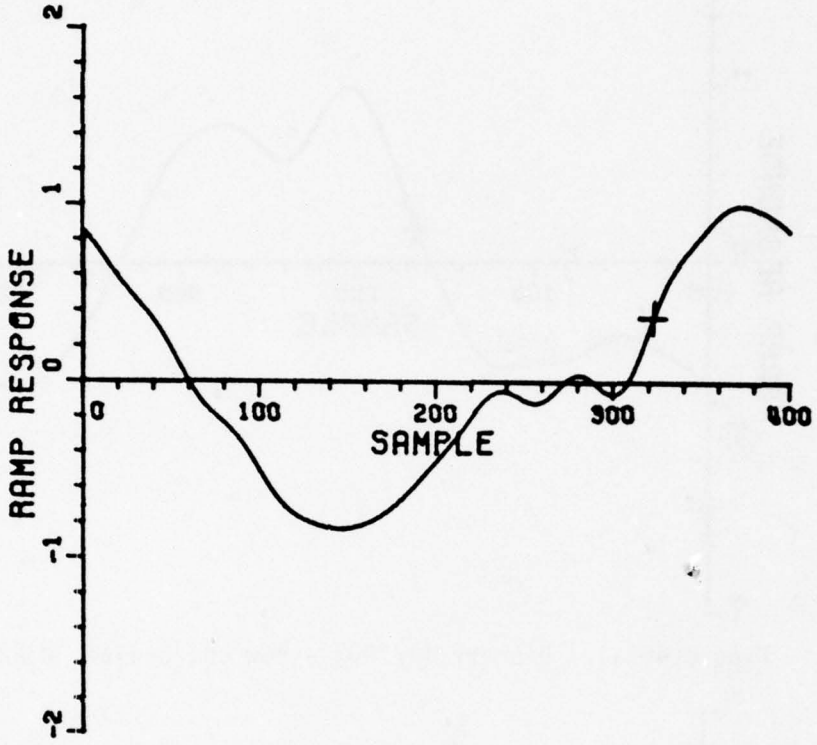

Figure 45(c). Missouri (1/700) - Starboard; Scale: 1.187.

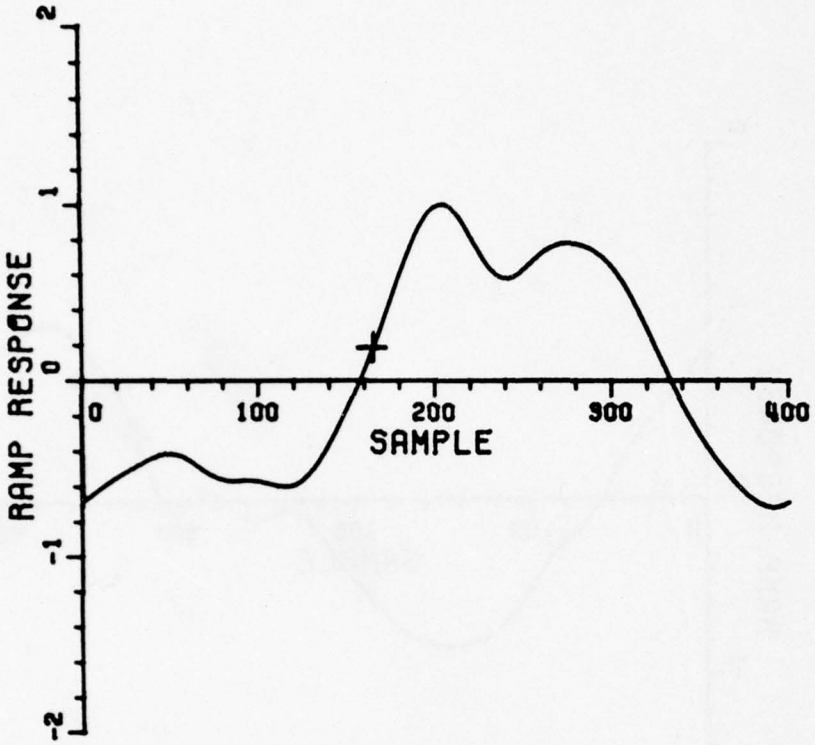

Figure 46(a). Bismark (1/700) - Bow on; Scale: 0.258.

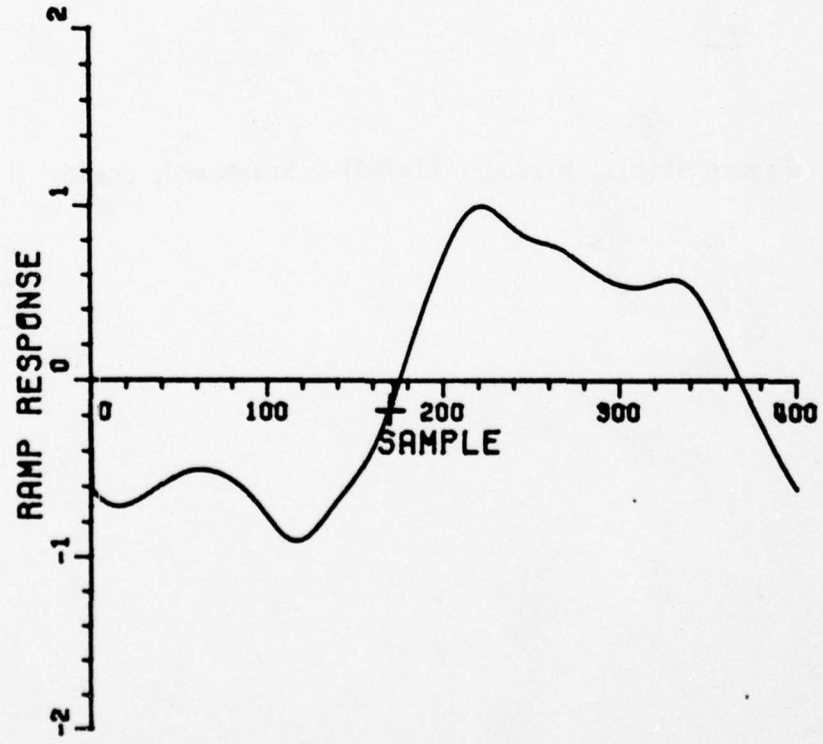

Figure 46(b). Bismark (1/700) - Stern; Scale: 0.239.

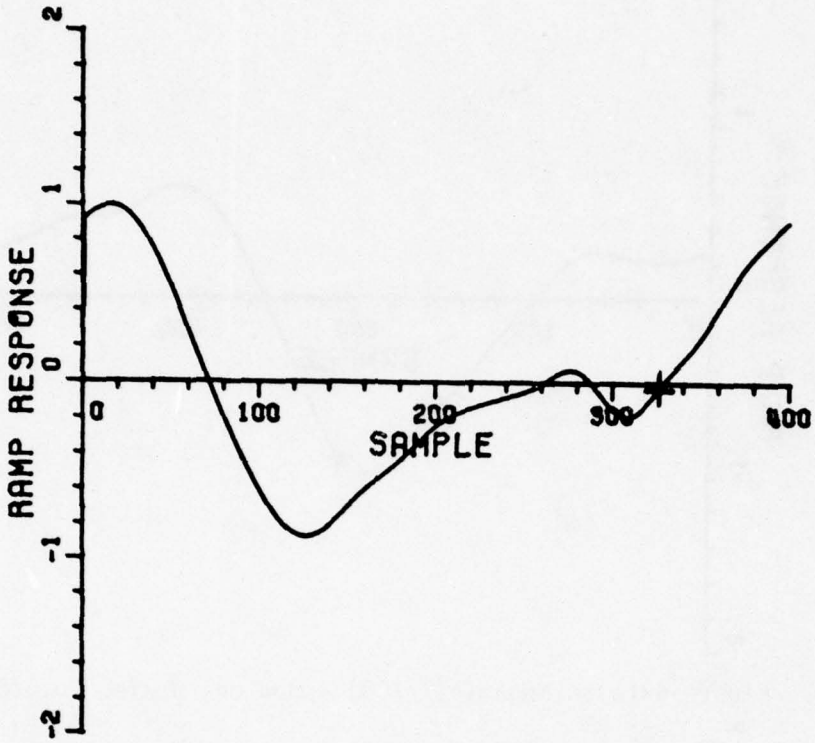

Figure 46(c). Bismark (1/700) - Starboard; Scale: 1.336.

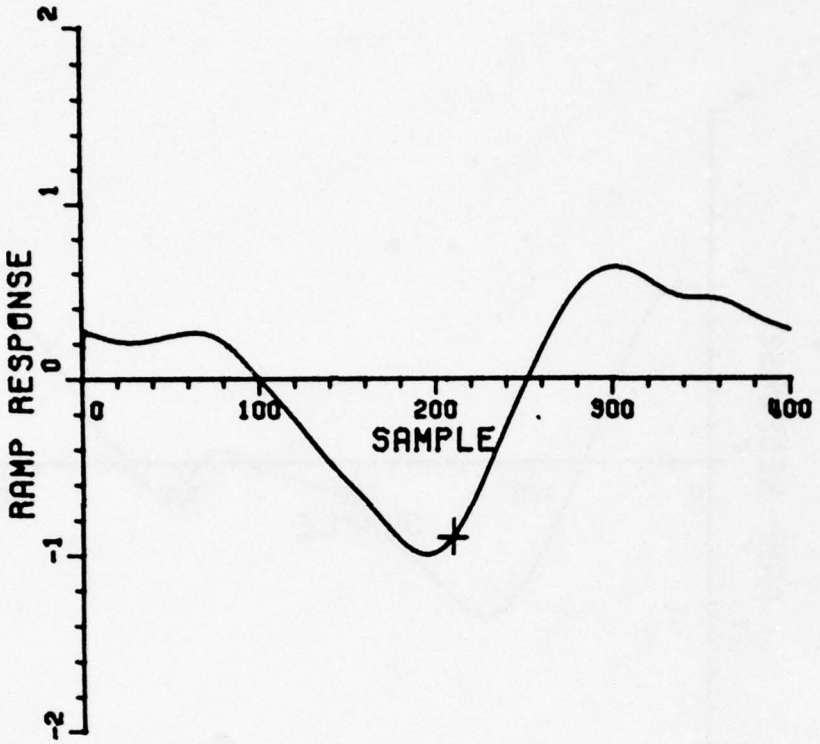

Figure 47(a). Mogami (1/700) - Bow on; Scale: 0.676.

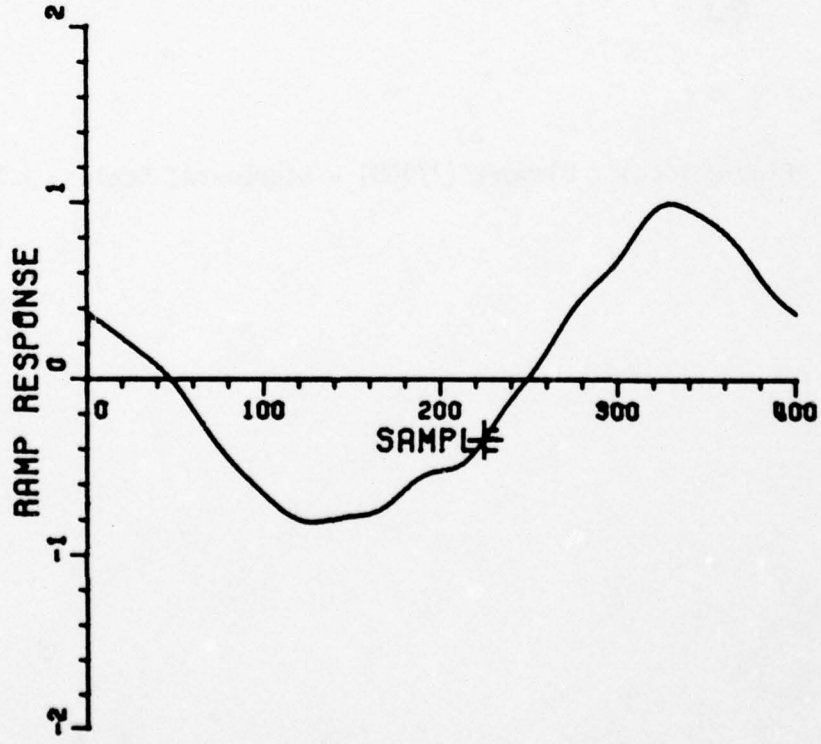

Figure 47(b). Mogami (1/700) - Stern; Scale: 0.215.

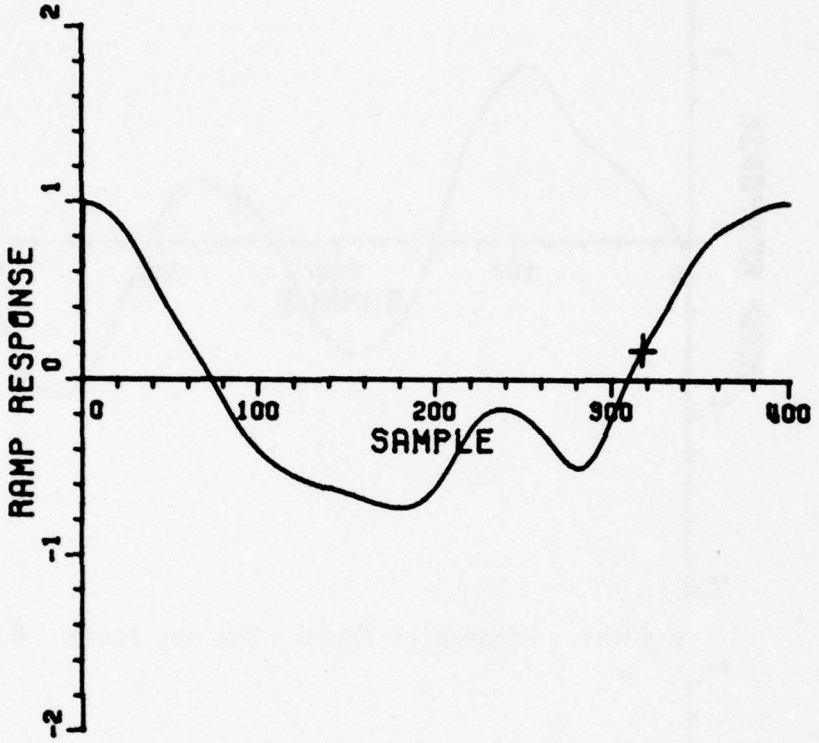

Figure 47(c). Mogami (1/700) - Starboard; Scale: 0.948.

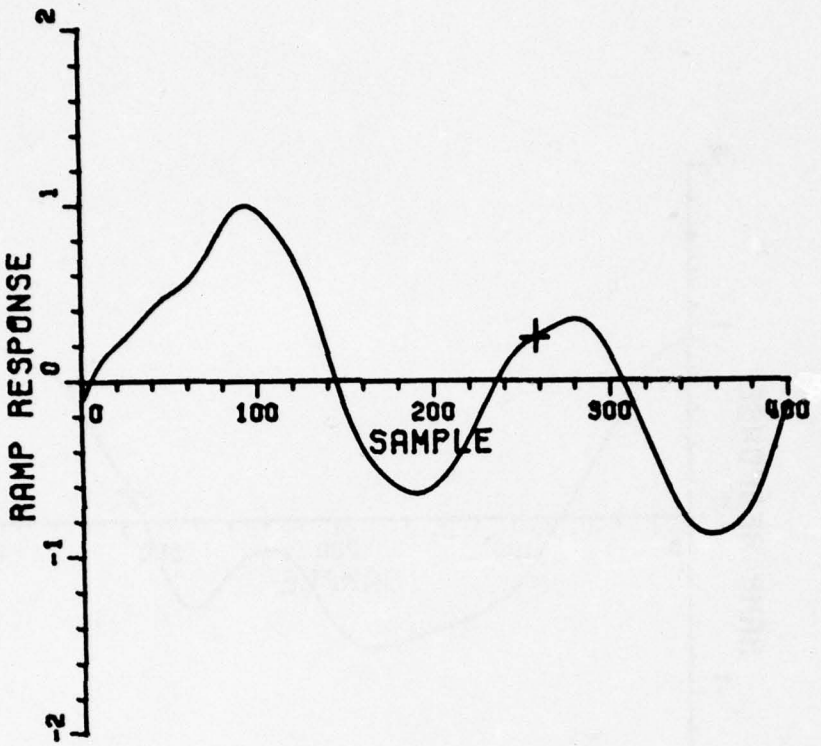

Figure 48(a). Hayanami (1/700) - Bow on; Scale: 0.148.

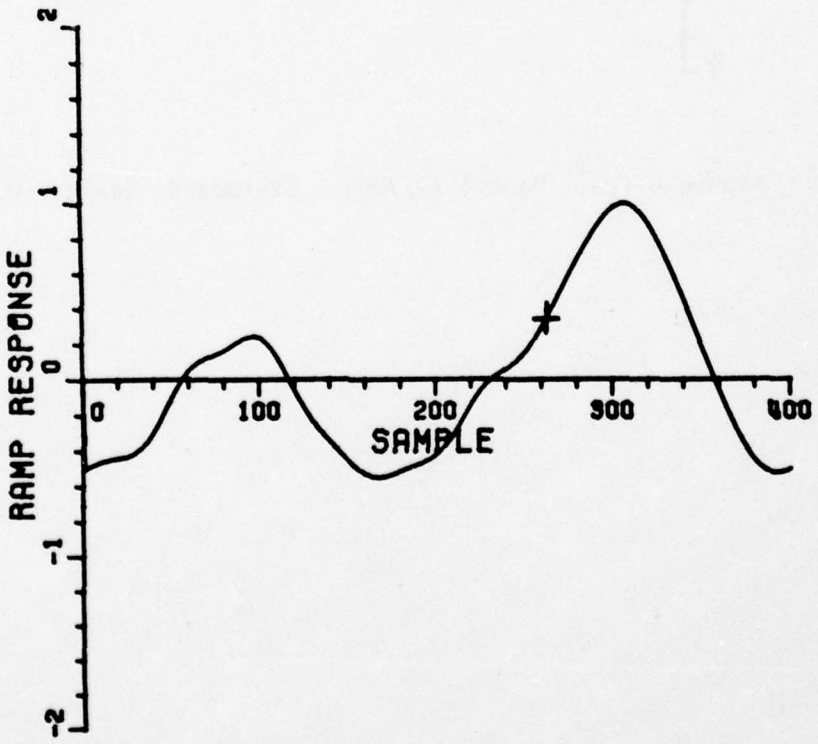

Figure 48(b). Hayanami (1/700) - Stern; Scale: 0.149.

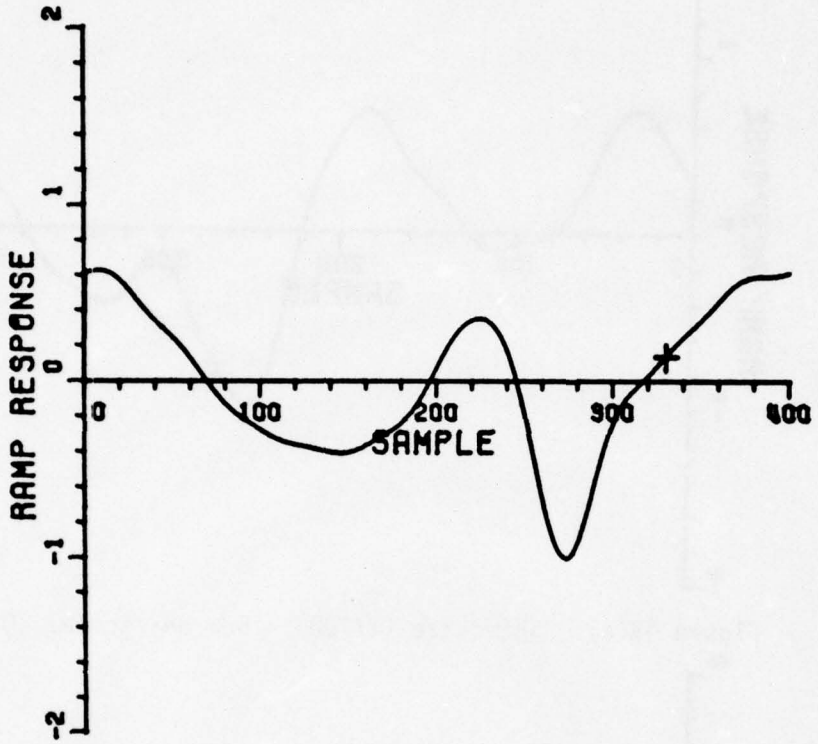

Figure 48(c). Hayanami (1/700) - Starboard; Scale: 0.464.

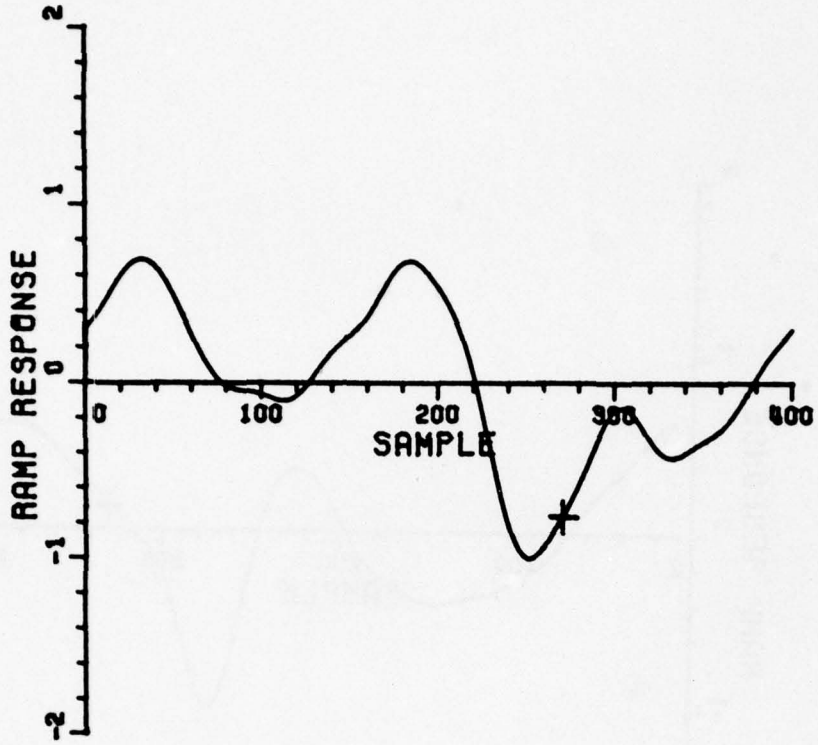

Figure 49(a). Shimokaze (1/700) - Bow on; Scale: 0.066.

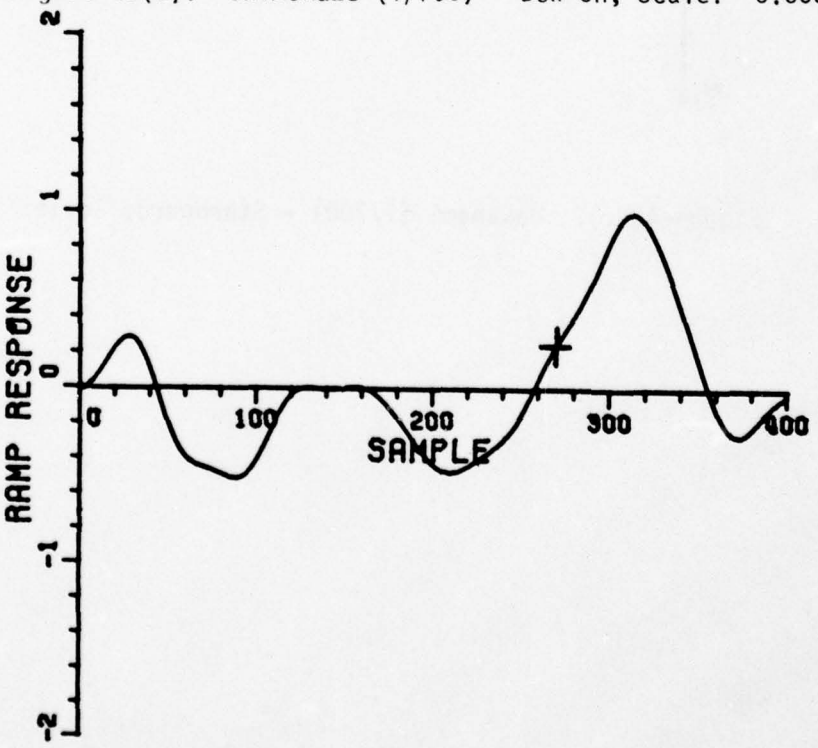

Figure 49(b). Shimokaze (1/700) - Stern; Scale: 0.079

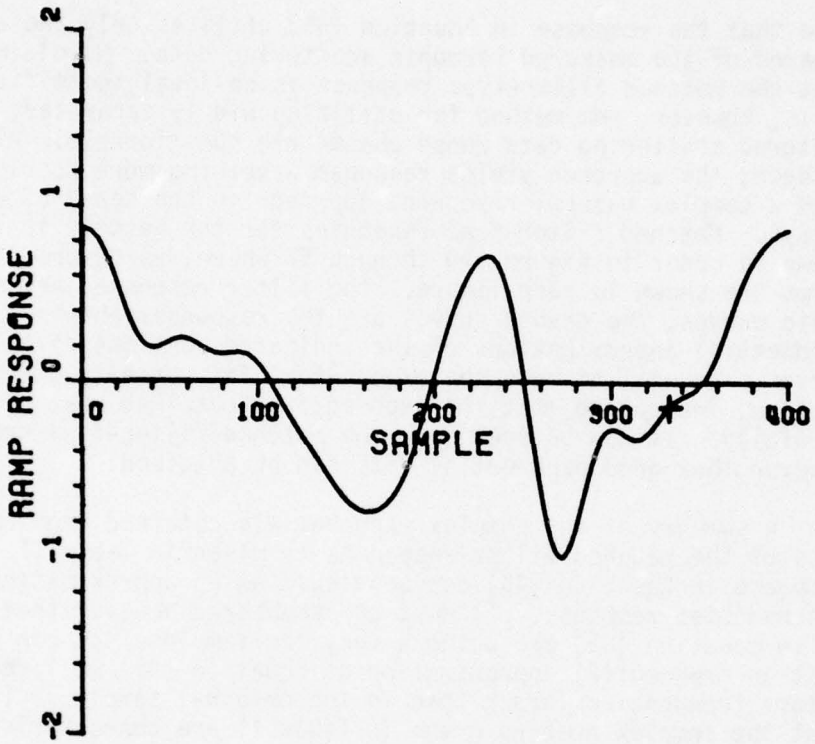

Figure 49(c). Shimokaze (1/700) - Starboard; Scale: 0.246.

$$f_{MO}(\theta,\phi,\hat{p},t) = \sum_{n=1}^{2N} \frac{|G(\theta,\phi,\hat{p},jn\omega_o)|^2}{n^2} \cos [n\omega_o t] \quad . \qquad (45)$$

Note that the response in Equation (45) utilizes only the amplitudes squared of the measured harmonic scattering data. No claim is made that the matched filter-type response is an ideal identification tool. It is, however, one method for utilizing widely separated, in frequency, measured scattering data whose phases are questionable. Also, as will be seen, the approach yields response waveforms more nearly compatible with a complex natural resonance approach in the sense of effecting decays. Matched filter-type responses for the vessels in Table I are shown in order in Figures 50 through 57 where, as before, three waveforms are shown in each figure. The filter responses are shown as solid curves; the dashed curves are the responses obtained from finite exponential approximations of the indicated portions of the solid curves. We will discuss the exponential fits briefly at the end of this section, indicating that the exponentials obtained must be interpreted carefully. It can be seen from the matched filter-type responses however that good exponential fits can be obtained.

A summary of the complex exponentials obtained from approximate fits of the matched filter responses is given in Table II. The response in Equation (45) can be viewed as an approximation to a matched step response. It must be remembered however that calculations as in Equation (45) are using a very few samples. It can be anticipated that an exponential approximation of Equation (45) will require oscillatory frequencies larger than in the original samples. It is maintained that the complex numbers given in Table II are characteristic of the vessels but no attempt to associate the numbers with particular component structures is made. In a following section it is shown that discrimination of the vessels can be achieved using the numbers in Table II and a predictor-correlator processing. However, Table II shows that the numbers are not yet excitation invariant. Swept frequency measurements over the same bandwidth covered by the discrete samples would be desirable and are planned for the future. An example of one such measurement has been made. Two 1/700 scale models of the Missouri were connected at the waterline using RF conducting tape. This forms a target-image pair. This configuration was then placed in a string holder used for free space swept frequency measurements. A bi-static angle of approximately 35° was used. Magnitude and phase information were recorded covering the 2150 to 4000 MHz frequency range for both vertical and horizontal polarization (results shown in Figures 58 and 59 respectively). Polarization is with respect to the plane of the target-image junction. The bistatic separation is in the plane orthogonal to the polarization vectors. For horizontal polarization, three regions (large response resonances) are of interest for both bow-on and stern-on incidence while nothing really significant is seen at broadside. Virtually the same situation exists for vertical polarization. It is true that certain modes are missing with this type of modeling but these would be included with the target on the ground plane.

TABLE II

COMPLEX POLES FROM SHIP DATA*
(Listed in order of decreasing residue magnitude)

Ship	Bow	Stern	Starboard
Midway (1/500)	-5.83±j26.1 8.01±j75.6 -147±j0.00	-18.2±j34.9 -36.7±j81.5 -5.52±j126 26.2±j29.2	-2.13±j27.2 -1.10±j0.00 -2.42±j74.0
Missouri (1/500)	-7.93±j9.70 -11.7±j107 -5.81±j5.98 2.89±j135	0.795±j13.2 -82.7±j0.00 -15.4±j87.4	-3.65±j12.4 -124±j0.00 -11.3±j79.1
Sverdlov (1/500)	-7.31±j26.0 5.84±j0.00 -1.13±j101	-0.168±j13.5 -12.9±j71.7 -66.4±j192	-26.4±j18.2 2.09±j0.00 -12.9±j95.1
Missouri (1/700)	-0.811±j8.78 -1.83±j42.3 -28.0±j137	-1.05±j9.29 -2.02±j0.00 -4.99±j96.5	-19.1±j0.00 -50.8±j0.00 -18.3±j74.1 0.320±j0.00
Bismark (1/700)	-15.6±j27.0 -24.2±j98.9 3.15±j74.7 15.5±j18.0	-16.4±j0.00 -0.753±j33.3 -30.2±j89.8 7.24±j0.00	-3.43±j18.6 -63.4±j0.00 -24.2±j61.7
Mogami (1/700)	-5.18±j15.6 -146-j137 -4.46±j28.1	-0.938±j7.03 -37.0±j0.00 -2.89±j88.6	-4.90±j8.33 -3.38±j45.2 -31.3-j137
Hayanami (1/700)	-1.63±j19.3 -2.15±j38.9 -3.27±j97.7	-1.66±j19.1 -1.20±j41.5 -5.37±j91.0	-10.3±j39.5 -1.88±j17.5 -10.5±j65.2 -2.84±j97.6
Shimokaze (1/700)	-5.76±j28.8 -4.97±j50.9 -0.724±j95.6 2.92±j0.00 5.85±j89.3	-6.33±j30.6 -44.4±j40.8 -8.42±j95.1	-16.7±j20.6 -25.8±j65.4 -1.60±j54.8 -2.96±j99.2

*The poles are scaled such that the imaginary parts are in MHz.

DATA FILE: SHP27
DATA ID : MIDWAY(1/500)-BOW ON
SHIFT : 0.0
NSTART : 1
NLAST : 200
POLES : 5
VSCALE : 14.673
NRMS ERR : 0.017858

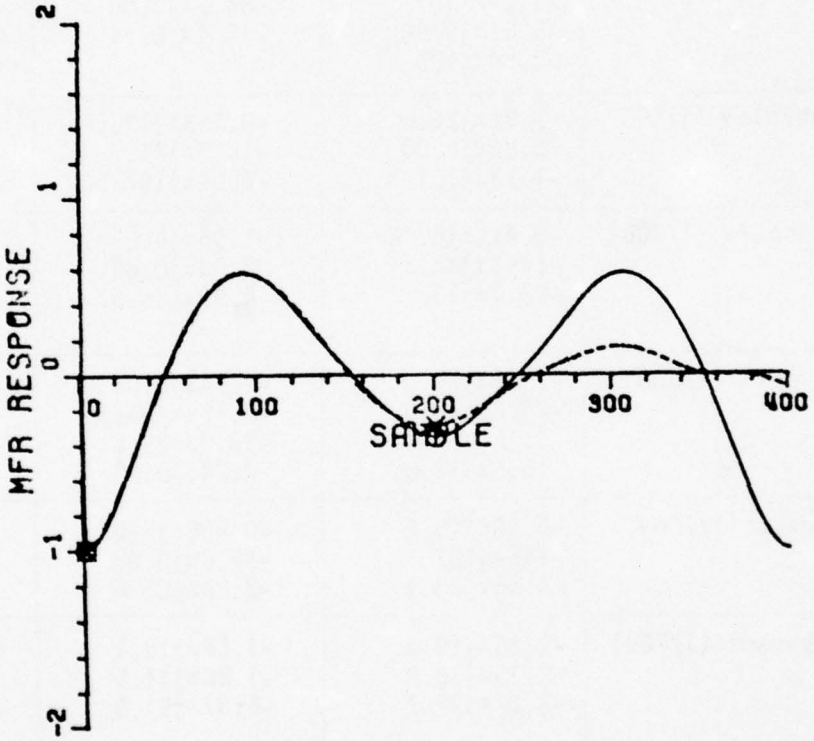

Figure 50(a)

DATA FILE: SHP28
DATA ID : MIDWAY (1/500) -STERN
SHIFT : 0.0
NSTART : 1
NLAST : 200
POLES : 8
VSCALE : 4.751
NRMS ERR : 0.029719

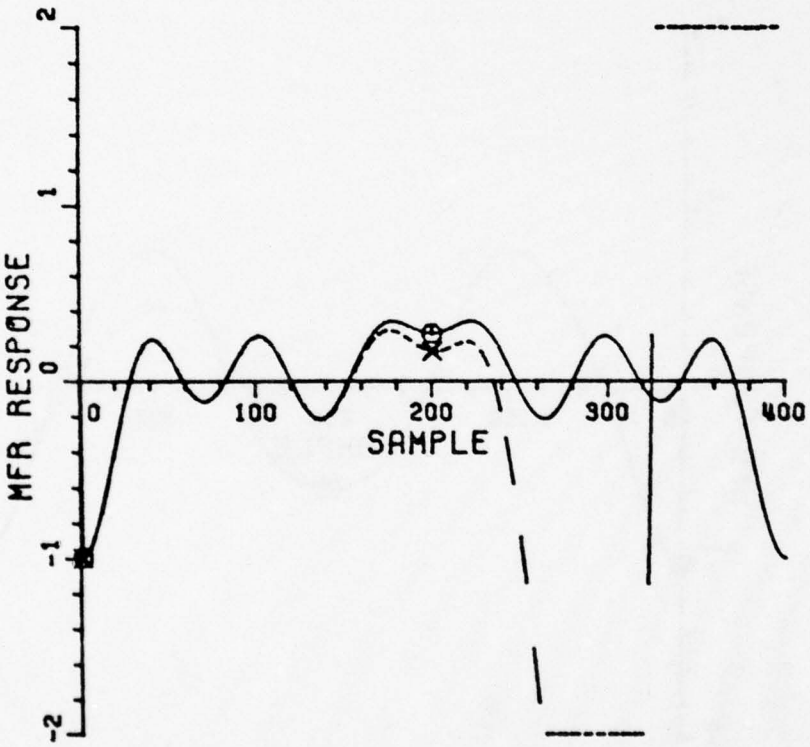

Figure 50(b)

DATA FILE: SHP30
DATA ID : MIDWAY(1/500)-STARBOARD
SHIFT : 0.0
NSTART : 1
NLAST : 200
POLES : 5
VSCALE : 586.824
NRMS ERR : 0.006126

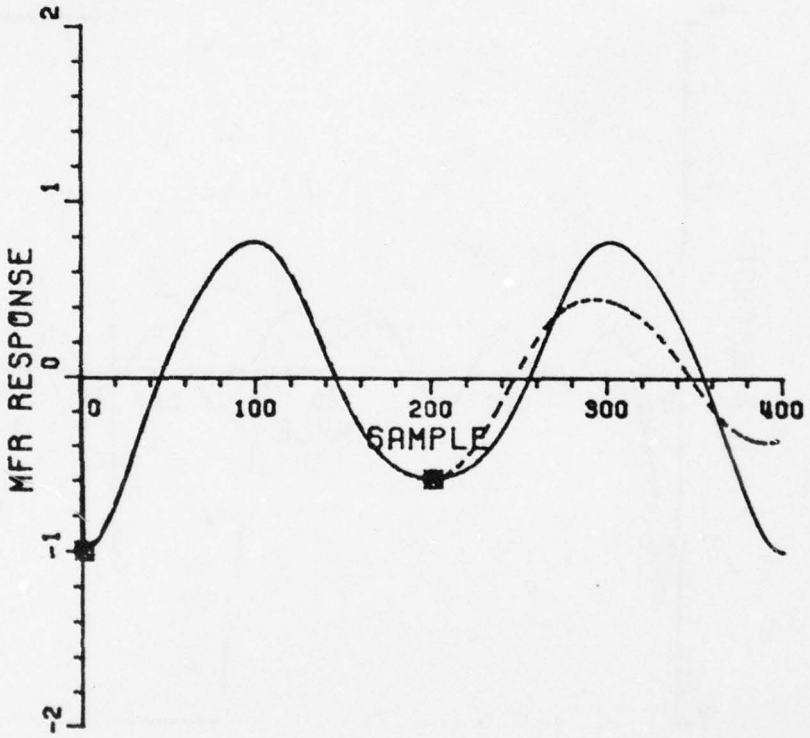

Figure 50(c)

DATA FILE: SHP1
DATA ID : MISSOURI(1/500)-BOW ON
SHIFT : 0.0
NSTART : 1
NLAST : 200
* POLES : 8
VSCALE : 4.404
NRMS ERR : 0.013600

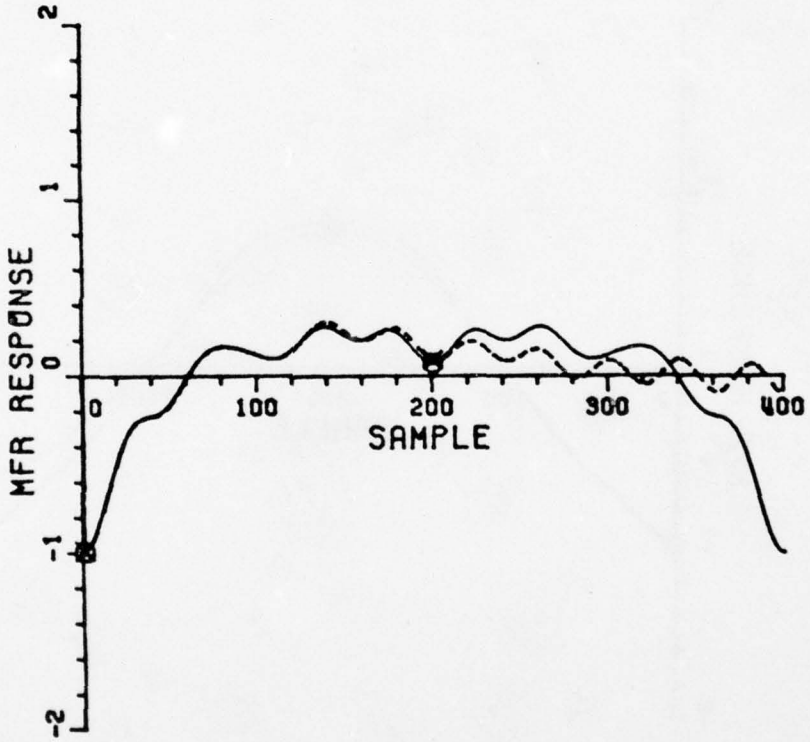

Figure 51(a)

```
DATA FILE:  SHP21
DATA ID   :  MISSOURI (1/500) -STERN
SHIFT     :  0.0
NSTART    :  1
NLAST     :  200
* POLES   :  5
VSCALE    :  6.953
NRMS ERR  :  0.035439
```

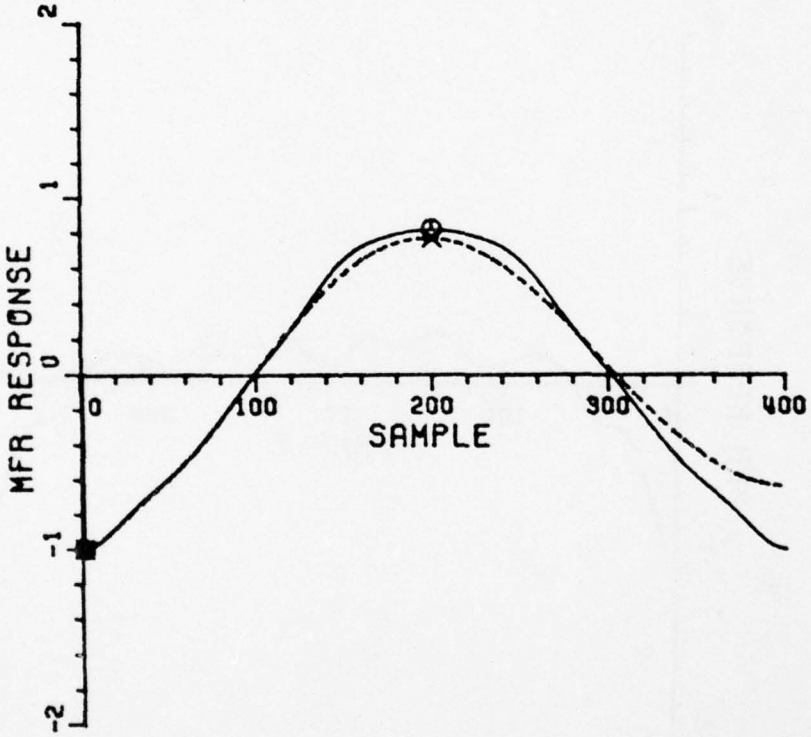

Figure 51(b)

DATA FILE: SHP23
DATA ID : MISSOURI (1/500) -STARBOARD
SHIFT : 0.0
NSTART : 1
NLAST : 200
* POLES : 5
VSCALE : 180.584
NRMS ERR : 0.019890

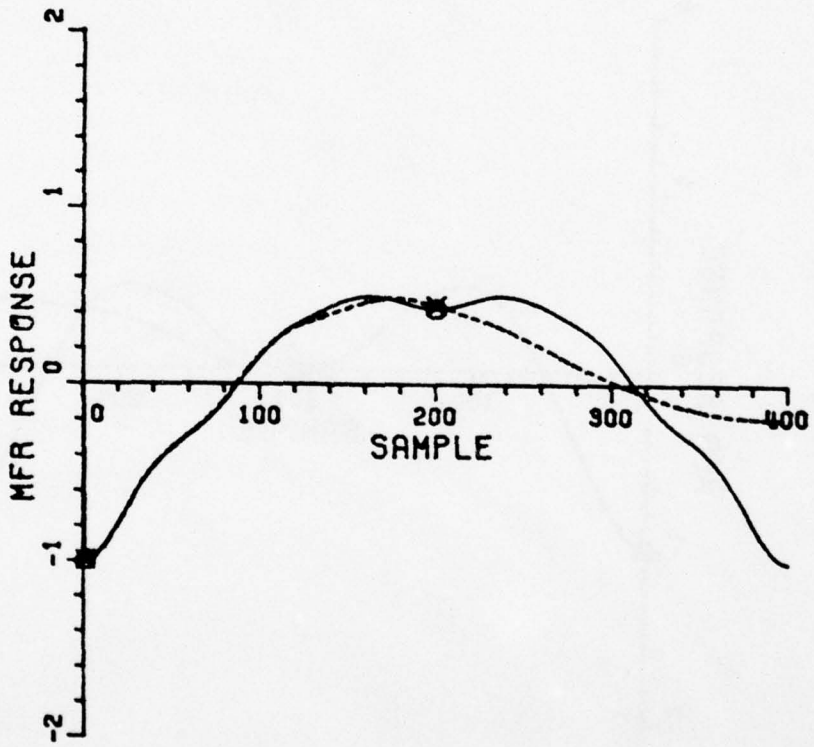

Figure 51(c)

DATA FILE: SHP2
DATA ID : SVERDLØV (1/500) -BØW ØN
SHIFT : 0.0
NSTART : 1
NLAST : 200
* PØLES : 5
VSCALE : 20.454
NRMS ERR : 0.008216

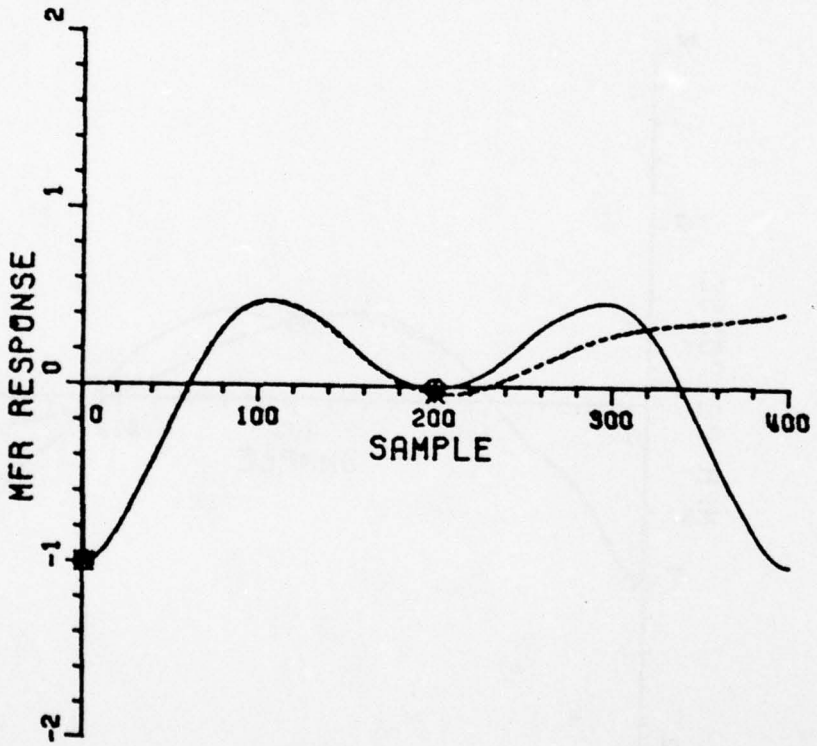

Figure 52(a)

DATA FILE: SHP25
DATA ID : SVERDLOV (1/500) -STERN
SHIFT : 0.0
NSTART : 1
NLAST : 200
* POLES : 5
VSCALE : 10.661
NRMS ERR : 0.004110

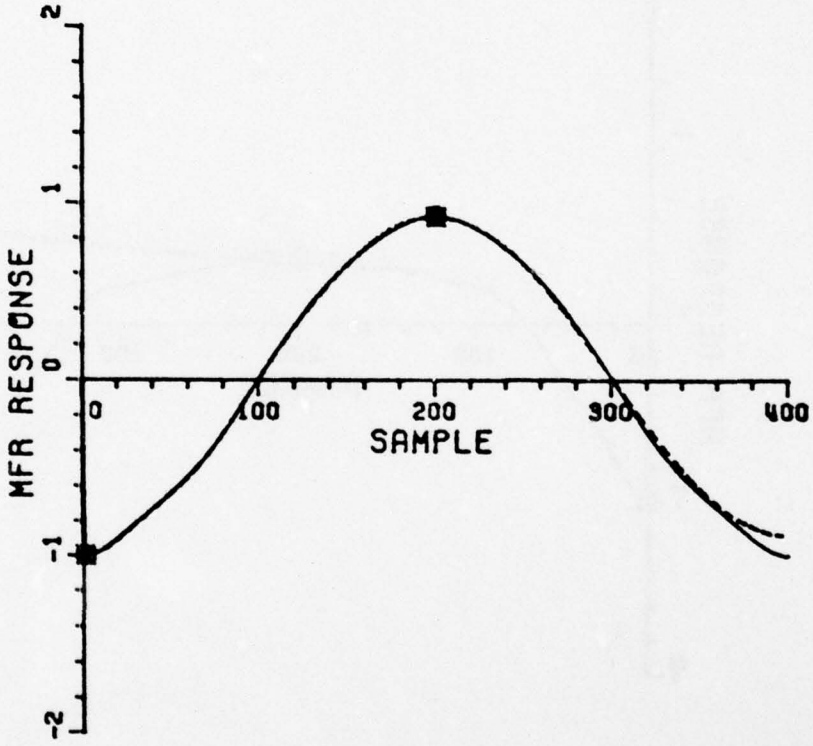

Figure 52(b)

DATA FILE: SHP26
DATA ID : SVERDLOV(1/500)-STARBOARD
SHIFT : 0.0
NSTART : 1
NLAST : 200
* POLES : 5
VSCALE : 104.963
NAMS ERR : 0.026664

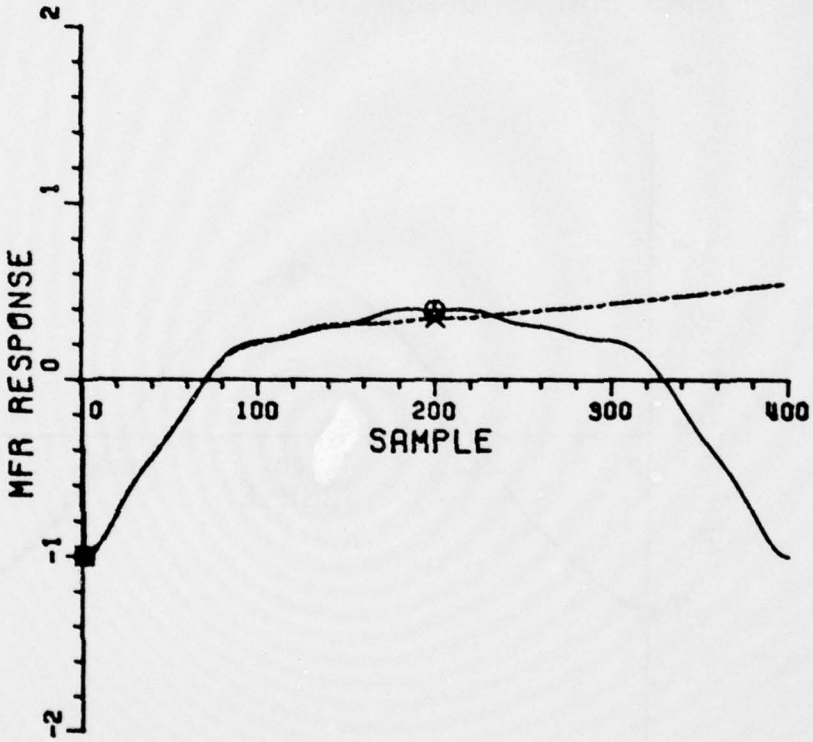

Figure 52(c)

DATA FILE: SHP15
DATA ID : MISSOURI (1/700) -BOW ON
SHIFT : 0.0
NSTART : 1
NLAST : 200
POLES : 5
VSCALE : 7.975
NRMS ERR : 0.041179

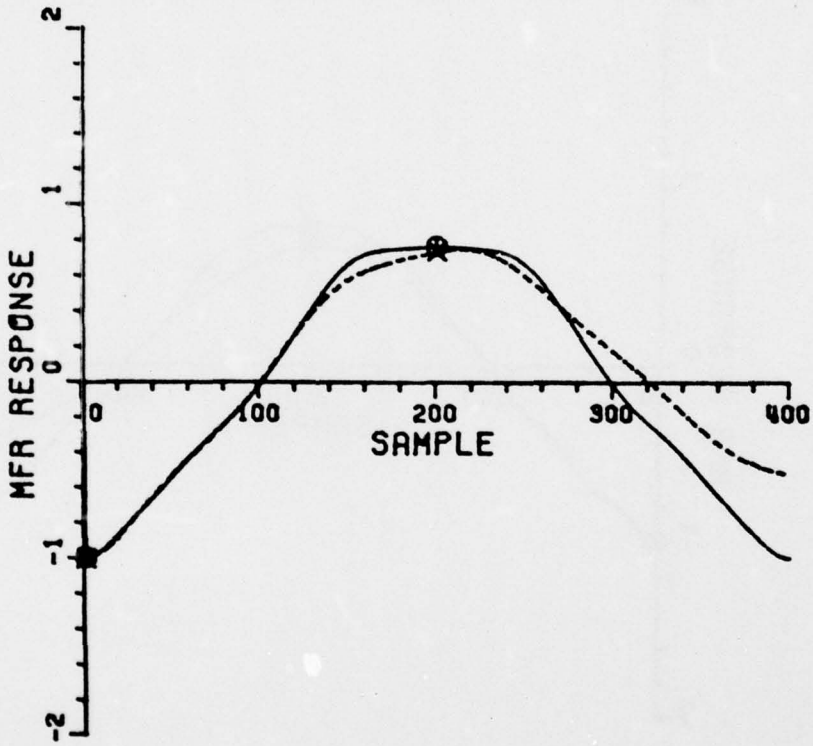

Figure 53(a)

DATA FILE: SHP16
DATA ID : MISSOURI (1/700) -STERN
SHIFT : 0.0
NSTART : 1
NLAST : 200
POLES : 5
VSCALE : 6.970
NRMS ERR : 0.066311

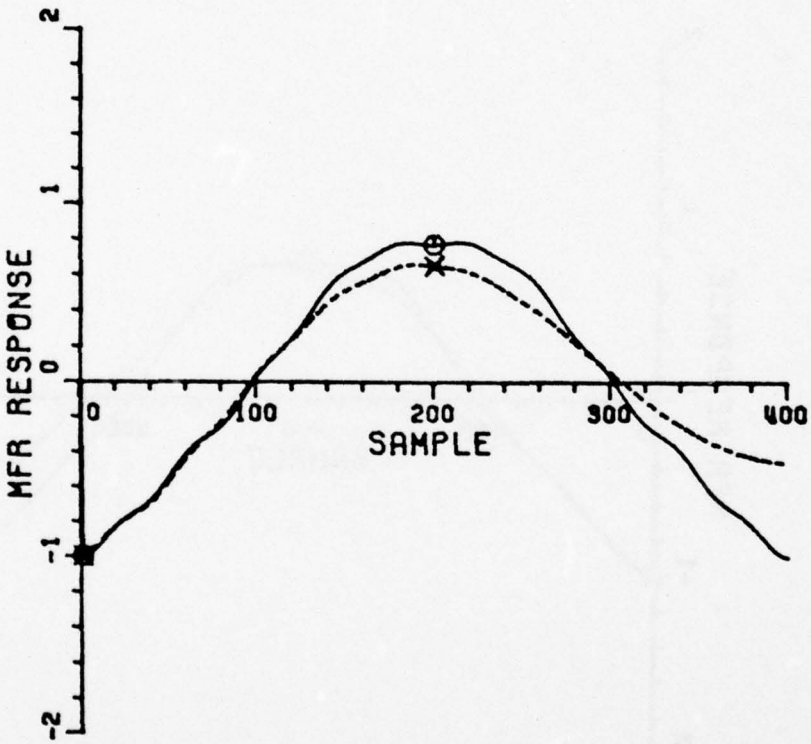

Figure 53(b)

DATA FILE: SHP17
DATA ID : MISSOURI (1/700) -STARBOARD
SHIFT : 0.0
NSTART : 1
NLAST : 200
POLES : 5
VSCALE : 47.930
NRMS ERR : 0.049238

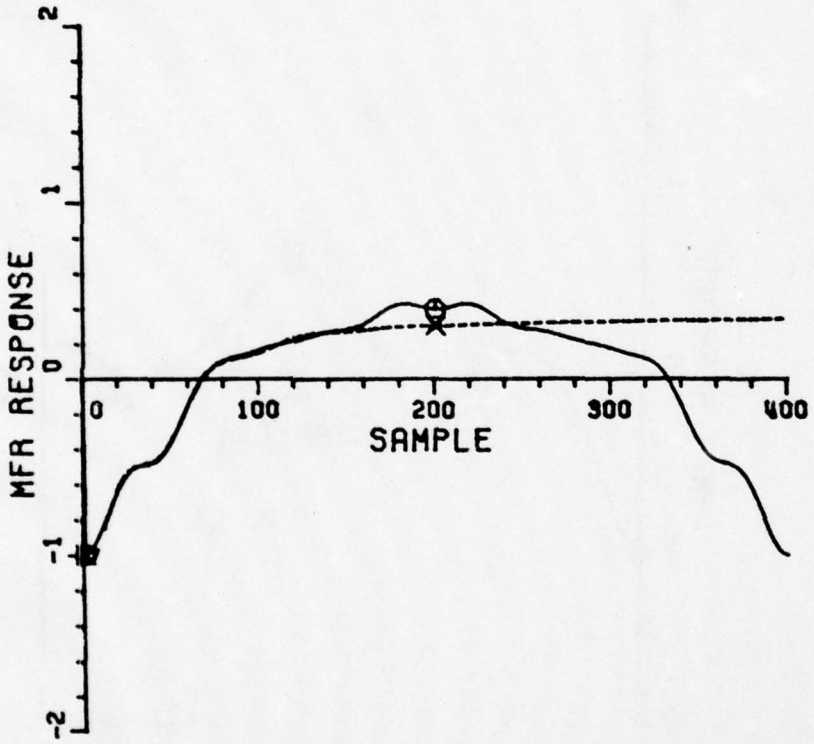

Figure 53(c)

DATA FILE: SHP3
DATA ID : BISMARK(1/700)-BOW ON
SHIFT : 0.0
NSTART : 1
NLAST : 200
POLES : 8
VSCALE : 2.871
NRMS ERR : 0.052903

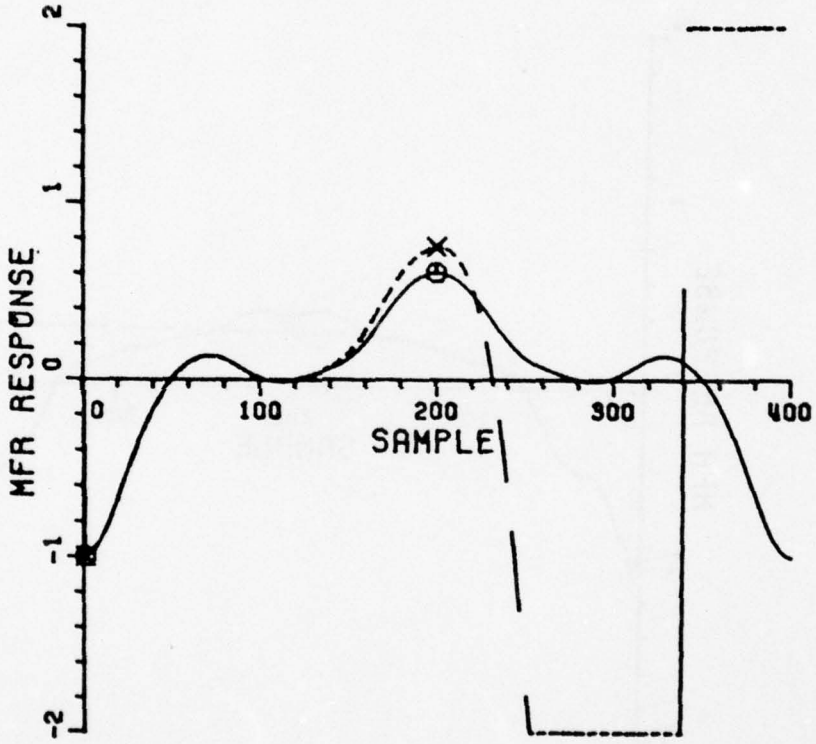

Figure 54(a)

DATA FILE: SHP20
DATA ID : BISMARK(1/700)-STERN
SHIFT : 0.0
NSTART : 1
NLAST : 200
POLES : 6
VSCALE : 2.597
NRMS ERR : 0.099977

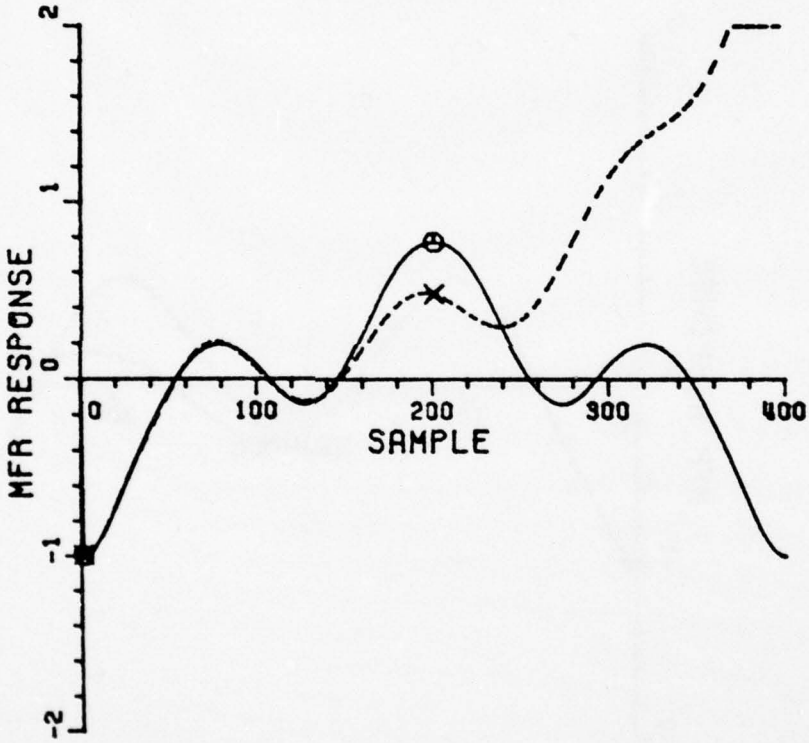

Figure 54(b)

DATA FILE: SHP5
DATA ID : BISMARK (1/700) -STARBOARD
SHIFT : 0.0
NSTART : 1
NLAST : 200
* POLES : 5
VSCALE : 69.311
NRMS ERR : 0.018386

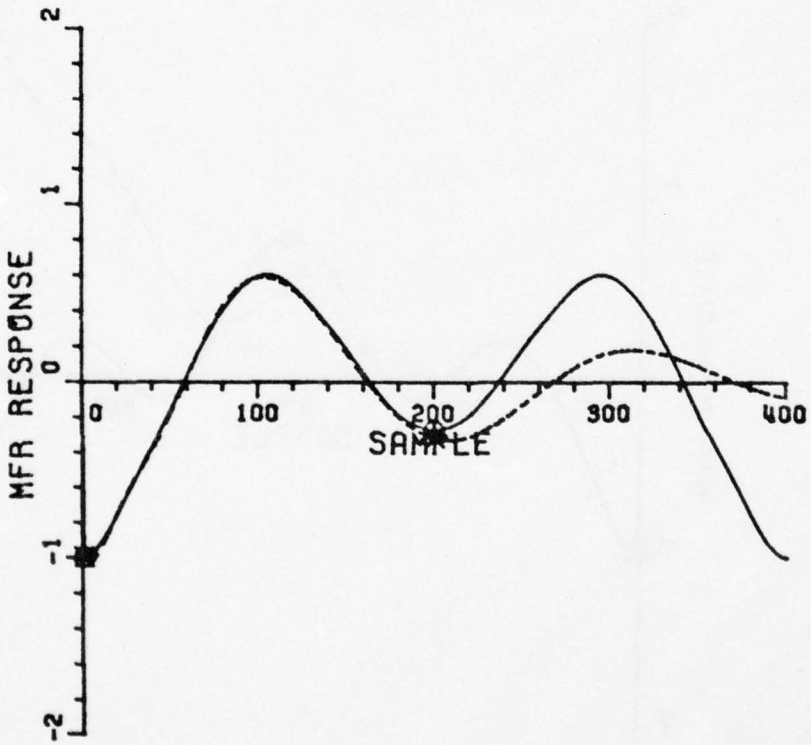

Figure 54(c)

DATA FILE: SHP4
DATA ID : MOGAMI (1/700) -BOW ON
SHIFT : 0.0
NSTART : 1
NLAST : 200
* POLES : 5
VSCALE : 13.045
NRMS ERR : 0.010912

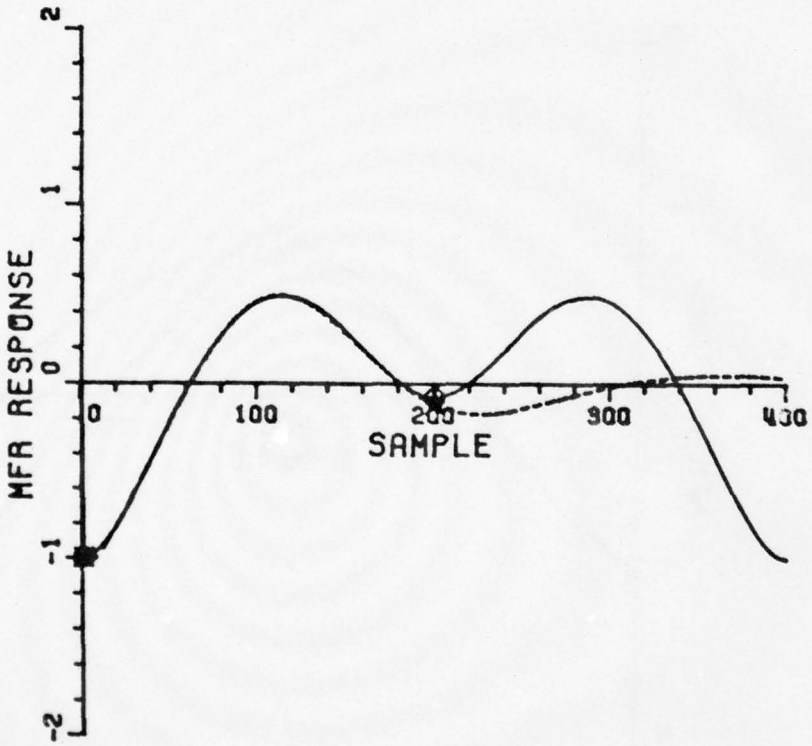

Figure 55(a)

AD-A050 047 OHIO STATE UNIV COLUMBUS ELECTROSCIENCE LAB F/G 17/9
RADAR IDENTIFICATION OF NAVAL VESSELS.(U)
DEC 77 D L MOFFATT, C M RHOADS N00014-76-C-1079
UNCLASSIFIED ESL-784558-1 NL

2 OF 2
ADA
050047

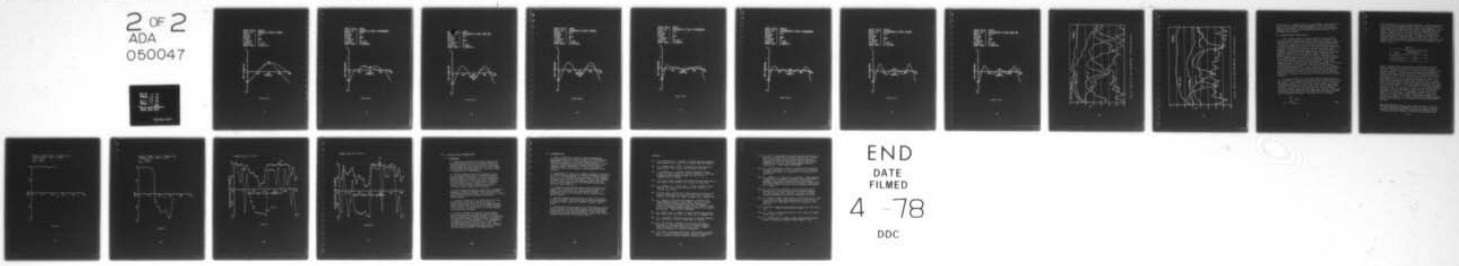

END
DATE
FILMED
4 78
DDC

DATA FILE: SHP19
DATA ID : MOGAMI (1/700) -STERN
SHIFT : 0.0
NSTART : 1
NLAST : 200
* POLES : 5
VSCALE : 1.173
NRMS ERR : 0.057112

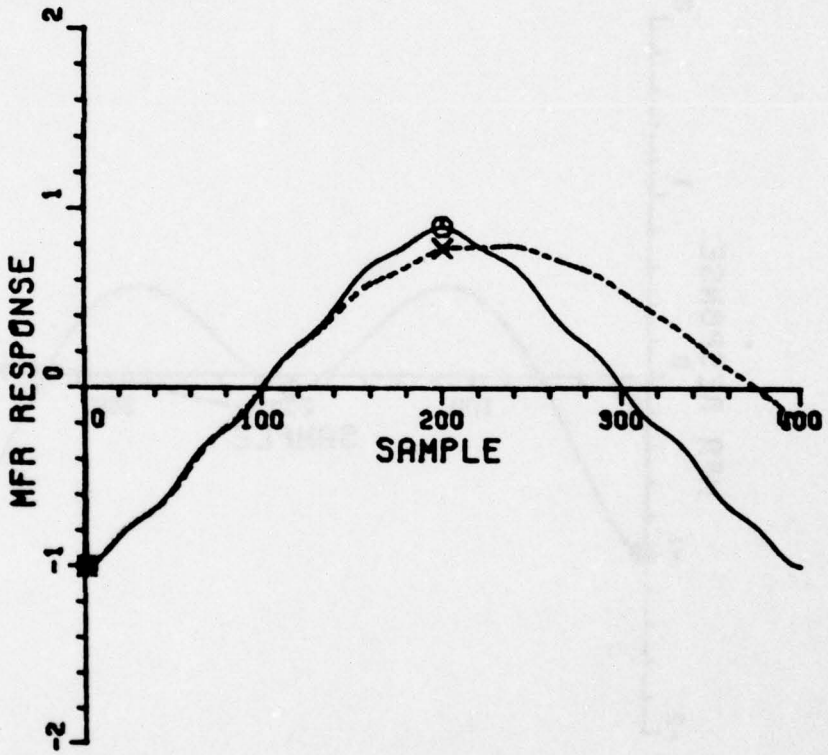

Figure 55(b)

DATA FILE: SHP6
DATA ID : MOGAMI (1/700) -STARBOARD
SHIFT : 0.0
NSTART : 1
NLAST : 200
* POLES : 5
VSCALE : 33.471
NRMS ERR : 0.030653

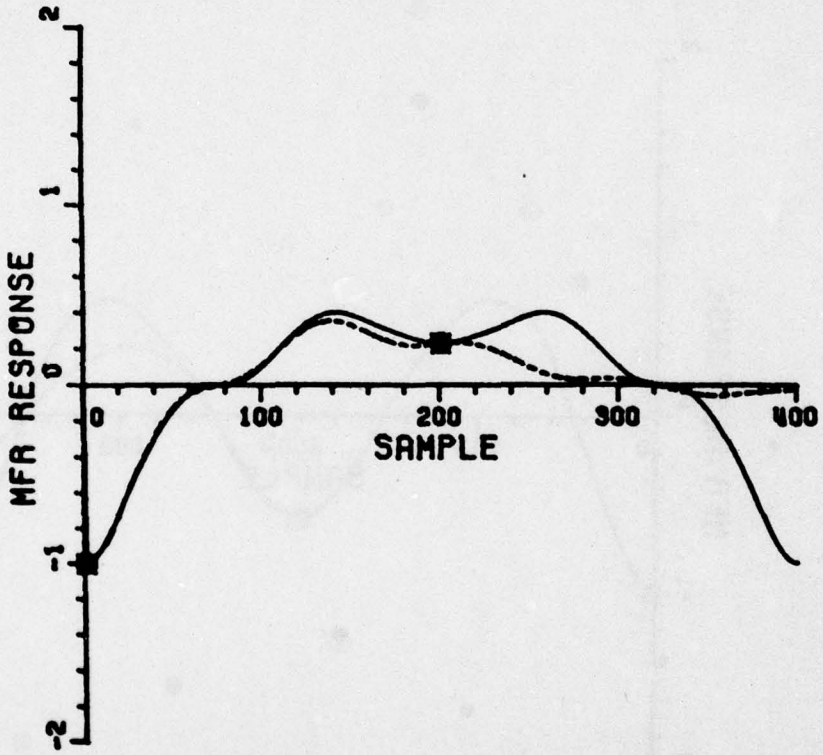

Figure 55(c)

DA[illegible]ILE: SHP7
DA[illegible]ID : HAYANAMI (1/700) -BOW ON
SHIFT : 0.0
NSTART : 1
NLAST : 200
POLES : 6
VSCALE : 1.512
NRMS ERR : 0.002519

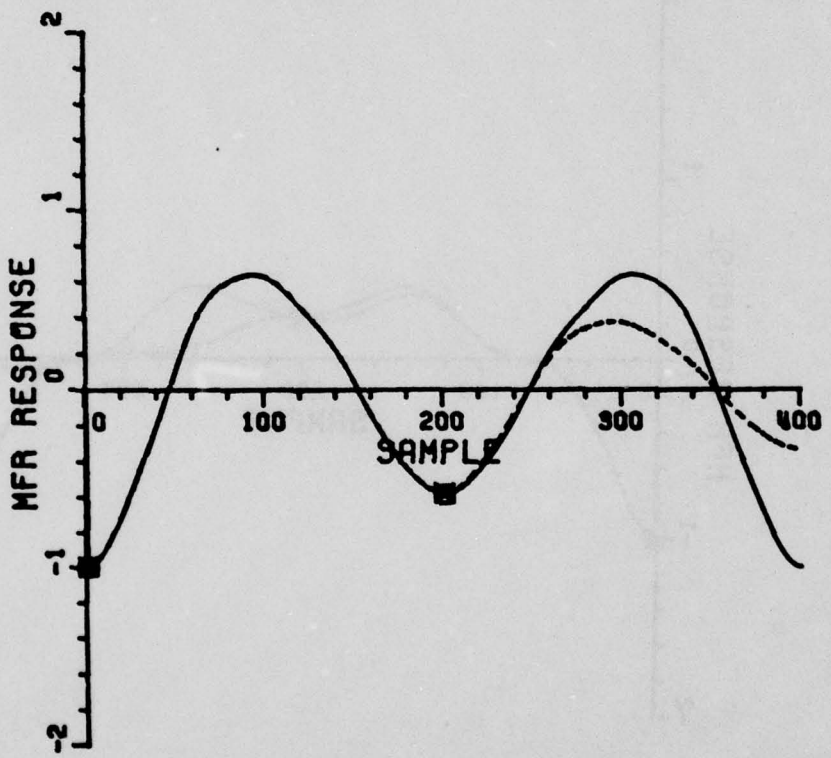

Figure 56(a)

DATA FILE: SHP8
DATA ID : HAYANAMI (1/700) -STERN
SHIFT : 0.0
NSTART : 1
NLAST : 200
* POLES : 6
VSCALE : 1.035
NRMS ERR : 0.007523

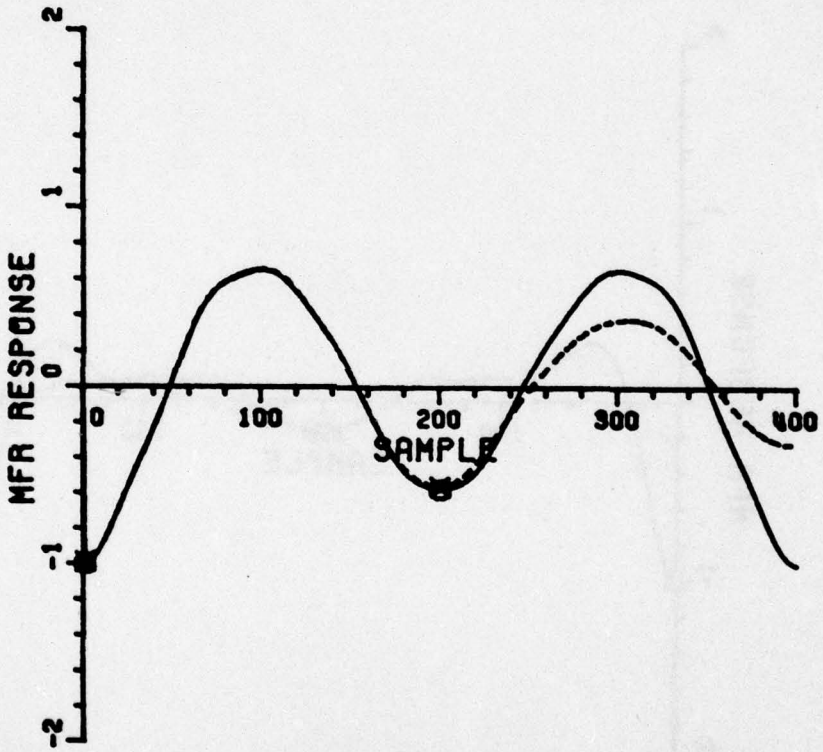

Figure 56(b)

DATA FILE: SHP9
DATA ID : HAYANAMI (1/700) -STARBOARD
SHIFT : 0.0
NSTART : 1
NLAST : 200
* POLES : 8
VSCALE : 14.073
NRMS ERR : 0.002537

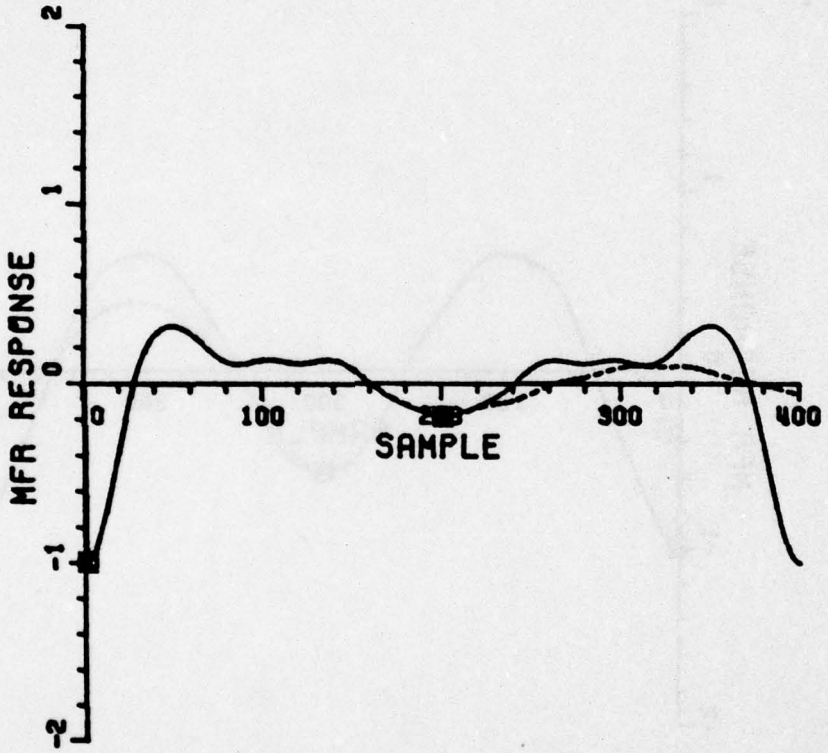

Figure 56(c)

DATA FILE: SHP13
DATA ID : SHIMOKAZE (1/700) -STARBOARD
SHIFT : 0.0
NSTART : 1
NLAST : 200
POLES : 8
VSCALE : 7.932
NRMS ERR : 0.004747

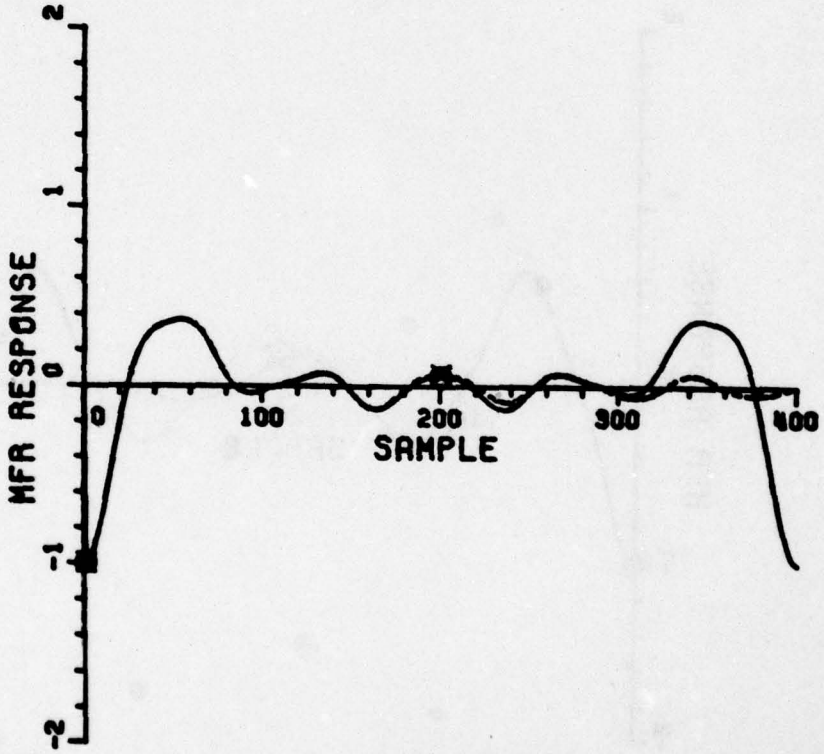

Figure 57(a)

DATA FILE: SHP12
DATA ID : SHIMOKAZE (1/700) -STERN
SHIFT : 0.0
NSTART : 1
NLAST : 200
POLES : 6
VSCALE : 0.376
NRMS ERR : 0.017830

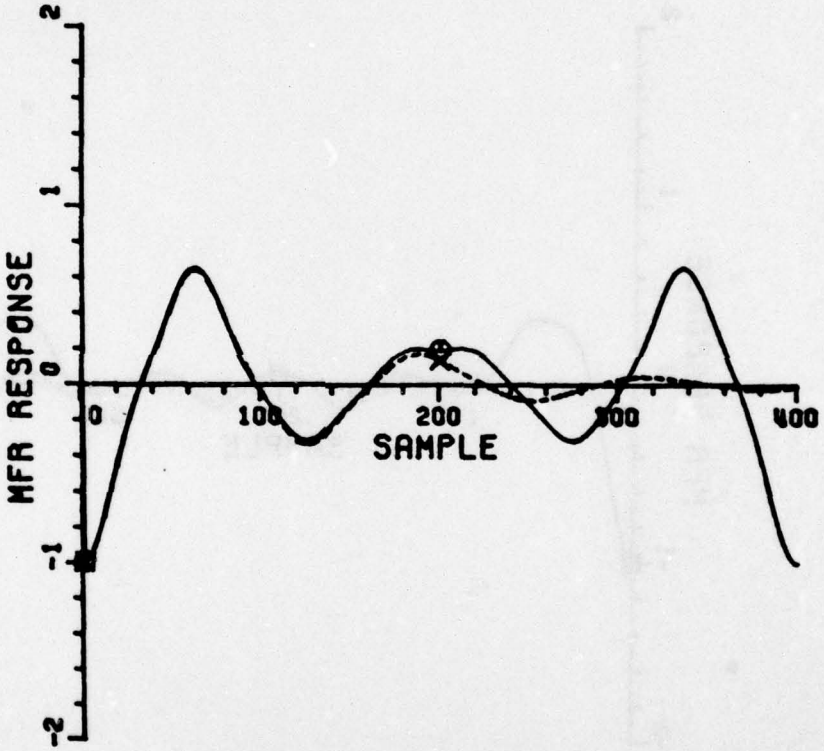

Figure 57(b)

DATA FILE: SHP11
DATA ID : SHIMOKAZE (1/700) -BOW ON
SHIFT : 0.0
NSTART : 1
NLAST : 200
* POLES : 9
VSCALE : 0.315
NRMS ERR : 0.001213

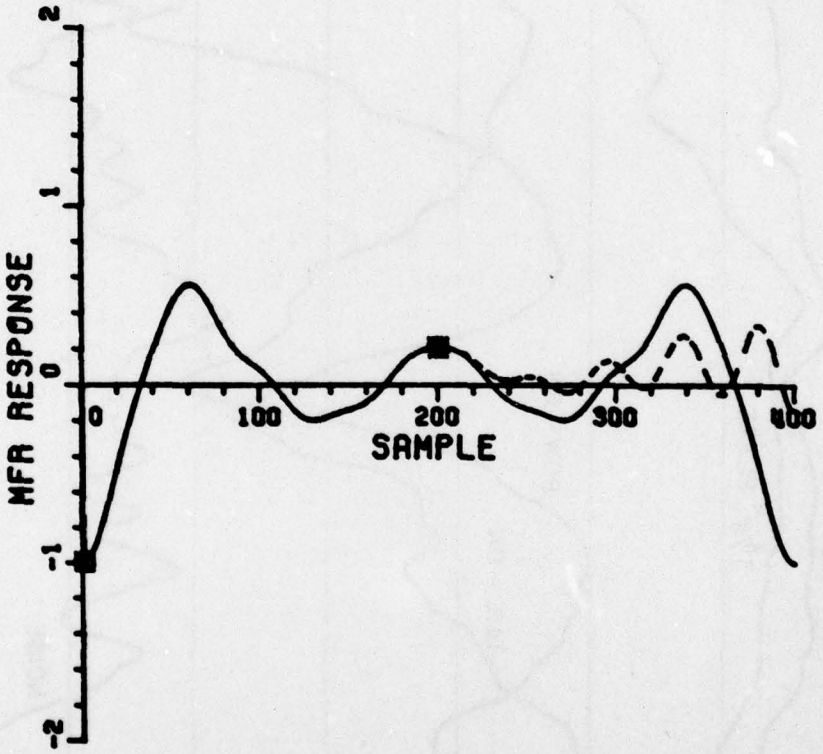

Figure 57(c)

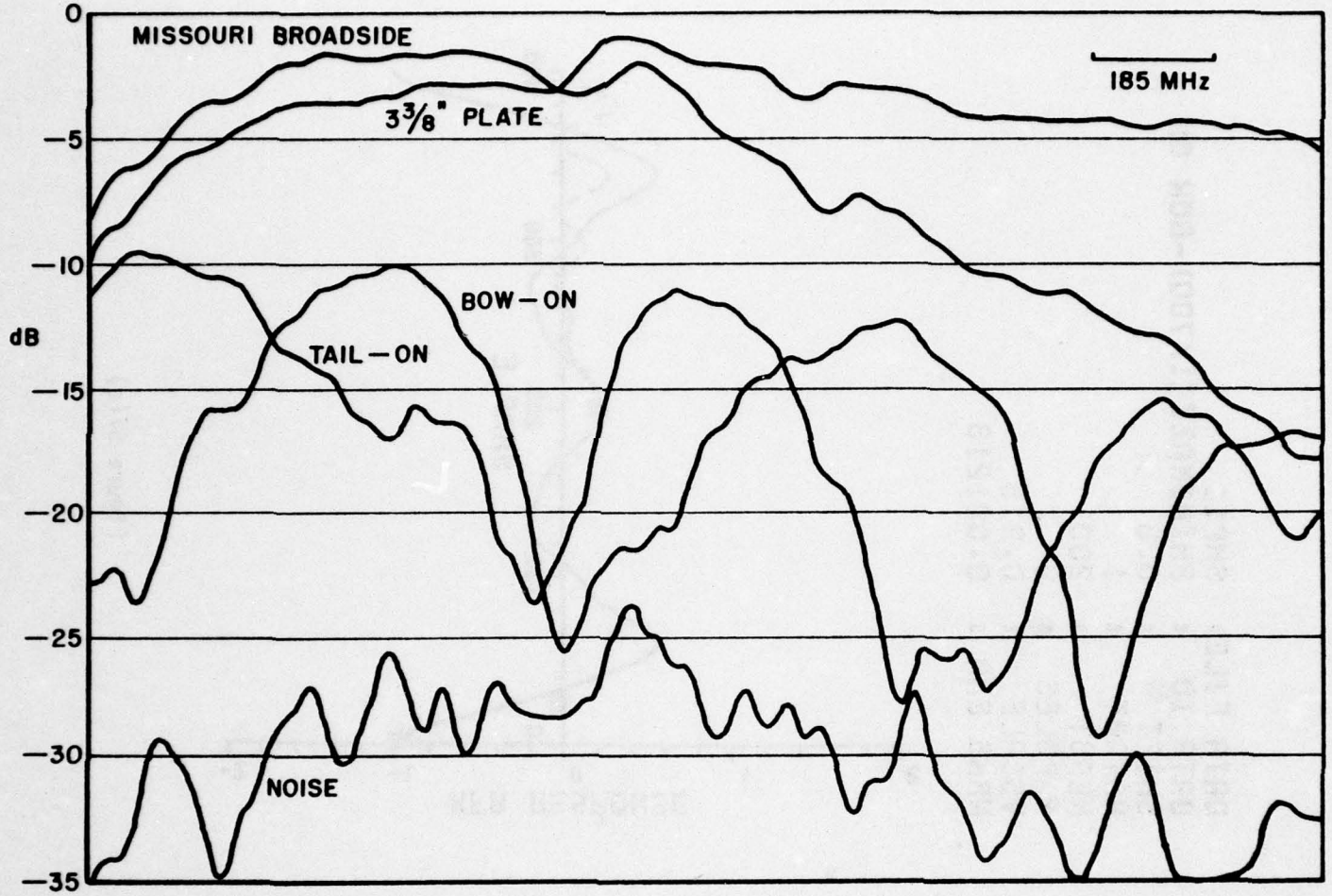

Figure 58. Missouri with image (2150-4000 MHz). Horizontal polarization.

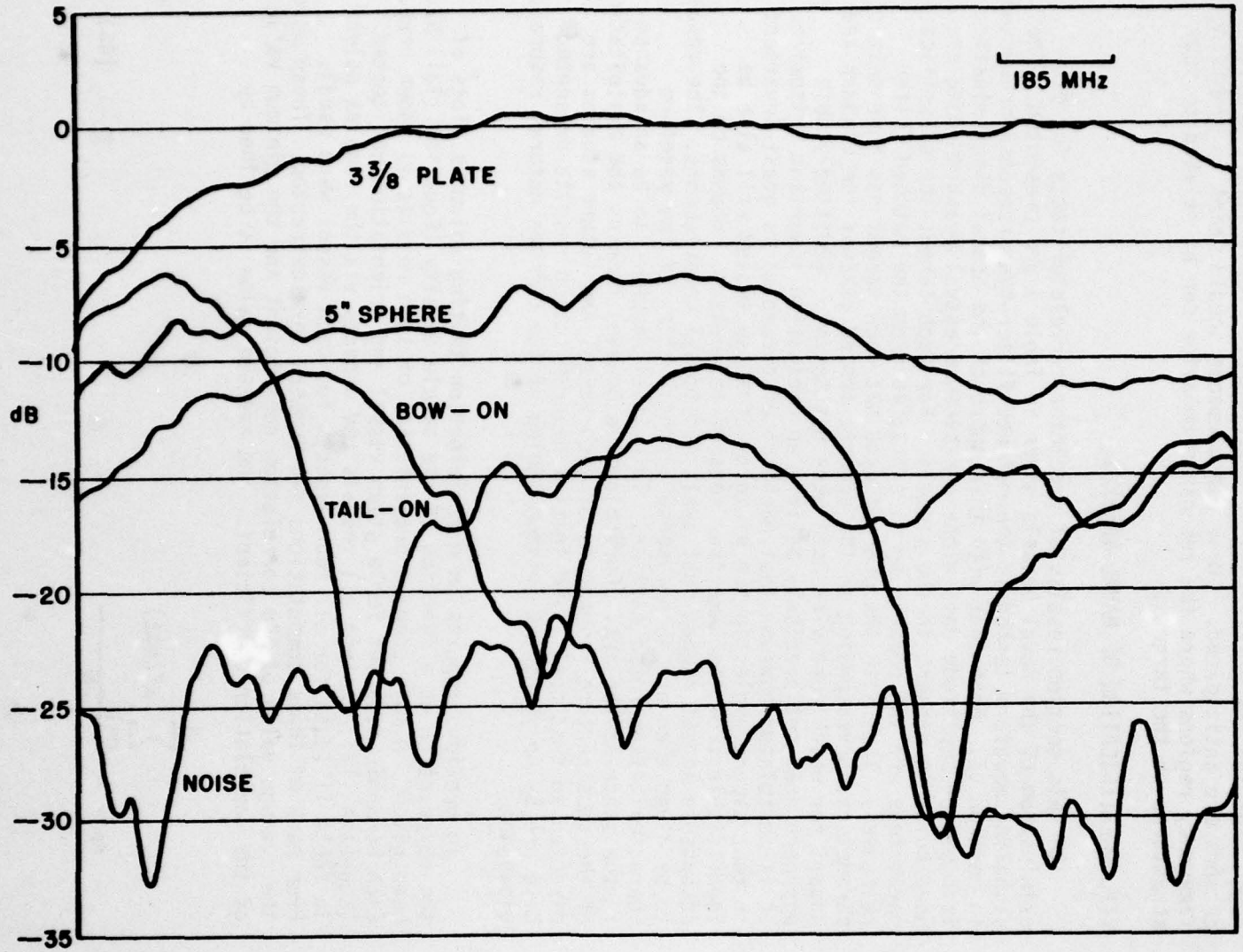

Figure 59. Missouri with image (2150-4000 MHz). Vertical polarization.

At this time it is planned to make such measurements on the ground plane range used for the multifrequency measurements. Only slight modifications are anticipated. These measurements should point to promising frequency regions where the resonance behavior can be related to substructures on the targets.

VII. IDENTIFICATION OF NAVAL VESSELS

In this section results of predictor-correlator tests for discrimination of the naval vessels given in Table I are presented. The signaling waveform tested is the matched filter-type response presented in Section VI. Note that with this approach the actual discrimination is based on amplitude data alone and because actual measured data are used noise is present in the signals. For each target the classification parameters are the complex poles extracted from the matched filter responses. Thus with the present data set each target has four sets of parameters corresponding to the aspects tested (except the Bismark and Mogami for which port view data were not taken). Admittedly this approach does not precisely satisfy an excitation invariant criterion. It is postulated however that each set of parametes is quasi-invariant in that aspect angles in the vicinity of those tested will also be identifiable from the same four sets of parameters. Bounds on the acceptable aspect ranges must await additional measurements. The results to be given then are in one sense a confirmation of the waveform characterization noted earlier. This itself appears to be an advance in the state-of-the-art. Our objective however remains the exploitation of the substructure resonances of each vessel and future studies are directed to that goal. The initial discrimination results presented here are by no means the optimum honing of the complex natural resonance viewpoint.

In previous reports on discrimination testing volumous plots of the correlation as a function of the sample density (Equation (13)) have been given. A more compact presentation of such results is shown here. Each harmonic data set for a given vessel and orientation was tested (Equation (13)) against all vessels and aspects via the complex poles in Table II (data for all four aspects for each vessel were used). From each of these computations two numbers were extracted. These were the average value of the correlation coefficient and the minimum value of the correlation coefficient. The average value is defined by

$$\langle \rho'' \rangle = \frac{\sum_{n=1}^{N} \rho''(n\Delta t)}{N} \tag{46}$$

where the summation is over all sample densities. A search was done for each of these correlation parameters for each vessel aspect to obtain the pole set which yielded the largest value for each parameter. Thus two simple identification parameters were tested. Two example plots are shown in Figures 60 and 61. In both cases the harmonic data for the Missouri (1/500) as viewed from bow-on was used. In Figure 60 the poles of the above data set were used. In Figure 61 the poles taken from the Shimokaze as viewed from the stern were used. Table III summarizes the results based on predictor-correlator processing of thirty harmonic data sets and thirty complex pole sets of all aspects of the ships in Table I.*

TABLE III

Method	Probability of Correct Classification
Maximize $<\rho''>$	0.77
Maximize (ρ''_{min})	0.70

There is obviously some risk involved in results based on a single number as opposed to thresholds selected over a range of sample densities. Nevertheless Table III is felt to be a fair estimate of our present capability. Figure 62 shows the results of the predictor-correlator processing of all pole sets with the harmonic data of the (1/500) scale Missouri viewed from bow on. The solid curve (actually the marked points) is for $<\rho''>$ and the dashed line for (ρ''_{min}). For these harmonic data the correct pole set was number one and it can be seen that both parameters yielded correct identification. It might appear that (ρ''_{min}) would be a more effective discrimination tool based on this isolated example. This may be somewhat misleading since based on the results of Table III it is felt that $<\rho''>$ is the more effective parameter of the two. An example of this is shown in Figure 63 where the harmonic data for the Mogami as viewed from the stern has been compared to all pole sets. For these data the correct pole-set is number 19. For this example, identification based on (ρ''_{min}) fails since pole-set number 16 was chosen. Identification based on $<\rho''>$, however, was successful. It is also felt that the averaging procedure should be less susceptible to noise than the one-point minimization procedure.

*The thirty data sets represent four views of all ships in Table I except the Bismark and the Mogami for which port data was not taken. The poles taken from the port view data are not listed in Table II since they are nearly identical to those for the starboard views.

Missouri (1/500) - Bow On ----Harmonic Data
Missouri (1/500) - Bow On ----Poles
$\langle \rho'' \rangle = 0.9956$
$\rho''_{min} = 0.9461$

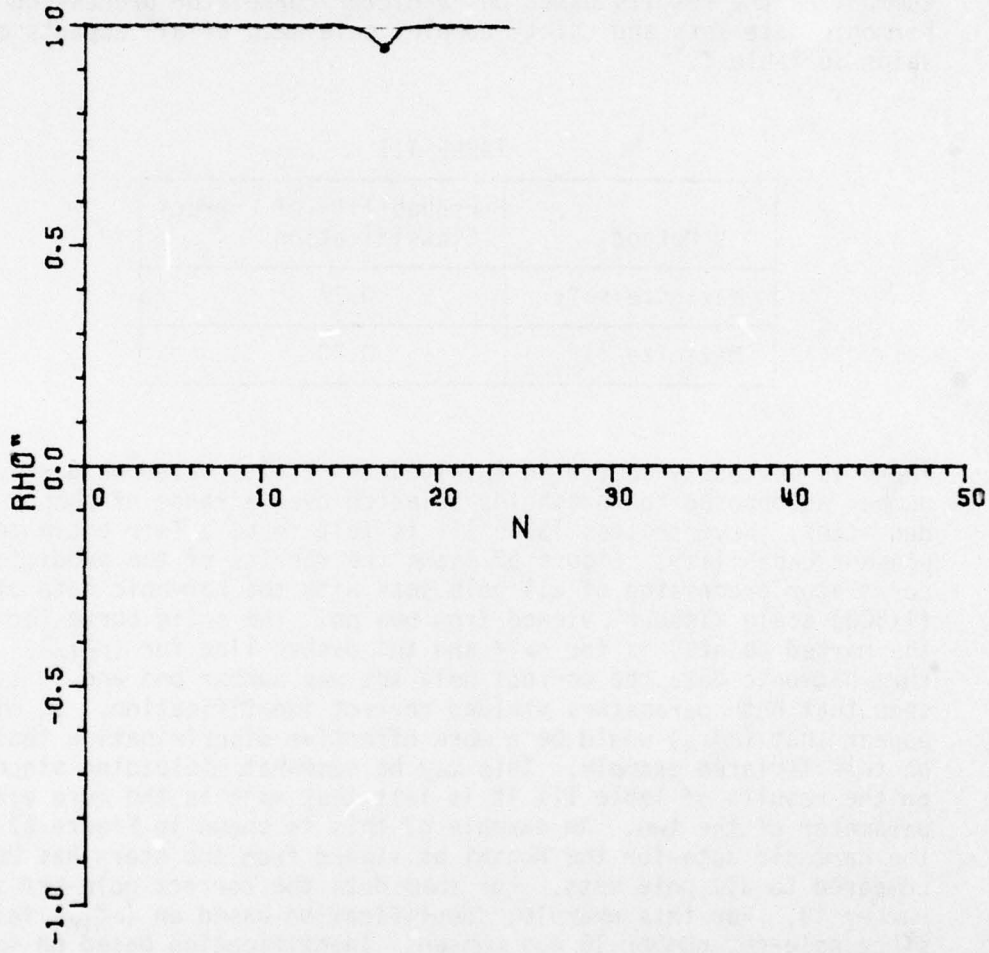

Figure 60

Missouri (1/500) - Bow On ----Harmonic Data
Shimokaze (1/700) - Stern ----Poles
$\langle \rho'' \rangle = 0.1072$
$\rho''_{min} = 0.9164$

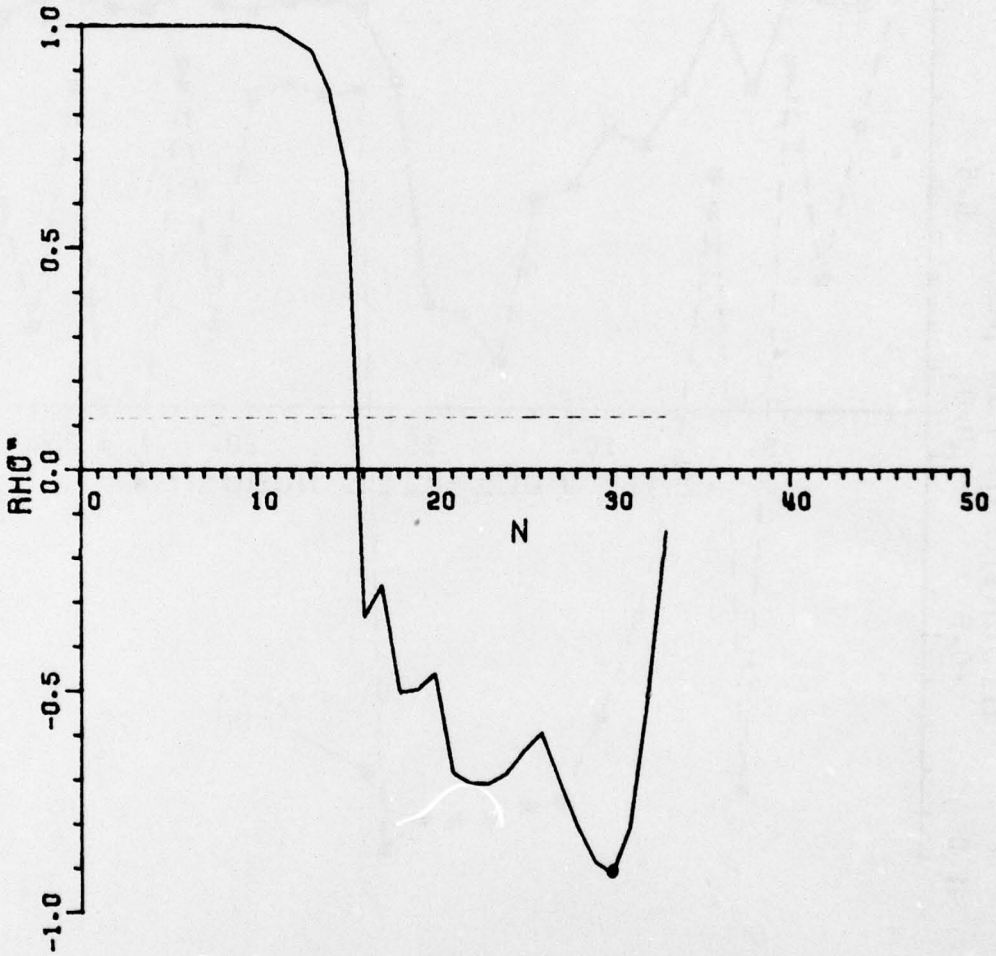

Figure 61

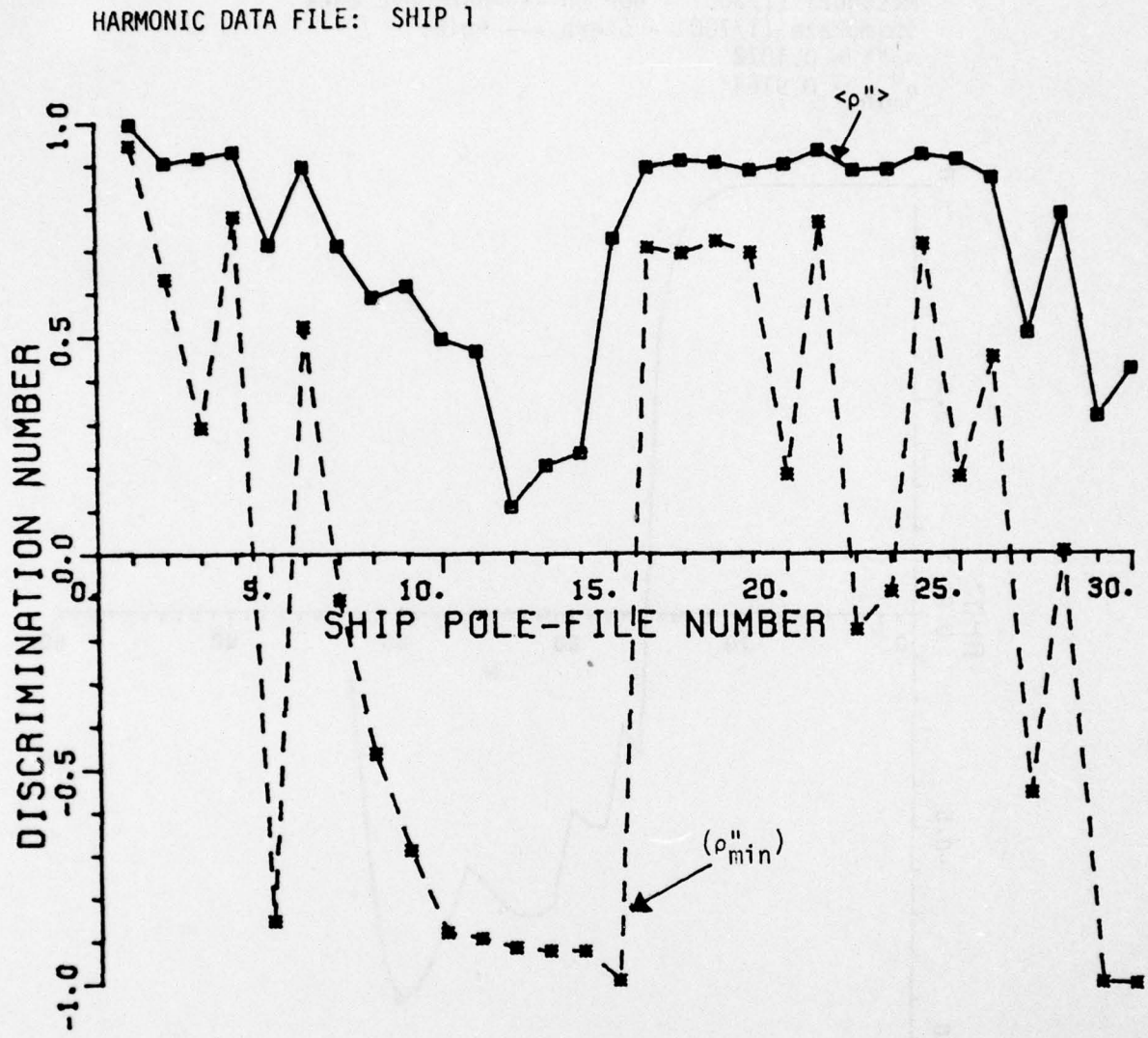
HARMONIC DATA FILE: SHIP 1
<ρ">
DISCRIMINATION NUMBER
1.0
0.5
0.0
-0.5
-1.0
0
5.
10.
15.
20.
25.
30.
SHIP POLE-FILE NUMBER
(ρ"min)

Figure 62

HARMONIC DATA FILE: SHIP 19

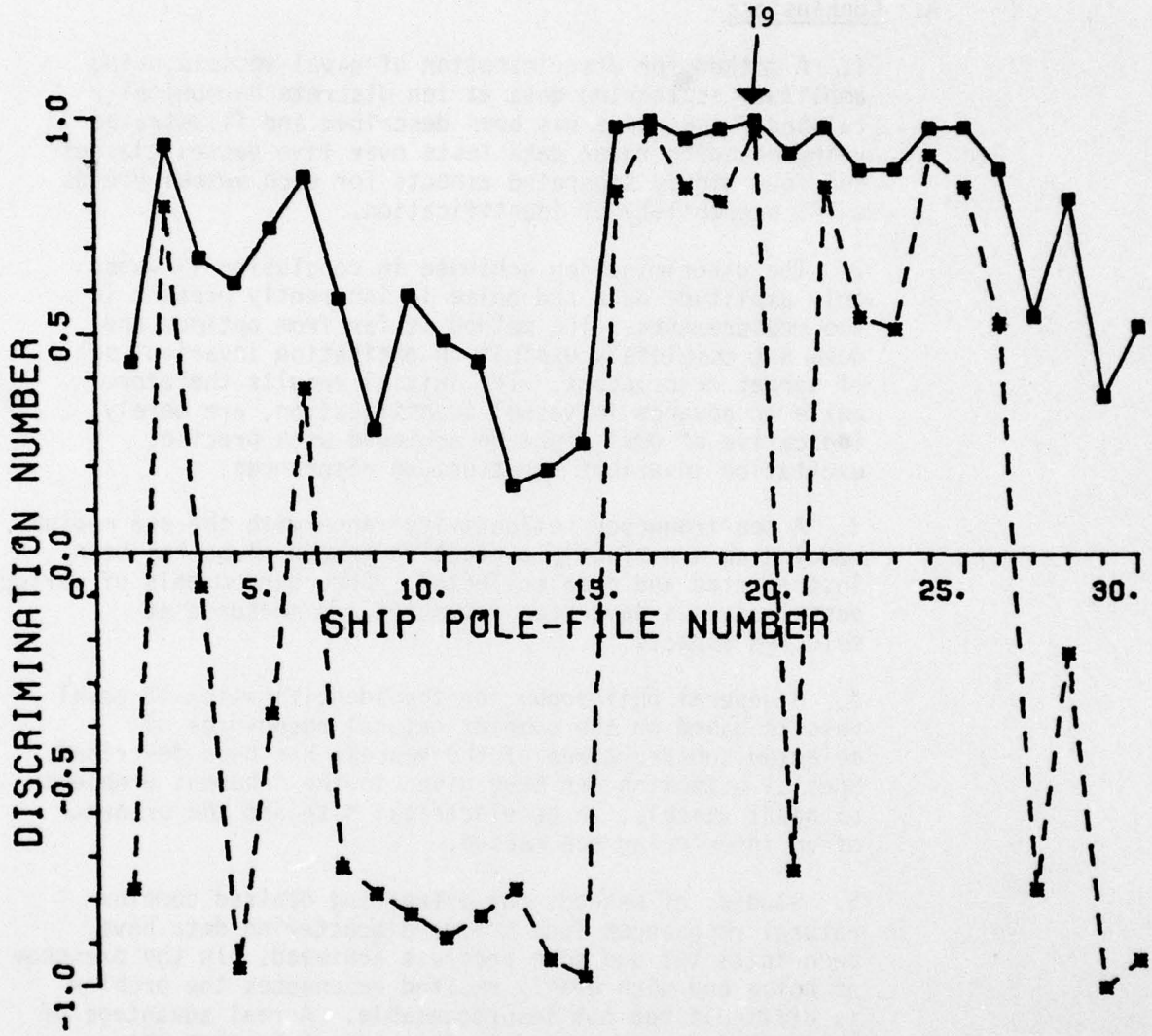

Figure 63

VIII. CONCLUSIONS AND RECOMMENDATIONS

A. Conclusions

1. A method for discrimination of naval vessels using amplitude scattering data at ten discrete harmonically related frequencies has been described and illustrated using measured radar data tests over five vessel classes and four widely separated aspects for each vessel yields a 77% probability of identification.

2. The discrimination achieved in conclusion 1) uses only amplitude data and noise is inherently present in the measurements. The method is far from optimum and does not completely exploit an excitation invariant set of target descriptors. The initial results therefore, while an advance in vessel identification, are merely indicative of what might be achieved with precise, excitation invarient substructure resonances.

3. A ten frequency reflectivity range with the sea medium modeled as a perfectly conducting ground plane has been instrumented and data collected. Some nine models of various vessel classes have been assembled and measured at selected aspects.

4. A general philosophy for the identification of naval vessels based on the complex natural resonances of selected substructures of the vessels has been described. Special attention has been given to the inherent problems of naval vessels; large electrical size and the presence of an interfering sea medium.

5. Studies of methods for extracting desired complex natural resonances from measured scattering data have been initiated and some progress achieved. In the presence of noise and with weakly excited resonances the problem is difficult but not insurmountable. A real advantage of the techniques described in this report is that the resonances need not be extracted in real time. That is, the discrimination procedure does <u>not</u> extract resonances from the signaling waveform of an unknown target.

IX. RECOMMENDATIONS

1. Swept, in addition to discrete, frequency measurements appear desirable for naval vessel targets. With swept frequency measurements, synthetic "chirp"-type processing will permit isolation of potentially interesting structure features. At the same time the measured data will suggest possible high return frequency regions. Modifications to convert the existing reflectivity facility to discrete or swept measurements are in progress.

2. Improvements are clearly still needed in methods for extracting the complex natural resonances of a target from measured response data. It is not intended that the main purpose of this program be directed to this goal (the same question arises on other programs) but some study will be made of alternative schemes, one such being via linear algebra to find that difference equation which satisfies several data sets.

3. A method for obtaining many complex natural resonances from measured data obtained with an internally located (within the target) source and receiver has been suggested [18,19]. Experimental tests of this procedure will be conducted during the next interim.

4. Additional measured scattering data on model naval vessels, in situ, are needed. These include swept frequency measurements at untested aspects and possibly additional classes of naval vessels.

5. Assuming that research progress on the identification of naval vessels continues to show workable methods, some study should be initiated on the actual size and complexity of full scale radar systems needed for the identification task. Ideally such a study should be started late in the upcoming interim.

REFERENCES

[1] E. M. Kennaugh and D. L. Moffatt, "Transient and Impulse Response Approximations," Proc. IEEE, Vol. 53, August 1965, pp. 893-901.

[2] D. L. Moffatt and R. K. Mains, "Detection and Discrimination of Radar Targets," IEEE Trans. on Ant. and Prop., May 1975.

[3] C. W. Chuang and D. L. Moffatt, "Natural Resonances of Radar Targets Via Prony's Method and Target Discrimination," IEEE Trans. on Aerospace and Electronic Systems, Vol. AES-12, No. 5, September 1976, pp. 583-589.

[4] J. D. Young, "Target Imaging from Multiple-Frequency Radar Returns," IEEE Trans. on Ant. and Prop., Vol. AP-24, No. 3, May 1976.

[5] K. A. Shubert, J. D. Young, and D. L. Moffatt, "Synthetic Radar Imagery," IEEE Trans. on Ant. and Prop., Vol. AP-25, No. 4, July 1977, pp. 477-483.

[6] R. Mittra and M. Van Blaricum, "A Novel Method for Extracting the SEM Poles and Residues of a System Directly from its Transient Response," 1974 Annual URSI Meeting, Boulder, Colo., October 1974.

[7] D. L. Moffatt, "Time Domain Electromagnetic Scattering from Highly Conducting Objects," Report 2971-2, May 1971, The Ohio State University ElectroScience Laboratory, Department of Electrical Engineering; prepared under Contract F19628-70-C-0125 for Air Force Systems Command, Laurence G. Hanscom Field, Bedford, Massachusetts. (AFCRL-71-0319) (AD 885883)

[8] D. L. Moffatt and K. A. Shubert, "Complex Rational Approximants," IEEE Trans. on Ant. and Prop., Vol. AP-25, No. 5, September 1977.

[9] M. S. Corrington, "Simplified Calculation of Transient Response," Proc. of IEEE, Vol. 53, No. 3, March 1965, pp. 287-292.

[10] M. L. Van Blaricum, "Techniques for Extracting the Complex Resonances of a System Directly from its Transient Response," Ph.D. Dissertation, 1976, University of Illinois at Urbana-Champaign, Department of Electrical Engineering.

[11] E. K. Miller, Brittingham and Willows, "The Derivation of Simple Poles in a Transfer Function from Real Frequency Information," Part 3, Lawrence Livermore Laboratory, January 10, 1977.

[12] D. A. Hill, "Electromagnetic Scattering Concepts Applied to the Detection of Targets Near the Ground," Report 2971-1, October 1970, The Ohio State University ElectroScience Laboratory, Department of Electrical Engineering; prepared under Contract F19628-70-C-0125 for Air Force Systems Command, Bedford, Massachusetts. (AFCRL-70-0250) (AD 875889)

[13] M. L. Van Blaricum and R. Mittra, "A Technique for Extracting the Poles and Residues of a System Directly from the Transient Response," IEEE Trans. on Ant. and Prop., Vol. AP-23, No. 6, pp. 777-781.

[14] D. L. Moffatt, L. C. Chan, and G. A. Hawisher, "Characterization of Subsurface Electromagnetic Soundings," Annual Report 4490-1, September 1977, The Ohio State University ElectroScience Laboratory, Department of Electrical Engineering; prepared under Grant ENG 76-04344 for National Science Foundation, Washington, D. C. 20550.

[15] M. L. Van Blaricum, "Techniques for Extracting the Complex Resonances of a System Directly from its Transient Response," Ph.D. Dissertation, 1976, University of Illinois at Urbana-Champaign, Department of Electrical Engineering, pp. 64-76.

[16] D. L. Moffatt, "Radar Target Detection and Discrimination," Short Course Notes for Radar Target Identification, 1977, The Ohio State University, Department of Electrical Engineering, 1976 and 1977.

[17] E. Guillemin, Theory of Linear Physical System, New York, Wiley, 1963.

[18] D. L. Moffatt, "Radar Identification of Naval Vessels, Proposal to ONR, March 11, 1976.

[19] D. L. Moffatt and C. M. Rhoads, "Radar Identification of Naval Vessels," Continuation proposal to ONR, October 1, 1977.